



KfK 3927
Mai 1985

Summary and Implications of Out-of-pile Investigations of Local Cooling Disturbances in LMFBR Subassembly Geometry under Single-phase and Boiling Conditions

F. Huber, W. Pepler
Institut für Reaktorentwicklung
Projekt Schneller Brüter

Kernforschungszentrum Karlsruhe

KERNFORSCHUNGSZENTRUM KARLSRUHE

Institut für Reaktorentwicklung

Projekt Schneller Brüter

KfK 3927

Summary and Implications of Out-of-pile Investigations of
Local Cooling Disturbances in LMFBR Subassembly Geometry
under Single-phase and Boiling Conditions

F. Huber

W. Pepler

Kernforschungszentrum Karlsruhe G.m.b.H., Karlsruhe

Als Manuskript vervielfältigt
Für diesen Bericht behalten wir uns alle Rechte vor

Kernforschungszentrum Karlsruhe GmbH
ISSN 0303-4003

Summary

The consequences of local cooling disturbances in subassemblies of LMFBRs have been investigated out-of-pile at KfK. Flow and temperature distributions in the disturbed region as well as cooling under boiling conditions up to loss of cooling were investigated. Fission gas release was simulated by gas injection. A total of 16 different blockages in 20 test set-ups were used, four of them under sodium and the rest under water conditions. Mainly planar plates of different sizes and arrangements were used as blockages. In some of the experiments performed in water also porous blockages were investigated. The test sections consisted of electrically heated pin bundles with a thermal-hydraulic characteristic corresponding to that of an SNR 300 subassembly. With different parameter settings the single-phase tests in water furnished a multitude of test results on flow and temperature fields and on the behaviour of gas in the recirculation zone. Concerning loss of cooling the results of the two 169 pin bundle tests performed in sodium with a 49 % central blockage and a 21 % wall blockage are discussed above all.

The temperature increase in the region of disturbed cooling is determined by the existing flow field. The latter does not only depend on the size of the blockage but also on the location and nature, e.g. a central or wall blockage, leak-tight or permeable.

In the experiments involving boiling two boiling patterns were observed: steady-state boiling and oscillating boiling. With increasing boiling intensity the boiling region grew to some extent, but it remained always confined to the blocked zone because of the relatively cold sodium flow around this zone. Therefore, a transition from local to cross boiling can be excluded. With oscillating boiling the limits of cooling were reached at much higher boiling intensity compared to steady-state boiling. The extension of the boiling zones and the loss of cooling conditions (dryout) were estimated from the single phase temperature distribution behind the blockage. Recalculations of experiments using

II

different codes led especially in the case of porous blockages to unsatisfactory results.

In the experiments simulating fission gas release it was found that under certain conditions gas accumulates in the reverse flow region behind a blockage and leads to loss of cooling. The experimental results have been applied to FBR conditions and are discussed. This includes the detection of a blockage by the DND system, the conditions to start boiling behind a blockage, the quantities of clad and fuel which may melt in case of a local loss of cooling and the conditions under which release of fission gas may influence the cooling.

Zusammenfassung

Out-of-pile-Untersuchungen von lokalen Kühlungsstörungen in Schnell-Brüter-Brennelement ähnlichen Stabbündeln unter Einphasen- und Siedebedingungen

Im Rahmen eines experimentellen Programms wurden die Auswirkungen von lokalen Kühlungsstörungen in Brennelementen von schnellen flüssigmetallgekühlten Brutreaktoren (LMFBR) im KfK untersucht. Untersucht wurden die Strömungs- und Temperaturverteilung im kühlungsgestörten Bereich sowie die Kühlbarkeit unter Siedebedingungen bis hin zum Versagen der Kühlung. Zur Simulation von freigesetztem Spaltgas wurden Versuche mit Gaseinspeisung durchgeführt. Insgesamt wurden 16 verschiedene Blockaden, davon 4 in Natrium, die übrigen in Wasser, eingesetzt. Die Blockaden bestanden überwiegend aus dichten ebenen Platten verschiedener Größe und Anordnung; in einigen Experimenten in Wasser waren sie definiert durchlässig. Als Teststrecken wurden elektrisch beheizte Stabbündel mit einer dem Brennelement des SNR 300 entsprechenden thermohydraulischen Charakteristik verwendet.

Die Einphasenversuche in Wasser lieferten umfangreiche Ergebnisse zu den Strömungs- und Temperaturfeldern und zum Verhalten von Gas in der Rezirkulationszone unter dem Einfluß verschiedenster Parameter. In der Diskussion zum Versagen der Kühlung werden im wesentlichen die Ergebnisse der beiden Natriumexperimente KNS1 und KNS2 mit einer 49%-Zentralblockade bzw. einer 21%-Eckblockade, verwendet. Die Temperaturerhöhung im kühlungsgestörten Bereich wird bestimmt durch das sich einstellende Strömungsfeld. Dieses hängt nicht nur von der Größe der Blockade, sondern auch von deren Lage und Art ab, z.B. Zentral- oder Eckblockade, dicht oder durchlässig.

In den Experimenten mit Sieden wurden zwei Siedeformen gefunden: Stationäres Sieden und oszillierendes Sieden. Mit zunehmender Siedeintensität dehnte sich die Siedezone zwar aus, blieb jedoch, wegen der den Blockadebereich umströmenden relativ kalten Flüssigkeit, auf den blockierten Bereich beschränkt. Ein Übergang vom

lokalen zum integralen Sieden kann daher ausgeschlossen werden. Bei oszillierendem Sieden wurde die Kühlbarkeitsgrenze bei höherer Siedeintensität als bei stationärem Sieden erreicht. Die Ausdehnung der Siedezone und die Bedingungen beim Versagen der Kühlung konnten anhand der einphasigen Temperaturverteilung hinter der Blockade abgeschätzt werden. Die Nachrechnungen von Experimenten mit verschiedenen Modellen führten besonders im Falle von porösen Blockaden zu keinen befriedigenden Ergebnissen.

In den Versuchen zur Simulation von Spaltgasfreisetzung wurde beobachtet, daß sich eingespeistes Gas unter bestimmten Bedingungen in der Rezirkulationsströmung hinter der Blockade ansammelt und damit zum Verlust der Kühlung führt.

Die experimentellen Ergebnisse wurden auf FBR Bedingungen übertragen und diskutiert. Dies schließt ein: die Detektion einer Blockade durch das DND-System, die Bedingungen, unter denen Sieden in der Blockade erreicht wird, die Mengen von Stahl und Brennstoff, die maximal ausschmelzen können, wenn ein örtlicher Kühlungsverlust im Blockade-bereich auftritt, und die Bedingungen, unter denen austretendes Spaltgas auf die Kühlung einwirkt.

<u>Content</u>	<u>Page</u>
1. Introduction	1
2. Description of Test Facilities	5
2.1 Test Loops	5
2.2 Test Sections	6
3. Experiments Performed and Experimental Procedure	10
4. Treatment of Recorded Signals	12
4.1 Flow Pattern in Isothermal Experiments	12
4.2 Single Phase Temperature Distribution	12
4.3 Boiling Behaviour	13
4.4 Behaviour of Injected Gas	13
5. Results and Analysis of Experiments under Single Phase Flow Conditions	14
5.1 General Shape of the Flow Pattern behind Planar Type Blockages	14
5.2 Characteristic Data of the Wake	14
5.3 Temperature Distribution Downstream of Impermeable Blockages	16
5.4 Influence of Leakage Flow through Blockages	20
5.5 Maximum Temperature Rise behind Blockages of Different Sizes	21
5.6 Temperature Rise in the Wake under Natural Convection Conditions	23
5.7 Influence of Pin Bowing	24
5.8 Summary of Thermal-Hydraulic Phenomena in the Wake	25
5.9 Summary of Experiments Performed under Single Phase Flow Conditions	27
6. Experimental Results Obtained under Boiling Conditions	30
6.1 General Course of Boiling	30

VI

6.2	Oscillatory Boiling	32
6.3	Steady-state Boiling	35
6.4	Comparison of Measured and Estimated Boiling Regions	37
6.5	Experimental Conditions at the Onset of Dryout	39
6.6	Summary of Boiling Tests	41
7.	Discussion of Dryout Conditions	44
7.1	Mechanisms of Liquid Supply into the Boiling Zones	44
7.2	Dryout Mechanisms	46
8.	Experiments with Gas Injection	49
8.1	General Behaviour of Gas in the Wake	49
8.2	Conditions Leading to Gas Accumulation	50
8.3	Influence of Gas on Cooling	53
8.4	Summary of Tests with Gas Injection	55
9.	Comparison of Experiments with 3-D Code Calculations	57
10.	Application of Results to Reactor Conditions	62
10.1	SNR 300: MK Ia Fuel Element Design	62
10.1.1	Flow and Temp. Fields under Single Phase Conditions	63
10.1.2	Cooling under Boiling Conditions	66
10.1.3	Implications of Gas Release	69
10.2	Application of Results to Different Subassembly Designs of the SNR 300	75
10.3	Conceivable Tendencies of Changes of the Size of the Subassembly	76
11.	Conclusions	78
12.	Nomenclature	84
13.	References	87

VII

Annex A: Definition of Normalized Temperatures	157
Annex B: Definition of Leakage FLOW	159
Annex C: Boundary Conditions for Gas Cavity Formation	160
Annex D: Graphs of Characteristic Boiling Signals	164

VIII

List of Tables

- Tab. 1 Survey of the Blockages Investigated
- Tab. 2 Technical Data of the KNS-Test Sections 1 and 2 and the Fuel Elements of the SNR 300
- Tab. 3 Range of Experimental Parameters with a 49 % Central Blockage in Water and Sodium
- Tab. 4 Range of Experimental Parameters with a 21 % Corner Blockage in Water and Sodium
- Tab. 5 Range of Experimental Parameters with a Porous 21 % Corner Blockage in Water
- Tab. 6 Range of Experimental Parameters with a Variable Blockage in Water
- Tab. 7 Conditions of the Experiments Represented in Figure 19
- Tab. 8 Conditions of Experiments Involving Permanent Dryout
- Tab. 9 Experimental Data Obtained under Dryout Conditions
- Tab.10 Benchmark Calculations with Local Blockages
- Tab.11 Summarized Values from the Discussion of the SNR 300 MKIa Subassembly Case

List of Figures

- Fig. 1 Local Blockages in Subassemblies,
Chain of events.
- Fig. 2 Schematic Diagram of the Water Loop.
- Fig. 3 Schematic Diagram of the KNS Sodium Loop.
- Fig. 4 Water Test Section with a 21 % Corner Blockage of Variable Porosity.
- Fig. 5 Schematic Diagram of the Test Section with Variable Blockage.
- Fig. 6 KNS Test Sections 1 and 2.
- Fig. 7 Subchannel and Pin Reference Identification.
- Fig. 8 Local Boiling Experiments Experimental Procedures.
- Fig. 9 Typical Flow Pattern Behind a Central Blockage and a Corner Blockage.
- Fig. 10 Length of the Reverse Flow Region as a Function of the Blockage Radius.
- Fig. 11 Influence of the Size of the Blockage on the Reverse Flow Velocity.
- Fig. 12 Influence of the Leakage Flow on the Wake Geometry and Reverse Flow Velocity.
- Fig. 13 Leakage Flow Causing the Dissolution of the Reverse Flow.

- Fig. 14 Normalized Temperature Field behind the 49 % Central Blockage.
- Fig. 15 Normalized Temperature Field behind the 21 % Corner Blockage.
- Fig. 16 49 % Central Blockage.
Normalized Temperature Profiles just before Boiling.
- Fig. 17 21 % Corner Blockage.
Normalized Radial Temperature Profiles.
- Fig. 18 KNS Test Section 2.
Influence of Main Flow Velocity on the Temperature Field.
- Fig. 19 Axial Peak Temperature Distribution Comparison of Different Blockages.
- Fig. 20 49 % Central Blockage, Fixed and Variable Radial Temperature Profiles.
- Fig. 21 21 % Corner Blockage, Fixed and Variable Radial Temperature Profiles.
- Fig. 22 Variable Corner Blockage.
Influence of Blockage Size on Axial Peak Temperature Distribution.
- Fig. 23 Variable Central Blockage.
Influence of Blockage Size on Axial Peak Temperature Distribution.
- Fig. 24 Influence of the Leakage Flow through the 21 % Corner Blockage in Water.

- Fig. 25 Influence of Leakage Flow on Max. Temperature Rise in the Wake.
- Fig. 26 Max. Temperature Rise behind Different Blockages (impermeable).
- Fig. 27 Central Blockage.
Max. Temperature Rise with and without Leakage Flow.
- Fig. 28 Corner Blockage.
Max. Temperature Rise with and without Leakage Flow.
- Fig. 29 49 % Central Blockage.
Influence of Boiling Experiments on the Max. Temperature Rise.
- Fig. 30 Identification of Important Thermal-Hydraulic Phenomena in the Wake of a Central Blockage.
- Fig. 31 49 % Central Blockage, Run 58E.
Typical Boiling Signals Recorded just before Permanent Dryout.
- Fig. 32 49 % Central Blockage.
Amplitude and Frequency of Vapour Volume Oscillations.
- Fig. 33 49 % Central Blockage.
Estimated Minimum and Maximum Boiling Regions.
- Fig. 34 21 % Corner Blockage, Run 485.
Typical Boiling Signals Recorded just before Permanent Dryout.
- Fig. 35 21 % Corner Blockage.
Approximated Boiling Regions.

XII

- Fig. 36 49 % Central Blockage.
Area of the Boiling Regions Compared with Estimate
from Single-Phase.
- Fig. 37 21 % Corner Blockage.
Area of the Boiling Region Compared with Estimate
from Single-Phase.
- Fig. 38 Excess Temperatures of Dryout Conditions.
- Fig. 39 Diagram Illustrating the Draining Liquid Film and
the Vapour Flow.
- Fig. 40 Experiments in Water.
Gas Cavities in the Wake.
- Fig. 41 21 % Corner Blockage Conditions of Gas Accumulation in
Sodium.
- Fig. 42 Minimum Reverse Flow Velocity for Gas Accumulations from
Different Experiments.
- Fig. 43 21 % Corner Blockage.
Dependence of Cavity Size on Main Flow Velocity and Gas
Injection Rate.
- Fig. 44 49 % Central Blockage.
Course of Temperature During Gas Accumulation.
- Fig. 45 21 % Corner Blockage.
Typical Signals of an Experiment with Pulsed Gas In-
jection.
- Fig. 46 21 % Corner Blockage.
Extension of the Cooling Disturbed Region in the Wake.

XIII

- Fig. 47 LMBWG Benchmark Calculations.
49 % Central Blockage in Sodium Radial Temperature Profile.
- Fig. 48 LMBWG Benchmark Calculation.
21 % Corner Blockage in Sodium Radial Temperature Profile.
- Fig. 49 LMBWG Benchmark Calculation.
49 % Central Blockage, Temperature Distribution.
- Fig. 50 LMBWG Benchmark Calculation.
21 % Corner Blockage, Temperature Distribution.
- Fig. 51 LMBWG Benchmark Calculation.
21 % Corner Blockage (variable) with Leakage Flow Radial Temperature Profile.
- Fig. 52 LMBWG Benchmark Calculation.
21 % Corner Blockage, Permeable Max. Temperature Rise vs. Leakage Flow.
- Fig. 53 Experimental Results from the Central Blockage Transferred to SNR 300 Conditions.
- Fig. 53a Max. Normalized Temperature Rise with and without Leakage Flow vs. Blockage Size.
- Fig. 53b Volume of the Wake above Specified Normalized Temperatures.
- Fig. 54 Experimental Results from the Corner Blockage Transferred to SNR 300 Conditions.
- Fig. 54a Max. Normalized Temperature Rise with and without Leakage Flow vs. the Blockage Size.

Fig. 54b Volume of the Wake above Specified Normalized Temperatures.

Fig. 55 Corner Blockage.

Minimum Main Flow Velocity for Gas Accumulation.

Fig. 56 Central Blockage.

Minimum Main Flow Velocity for Gas Accumulation.

Fig. 57 Leakage Flow Conditions Related to Reverse Flow and Gas Accumulation /25/.

Fig. 58 Upper Limits of Gas Cavity Volumes.

Fig. 59 Gas Entrainment Rate from the Cavity.

Acknowledgement

The authors wish to thank all colleagues who participated in the realization and analysis of the experiments and contributed to the success of this project by their engagement.

1. Introduction

Current approaches to study the safety of LMFBRs require a systematic treatment of the progression of possible incidents from initiation as a result of rather minor events. Within this context, local cooling disturbances in single fuel subassemblies have to be considered as initiating mechanisms /1, 2/.

A survey of the knowledge available of propagation incidents is given in /3/. Two major phases govern the course of this incident:

- (1) Propagation of failures from a few pins throughout the subassembly (pin-to-pin propagation).
- (2) Further propagation from the failed subassembly to adjacent elements (subassembly-to-subassembly propagation).

To classify this research work within the LMFBR safety analysis a survey of the chain of events with respect to local cooling disturbances by planar blockages is reproduced in Fig. 1. Axial extended blockages are also possible and may lead to other type of boiling /6/. The chain of events starts with the growth of a blockage detection excluded. According to present knowledge /4, 5/ a planar blockage should be formed mainly by fuel particles from the subassembly considered because foreign particles are very unlikely to penetrate through several grid spacers into the core region. Blockages up to local flow obstructions behind which cooling is seriously impaired may build up within days or weeks. During this time the fuel released is very likely to be detected.

In the studies described it is assumed, however, that a blockage of a certain size has built up which leads to a local temperature increase. The subsequent development of the failure could follow two paths of events. Either pins fail prior to local boiling and fission gas is released and accumulates temporarily behind the blockage or boiling starts locally behind the blockage. Both paths could finally lead to a local loss of cooling followed by

clad and fuel melting. Fuel melting is considered as a switch point from where on the chain of events could proceed to more serious failures in the subassembly. The experiments described in this report concentrate on the events involving the formation of local blockages up to local loss of cooling (local dryout).

After clad and fuel melting secondary blockages could build up which in turn could lead to progress of clad and fuel melting. This stage of the events is covered by another series of experiments /6/. In Fig. 1 two other imaginable chains of events following local boiling or fuel melting are shown. They will not be discussed because they can be ruled out, on the basis of results of earlier experiments and analysis.

The general aim of the studies is to demonstrate that the consequences of a local blockage do not lead to rapid propagation of damage within a pin bundle.

Therefore, the aims of these experiments were:

- Definition of the temperature profiles to be anticipated downstream of blockages as a function of various physical parameters, such as flow, power, leakage flow through the blockage, inlet temperature, etc.
- Establishment of the types and courses of boiling events downstream of blockages.
- Assessment of the margin between the onset of boiling downstream of a blockage and the onset of dryout.
- Determination of the effects of gas in connection with the aims stated above
- Collection of experimental data to validate codes like SABRE /7/ which enable temperature profiles to be predicted for non-boiling situations.
- Pinpointing of the detection limits of blockages in relation to the capabilities of measuring devices.
- Demonstration whether in case of decay heat the blocked region can be cooled by natural convection.

-- Estimation of the possible amount of clad and fuel at risk of melting for planar blockages.

A survey of the type and size of the blockages investigated in the past years within the out of pile experimental programme and the respective references /8-26/ are reproduced in Table 1. This table does not include the experiments in which blockage formation was studied /5/ and the in-pile experiments /6/. The bundle geometry for the blockages listed in Table 1 corresponds largely to the subassembly of the FBR SNR 300 MkIa design (with spacer grids). The cross sections of the test sections were varied between full and half bundle and a 60° sector. The tests were carried out in water and sodium as well. In most cases planar, solid blockages were built in the bundle. Such blockages are generally considered to be more probable in gridded fuel pin clusters than in wire-wrapped fuel assemblies; consequently most experimental and theoretical effort concentrated on planar blockages which produce a recirculating wake if the blockage permeability is low or zero.

The experimental work carried out at KfK on local cooling disturbances culminated in two series of local blockage experiments in sodium (Table 1, blockages 9 and 10) in the KNS sodium boiling loop. The results of this work is one of the main subjects of this report. The two test sections simulated SNR 300 MkIA fuel elements with a 49 % central blockage in the first test section (KNS I), and a 21 % corner blockage in the second (KNS II). In the course of this work pin cooling in the wake of the blockage was investigated under single-phase conditions boiling conditions up to dryout and under conditions simulating gas release from failed pins.

Since in a subassembly a permeable blockage may be more realistic than an impermeable one, additional experiments in water with a permeable 21 % corner blockage (Table 1, blockage 15) were carried out. The main objectives of these experiments were to ascertain

the influence of leakage flow on the flow velocity and temperature distribution in the wake, and on the phenomenon of gas accumulation. Findings from the latest experiments performed in a water test section (blockage 16) with a blockage of variable size, position and porosity are included.

An attempt has been made to understand the physical basis of the more significant features of the results presented. In particular the large variation of the conditions at the start of boiling up to the onset of permanent dryout requires understanding of pin cooling mechanisms and their limitations. They have been studied for the simplest case of dryout in steady state boiling by Clare, A.J. /27/, and the main findings are summarized here. As the dryout margin is affected by the boiling regime, some attention has been paid identifying the factors which govern the boiling behaviour.

Based on the numerous experimental data, the maximum temperatures behind various planar blockages were estimated under adverse cooling conditions e.g. a certain leakage flow through the blockage. Furthermore, the volumes behind planar blockages at or above a specified temperature limit were determined. From these considerations the maximum amounts of fuel at risk of melting behind blockages have been deduced; thus it was possible to define an upper limit for the propagation potential of local cooling disturbances. By calculations with simple models taking into account the measured reverse flow conditions behind a wake in the SNR 300 MKIa subassembly geometry the tendencies could be outlined which should exist in case of a change of the subassembly geometry. The latter point should be treated furthermore as soon as validated 3D codes will be available.

The work described was carried out under cooperation of the United Kingdom Atomic Energy Authority, the ECN in Petten (Netherlands), and Tokyo Shibaura Electric Company (Toshiba) of Japan.

2. Description of Test Facilities

2.1 Test Loops

Water Loop

Figure 2 shows a schematic diagram of the water loop used for the experiments. The main components are: the storage tank, the expansion tank, the pump and the damping tanks. The main technical data of this loop are:

- max. mass flow	22.5 kg/s
- max. pressure head	10 bar
- max. operating temperature	90°C
- diameter of the main pipe	100 mm

The test sections for the investigation of local cooling disturbances with local blockages were installed at position (2) in the loop (see Fig. 2). Position (1) between the damping tanks was used for other experiments. The water in the storage tank (5 m³) served as a heat buffer for the heat from the test section. Consequently the inlet temperature of the test section could be kept nearly constant during one run.

Compact Sodium Boiling Loop (KNS)

The compact sodium boiling loop (KNS) was specifically developed and built for the purpose of implementing boiling tests with large bundles that are similar to fuel elements. Figure 3 is a simplified flow diagram of this loop.

For safety reasons the main loop is contained in a protection vessel filled with nitrogen throughout the test operations.

The design data of the KNS loop are:

- temperature	700	°C
- mass flow	18	kg/s
cooling capacity	1.2	MW
- nominal width of the main tube to test section	80	mm
- nominal width of the bypass	50	mm

The KNS loop is connected to the sodium tank test facility (NABEA) /28/ which supplies both the argon cover gas and the sodium. This facility also serves to purify the sodium and as a cooling loop. The buffer tank and its gas plenum simulate the inlet plenum of the reactor. The flow through the test section is generally controlled by a combination of throttle valve SV1 and the bypass throttle valve SV3. The throttle valve SV2 between the buffer tank and the test section is used to adjust the pressure drop to SNR 300 conditions. Downstream of the test section is the "mixing section" where the sodium from the test section merges with that from the bypass. The sodium is passed from here through a sodium/sodium heat exchanger and returned to the pump tank at its original temperature. The mixing section and the free sodium surface of the pump tank simulate the reactor outlet plenum.

2.2 Test Sections

In the following paragraphs only those test sections will be briefly described which furnished the results mainly used in this report.

Water Test Section with a Porous 21 % Corner Blockage

The test section and the blockage used in the water experiment with a porous 21 % wall blockage /21, 23/ are shown in Fig. 4. The test section represents one half of the SNR 300 fuel subassembly, divided along the vertical plane of symmetry through the blockage. A glass wall replaced this plane. The fuel pins were simulated by electrical heaters with the same diameter and pitch as those in the sodium experiments. The heated length was about 700 mm and the maximum heat flux 27 W/cm^2 . The porous blockage was installed in the corner of the test section. The size and position are identical with those of the second sodium test-section wall blockage. The blockage had a box geometry and was divided into two chambers by an impermeable intermediate plate. The porosity was simulated by holes, diameters 1 mm and 1.5 mm, respectively, drilled in the upper and lower plates of the block-

age in the subchannel region (Fig. 4). A portion of the main flow in the test section was discharged through the lower chamber into an auxiliary loop and then returned via the upper chamber into the wake. By this auxiliary loop the leakage flow through the blockage could be controlled independently of the main flow thus allowing to study the influence of the leakage flow over a wide range (definition of leakage flow see Annex B). Gas injection was provided behind the blockage and upstream of the blockage into the main flow. The injected gas was used to make visible the flow and to investigate the conditions for gas accumulation. The same test section, although equipped with an impermeable 21 % corner blockage, was also used in the experiments of Fukuzawa /20/.

Water Test Section with Variable Blockage

Figure 5 shows schematically the main part of the test section which allows to vary the type, the size and porosity of the blockage /24, 25/. This test section is a modification of the test section described above. To simulate different types of blockages each individual cell of the grid which simulates the position of the blockage is connected to a flow distributor by flexible tubes. The inlet flow is divided in two distributors, one for the channels of the unblocked region (A) and one for the channels which simulate the partially or total blockaged flow area (B). In the case of the impermeable blockage the flow to distributor B is interrupted. In the case of a permeable blockage simulation the flow through the blockage (distributor B) is set to the desired flow rate. In contrast to a fixed blockage in this test section the main flow is uniform over the cross-section of the unblocked region. This will also cause a difference in the flow behaviour behind the blockage.

To investigate the influence of the first grid down-stream of the blockage this grid was axially displaceable. Figure 5 shows also the gas injection system. The flow in the wake was directly observed and recorded by high speed cinematography. To measure the

temperature field behind the blockage in the case of the two water test sections thermocouples were inserted through the window into the subchannels between the first and the second pin rows.

Sodium Test Section

A full description of the two test sections used for the experiments in sodium is given by Huber et al. /29/. The main features are illustrated in Fig. 6 of this report. The most important technical data of the two test sections together with those of the SNR 300 fuel elements are shown in Tab. 2. The bundles had 169 pins of 6 mm diameter and a triangular pitch of 7.9 mm which corresponds to SNR 300 Mk1A fuel element conditions. The upper part of the test sections (unheated length, flow mixer and outlet) also follows the SNR 300 design. 90 out of 169 pins were heated over a length of 290 mm. The heater design was for a maximum heat flux of 170 W/cm^2 at a heater wall temperature of $950 \text{ }^\circ\text{C}$; so, the total power of each test section was 840 kW.

The blockages were 3 mm thick and positioned within a spacer grid, 40 mm from the beginning of the heated length. In test section 1 the hexagonally shaped blockage was in the centre of the test-section; it enclosed 91 pins and blocked about 49 % of the total flow area. The cross section illustrates the shape and position of the blockage and also the positions of the heater and dummy pins. In test section 2 the blockage was positioned in a corner of the test section and blocked about 21 % of the total flow area. There was a total of 36 pins within the blockage boundary. Figure 7 shows the subchannel and pin reference definition of the two sodium test sections.

The test sections were instrumented with:

- about 100 thermocouples, most of them embedded in the heater pin walls and located at different levels downstream of the blockage;
- chen-type void detectors distributed in the wake;

- static and dynamic pressure transducers at various positions;
- acoustic monitors at various positions in the test section and the loop;
- flowmeters at the inlet and outlet of the test section.

To investigate the effects of gas released into the coolant from failed fuel pins, gas could be injected. In the case of KNS-test section 1 it could be injected only upstream of the blockage into the main flow. By contrast, the gas injection equipment for KNS-test section 2 allowed gas to be injected directly into the wake as well as upstream of the blockage, either continuously or in a pulse mode.

3. Experiments Performed and Experimental Procedure

As already mentioned in chapter 1 the results of the experiments with the 49 % central blockage (Tab. 1, Nos. 9 and 13), the 21 % corner blockage (Tab. 1, Nos. 10, 11, 14 and 15) and with the variable blockage (Tab. 1, No. 16) will be treated preferably. Among these experiments those carried out in sodium are of major interest, because they have the character of performance tests with respect to the SNR 300 fuel element.

Dependent on the experimental conditions and the aims pursued, these experiments are grouped into five types:

- F isothermal experiments in water to study the flow behaviour in the wake;
- G isothermal experiments in water and sodium with gas injection to study the conditions of gas accumulation;
- S single phase experiments in water and sodium to measure the temperature distribution in the wake;
- S/G single phase experiments in sodium with gas injection to study the influence of gas on the temperature distribution;
- B boiling experiments in sodium to study the boiling behaviour;
- B/G boiling experiments with gas injection to study the influence of gas on the boiling behaviour.

A survey of the experimental conditions of the different experiments is given in Tables 3-6. In the single phase and boiling experiments the most important parameters are the flow rate and the heat flux expressed as the power to flow ratio or the axial temperature gradient in the bundle. The conditions for the onset of boiling were determined from the results of the single phase experiments. Boiling was increased by either stepwise decreasing the inlet flow rate (Fig. 8, Type I) or by stepwise increasing the pin power (Type II). With the data recording system several steps of 1 min duration were recorded. Under dryout conditions the power was switched off when the temperature in the heater

wall exceeded the saturation temperature by about 50 K. In the sodium experiments with gas injection the injection rate is related to peak temperature and pressure in the wake. In the experiments conducted in water the injection rate is usually given for standard temperature and pressure. In the 21 % corner blockage experiments in sodium gas was also injected to simulate fission gas release from a real pin failure. In this case gas was stored in a small tank of 12 cm³ volume at a pressure of 6, 12 or 24 bars. The gas flow rate and pressure decreased with time. The release is characterized by the half life period of the gas pressure in the tank which is adjusted by a throttle valve.

In similar experiments in water with the 21 % corner blockage /20/ a gas plenum of 13 cm³ volume at 10 bars pressure was used.

In the phenomenological experiments in water with variable flow through the blocked area (blockages No. 15 and 16) the flow through the blockage was increased in steps until the reverse flow in the wake disappeared.

4. Treatment of Recorded Signals

4.1 Flow Pattern in Isothermal Experiments

In the water experiments the flow was visualized by the addition of gas. This was recorded by photographs and high speed cinematography. The flow behaviour characterized by local flow direction, turbulence and mixing between the main flow and the flow in the wake was derived from the cine film. The wake geometry was measured from the photos. The velocity of the recirculating flow was evaluated from the movement of single bubbles between single pictures of the cine film.

4.2 Single Phase Temperature Distribution

From the recorded temperature signals mean values over a time interval of about 10 seconds were calculated. With these data the normalized temperatures (see Annex A) were calculated. Both, the real and the normalized temperatures were printed in lists. In these lists the data are arranged by their axial and radial positions within the bundle. Furthermore, these data were used to produce axial temperature profiles of different subchannels and isotherms of the whole wake region. However, because of the limited number of thermocouples the measured temperatures had to be inter- or extrapolated to generate a complete picture of the temperature field. In the sodium experiments the velocity of the reverse flow was determined from a heat balance using the axial temperature profile in a specified subchannel.

The peak temperature in the wake is not known exactly because it does not necessarily appear at a thermocouple position. Therefore the peak temperature is calculated mainly from the conditions prevailing at the onset of boiling.

4.3 Boiling Behaviour

Besides the mean values (see 4.2) large scale plots of temperature, void, flow and pressure signals were produced as a function of time. The time at which boiling started locally was clearly be detectable from the first appearance of pressure spikes due to collapsing bubbles. Since the saturation pressure is known the peak temperature has to coincide with the saturation temperature. The boundaries of the expanding boiling region were deduced from thermocouple and void detector signals. They provide information about a limited number of positions in the wake. Therefore, the accuracy of the boiling region is limited. Movements of the vapour/liquid interface are mainly inferred from the signals of thermocouples close to the boundary. Such thermocouples show the saturation temperature with frequent or occasional excursions to subcooled levels as the boundary moves back and forth. In the case of oscillatory boiling the inlet and outlet flowmeter signals exhibit sinusoidal variations. The integrated difference of these signals provides the amplitude of the vapour volume oscillations. In view of the uncertainties associated with identifying the vapour region from temperature and void signals, the vapour volume fluctuations deduced from flowmeter signals are particularly useful.

4.4 Behaviour of Injected Gas

In the water experiments the behaviour of injected gas was recorded and analyzed as described in 4.1 to determine the flow pattern. In the isothermal sodium experiments the behaviour of the injected gas was deduced from the void detector signals. In the experiments with heat input additional information from the thermocouples was used. The problems faced in determining the boundaries of gas accumulations were about the same as those in the boiling regions.

5. Results and Analysis of Experiments under Single Phase Flow Conditions

5.1 General Shape of the Flow Pattern behind Planar Type Blockages

To be able to interpret the measured temperature fields it is necessary to know the flow conditions prevailing downstream of the blockage. Results are available from earlier experimental work. It was found that at sufficiently high Reynolds numbers a quasi steady-state recirculation flow pattern will form downstream of a blockage. Hannappel /19/ studied the flow patterns in both a 49% central blockage and a 21% corner blockage in water arranged as in the KNS test-sections. In addition to the influence of flow velocity he also studied the influence of the presence of a spacer grid on the length of the recirculation zone. In Fig. 9 two typical flow patterns (behind a central blockage and a corner blockage) are reproduced. The flow patterns behind the two blockages are similar. The arrows on the flow paths indicate the approximate direction of the flow. In both cases there is a fully developed reverse flow (3) towards the blockage. In case of the central blockage it is located in the centre of the recirculating zone and in case of the corner blockage it is near the wall. The recirculation zone is separated radially from the main flow by a thin transition zone (5) where there is intensive mass exchange due to turbulence between the recirculating flow and the main flow. The length of the recirculation zone is determined by the position of the rear stagnation point (2).

5.2 Characteristic Data of the Wake

Characteristic data of the wake are the axial extension of the reverse flow region, the position of the vortex centre and the reverse flow velocity. As known from the phenomenological experiments /19, 24/, the axial extension of the reverse region is in-

fluenced by the size of the blockage, the main flow velocity and in the case of large blockages, by the next grid downstream of the blockage.

In the water experiments with variable blockages /24/ it was found that at main flow velocities below 4 m/s the axial extension of the reverse flow region increased with increasing main flow velocity. At higher velocities it was nearly independent of the main flow. The influence of the size and position of the blockage and the adjacent downstream grid spacer is shown in Fig. 10. In this figure the length of the reverse flow region is plotted versus the radius of the blockage for central blockages and the corner blockages with and without grid at a main flow velocity of 3 m/s. Up to a radius of about 35 mm, which corresponds to a 14% corner blockage and a 40% central blockage, the length of the reverse flow region of the two types of blockages is similar and there is no influence of the grid. In this range the ratio of L_R/R can be estimated to be approximately 2.6. In the case of larger blockages the length of the reverse flow region is shortened by the spacer grid.

The influence of the size and type of the blockage, either central or corner blockage, on the reverse flow velocity is shown in Fig. 11 /24/. As indicated in this figure the reverse flow velocity is related to the mean value of the main flow velocity. It is of interest that in both cases this relation is nearly independent of the size of the blockage. This is even true for large blockages in which the reverse flow is influenced by the grid. The ratio is about 0.5 for the central blockage and 0.28 for the corner blockage.

In Fig. 10 and 11 results from other experiments are entered in addition. It follows from Fig. 10 that for fixed blockages the reverse flow region seems to be somewhat longer than for the cases of variable blockages. Figure 11 shows that the reverse flow velocity in the sodium experiments is lower, too. This dif-

ference may be due to the absence of a contraction of the main flow and the uniform velocity of the main flow in the unblocked flow area in case of variable blockage.

In a permeable blockage the wake geometry and the flow in the wake are influenced by the leakage flow through the blockage (definition of the leakage flow, see Appendix B). In Fig. 12 an example of the influence of the leakage flow on both the length of the reverse flow region and the reverse flow velocity is given for a 21% corner blockage (results from /24/). It is seen that the leakage flow greatly influences the distance between the blockage and the bottom of the recirculating flow, but has little influence on the length of the wake region (L_R). With increasing leakage flow the vortex becomes shorter and the reverse flow velocity decreases about linearly. At a leakage flow of about 11% the reverse flow ceases. This behaviour was observed for all sizes of blockages. However, the leakage flow at which the reverse flow ceases is dependent on the size of the blockage.

For the central and corner blockages the rate of leakage flow at which the reverse flow ceases is shown in Fig. 13. In both cases this leakage flow increases about linearly with the size of the blockage. Because of the higher reverse flow velocity in the central blockage case the leakage flow necessary to interrupt the reverse flow is much higher than in a corner blockage. It is important to realize these boundary conditions because blockage formation by particles always starts at high porosity corresponding to a high leakage flow.

5.3 Temperature Distribution Downstream of Impermeable Blockages

It will be anticipated here that detailed knowledge of the single phase temperature field and the parameters influencing it allows to predict the conditions for the onset of boiling and to estimate the extension of the boiling region for a variety of conditions. The temperature distribution downstream of a blockage is

determined mainly by the flow pattern and, especially, by the formation of a reverse flow region. Therefore, the temperature distribution depends directly on the parameters influencing reverse flow. Important experiments in two full bundle test sections under sodium conditions were performed /12, 13, 16/. Therefore typical temperature distributions of these two series of experiments will be discussed first.

Figure 14 shows the temperature distribution in the wake of the 49% central blockage in the more general form of normalized isotherms (see also Annex A). These isotherms are obtained from the measured radial temperature profiles (Fig. 16) under single-phase conditions close to boiling (Test 17/1, Run 20A) at an inlet flow velocity of 3.8 m/s, a pin power of 129 W/cm^2 , and an axial temperature gradient of 244 K/m. The actual temperature difference between single isotherms can be calculated by using equation (A1).

The temperature field is basically toroidal as a result of flow recirculation. The presence of the cold reverse flow in the centre of the wake causes the temperature rise in this region to be only about half the peak temperature. The peak temperature occurs some 50 mm downstream of the blockage in the region of the vortex centre. This region is located within a short distance of the main flow which causes very steep radial temperature gradients in the direction of the main flow. From the conditions at the onset of boiling a peak temperature of $\theta \approx 1.26 \text{ m}$ was derived. With the axial temperature gradient in the centre of the wake, a reverse flow velocity of about 60% of that in the undisturbed cross section of the bundle was determined.

In all the tests with the 49% central blockage the temperature distributions were found to be very similar. A pronounced influence of the test parameters was not observed. There exists, however, a little dependence upon the flow velocity and power to flow ratio. There is experimental evidence that the influence of

the flow velocity would be more significant in the absence of the spacer grids.

Figure 15 illustrates a typical temperature field in the wake of the 21% corner blockage. The normalized isotherms are obtained from measurements made at an inlet flow velocity of 4 m/s, a heat flux of 101 W/cm^2 , an inlet temperature of $397 \text{ }^\circ\text{C}$, and an axial temperature gradient of 169 K/m (see Fig. 17). The fundamental form of the temperature field is similar to that of the central blockage, i.e. a sector of a torus produced by the recirculating flow. The peak temperature lies about 40-50 mm downstream of the blockage in the region of the vortex centre. In the case of a main flow velocity of 4 m/s a normalized peak temperature of $\theta = 2.2-2.3 \text{ m}$ was determined. This is about twice that for the central blockage. Because of the higher temperatures and the shorter wake region the temperature distribution is peakier and the radial temperature gradients are steeper than those of the central blockage. A maximum reverse flow velocity of about 17% of that of the main flow velocity was determined. This is only one third of that of the central blockage.

In contrast to the 49% central blockage the temperature field behind the 21% corner blockage is dependent on the main flow velocity. With decreasing main flow velocity the temperature rise also decreases and the region of high temperature moves towards the blockage (see Fig. 18). The change in the temperature field is caused by the reduction of the length of the recirculating zone and the reverse flow velocity. The influence of the power to flow ratio was small in every case.

With these two types of blockage experiments in water were also carried out as can be seen from Table 1. The results of the water experiments /10, 15, 23/ can be well compared with those performed in sodium except for the experiments with the variable blockages.

For both fixed and variable blockages in Fig. 19 the peak temperatures in the wake versus the axial position are shown for experiments in water and in sodium performed at similar flow velocities. The experimental conditions are listed in Table 7. It follows from Fig. 19:

Fixed blockages

The general shape of the axial temperature distribution and also the amplitude and position of the maximum peak temperatures are similar in water and sodium. In the central and corner blockages the maximum lies 40 to 60 mm downstream of the blockage. The maximum temperature rise behind the corner blockage is nearly twice that of the central blockage.

Variable blockages

The temperature rise is very low compared with the two types of blockages considered before. In the corner blockage the course of the axial distribution looks similar to that with fixed blockages. The maximum arises again 40 mm downstream of the blockage. This is different in the case of the central blockage. Here the maximum lies close to the blockage.

To illustrate further the differences between fixed and variable blockages the radial temperature profiles at different measuring planes are shown in Figs. 20 and 21 for a central blockage and a corner blockage both in sodium and in water (variable blockage). In the variable blockage the strong temperature rise in the region of the vortex centre is missing. The temperature distribution is very flat without a pronounced maximum, above all for the central blockage.

To illustrate the influence of the blockage size on the temperature field the peak temperatures measured in the single measuring planes of all variable blockages investigated are shown in Figs. 22 and 23.

In case of corner blockages (Fig. 22) except for the 64% blockage, there is always a clear maximum somewhat downstream of the blockage. The distance of the maximum from the blockage increases with increasing blockage size. For the central blockage (Fig. 23) the shape of the axial distribution is similar in all cases. The temperature increases only slightly towards the blockage with a small maximum near the blockage. The size of the blockage influences only the amount of the temperature rise.

5.4 Influence of Leakage Flow through Blockages

The influence of the blockage porosity on the temperature field was investigated only in water /23, 25, 26/, firstly with a fixed 21% corner blockage (Tab. 1, blockage No. 11), and secondly with the variable blockages (Tab. 1, blockage No. 16). In both cases the leakage flow (definition see Annex B) was varied continuously over a wide range.

In most of the experiments a heat flux of about 27 W/cm^2 was used. To obtain information about the influence of the main flow velocity, different velocities were chosen, usually 3 and 4 m/s. The leakage flow was varied between zero and a value somewhat higher than the leakage flow causing dissolution of the reverse flow. A great number of experiments were carried out. From the data available only some typical data of normalized temperatures in the wake will be used in this paper to compare different experiments.

Figure 24 shows the variation of the maximum temperatures at different axial measuring planes versus the leakage flow rate for the fixed corner blockage (No. 11). The following statements which are valid only for this 21% corner blockage, can be derived from this figure:

- The reverse flow dissolves at around 7% leakage flow.
- The temperature distribution is greatly influenced by the leakage flow.

- The position of the peak temperature moves away from the blockage (35 to 55 mm) as the leakage flow is increased.
- The peak temperature remains nearly constant for leakage flow rates less than 4%.
- For leakage flow rates greater than 4% the peak temperature decreases sharply reaching about half its maximum value as the reverse flow disappears.

In Fig. 25 the influence of the leakage flow on the maximum temperature rise in the wake is shown for 33% and 49% central blockages and 21% and 37% corner blockages. These data were obtained from experiments performed in water with the variable blockages. The results from the 21% blockage discussed before are also shown. In all cases the peak temperature increases more or less with increasing leakage flow to reach a maximum. The degree of increase is strongly influenced by the type and size of the blockage. For instance, for the 21% corner blockage the maximum increase is about 10%, whereas that for the 37% corner blockage is about 100%. In case of the 49% central blockage the peak temperature increases markedly over a small range of leakage flow only. As already stated before the maximum normalized temperatures may vary considerably even for the same size of blockage, e.g. there is a factor of three between the two 21% corner blockages.

The leakage flow causing the dissolution of the reverse flow increases with increasing blockage size but depends again also on the nature of the blockage. In all experiments the leakage flow, which causes the maximum temperature rise, is about the same (mostly somewhat lower) as that one which leads to the dissolution of the reverse flow.

5.5 Maximum Temperature Rise Behind Blockages of Different Sizes

The maximum temperature rises (peak temperatures) obtained in different experiments in the wake of two blockages - the impermeable corner and central blockage types - are compared in

Fig. 26. The solid lines represent results of experiments in water involving the variable blockage, the single points mark results from earlier tests conducted in water and sodium with fixed blockages.

As discussed in the preceding chapter the temperature rises obtained in the tests with variable blockages are only 30 to 40% of those obtained in tests with fixed blockages in water and in sodium as well. This finding is valid for all series of experiments performed so far.

In case of the corner blockage (solid line) the maximum temperature rise is about twice that of the central blockage. This ratio agrees well with results from experiments with fixed blockages. In both cases there is a clear dependence of the peak temperature on the size of the blockage. The maximum temperature rise increases to a maximum with increasing blockage size. In the case of a corner blockage this maximum is reached when about 45% of the flow area is blocked whilst for the central blockage the value is 55%. Further increase in the blockage size causes a reduction in the maximum temperature rise in the wake of the blockage. This general behaviour is caused by the contrary influence of the blockage size on the extension of the wake and the recirculating flow. The extension of the wake increases with increasing blockage size causing an increase of the temperature rise. However, the velocity of the recirculating flow increases also and improves the heat transfer from the wake into the main flow.

Figures 27 and 28 show for all experiments the maximum temperature rise with and without leakage flow and its dependence on the blockage sizes and main flow velocities. In case of the central blockage (Fig. 27) the maximum temperature rise measured with respect to the related leakage flow increases with the size of the blockage up to values of about three times that without leakage flow. The results for the corner blockage (Fig. 28) are

somewhat different from those for the central blockage. Up to blockages of about 30% the peak temperature is hardly influenced by the leakage flow. For larger blockages the temperature rise with leakage flow is about a factor 1.6 higher in the maximum than that without leakage flow. In case of the corner blockage the influence of the main flow velocity is small and does not depend on the blockage size.

From the foregoing discussion and the results of chapters 4.3 and 4.4 it can be stated that different blockage configurations influence mainly the level of the temperature fields in the wake region and to a minor extent the general shape. Therefore, it seems to be justified to use the general dependence of the temperature fields, obtained from experiments in water with variable blockages, and transfer it to sodium conditions with fixed blockages of different sizes. The discussion in Chapt. 10 is based on this assumption.

5.6 Temperature Rise in the Wake under Natural Convection Conditions

The flow velocity arising under natural convection conditions will depend on the reactor design, but will be very low in any case. Tests of this kind, therefore, belong to the domain of conditions with low flow velocities. The point of interest in such experiments was to find out whether a reverse flow will exist downstream of the blockage or whether the buoyancy forces prevail causing an entirely different flow and temperature distribution. The experiments were carried out within the KNS-test series. Due to differences in the heated length, in the temperature distribution of the whole circuit, and in the effective heights for the buoyancy forces, the experimental setup is substantially different from reactor conditions in the case of natural convection. The experimental results are therefore more of a qualitative nature. Heat fluxes of 10 and 20 W/cm² were used as parameter the latter value being somewhat higher than that for the case of decay heat removal.

The main flow velocity was found to be about 0.1 m/s. In both blockage cases the temperature rise in the wake was small compared with that of forced convection (10 to 20 %) and the temperature fields were different, too. This indicates that the flow distribution in the wake had changed.

Although the result of these experiments may not be directly applied to real reactor conditions they are important, because they show that in the case of natural convection the temperature rise due to the blockage is small compared with that under normal flow.

5.7 Influence of Pin Bowing

In the sodium experiments with the central blockage the single-phase temperature distribution changed significantly after boiling tests that had been conducted in the meantime. This is due to plastic deformations of pins caused by the steep temperature gradients combined with the high temperatures during boiling. As a result of these deformations the temperature distribution in the wake depends on the power to flow ratio which was not observed prior to the boiling tests. As an example the normalized peak temperatures versus the power to flow ratio before and after boiling tests are given in Fig. 29 . However, at high values of the power to flow ratios, as needed in the boiling experiments, a difference before and after boiling experiments was not observed. Post-test examinations of the test section showed radial displacements of the pins up to 1.5 mm in the high temperature ranges /12/.

In the experiments with the corner blockages such an influence was not found. In the post-test examinations of this test section a maximum radial displacement of the pins of about 1 mm was found. This is apparently not enough to influence the temperature field significantly.

5.8 Summary of Thermal Hydraulic Phenomena in the Wake

As shown by the result presented the flow pattern and the related temperature profiles in the wake of blockages are very complex. For a better understanding of the behaviour of the wake the most relevant thermal-hydraulic phenomena will be indicated. In Fig.30 the main regions of interest are marked. In case of a fixed blockage the flow towards the blockage is diverted and accelerated to the unblocked cross-section of the lower grid spacer. This leads to a flow contraction (1) in this area and simultaneously to an additional enlargement of the blocked area. The flow leaves this part of the grid spacer as an annular jet which closes and slows down (2) by transverse flow until it reaches the second spacer grid. This jet generates the driving pressure for the reverse flow. According to Bernouilli the lowest static pressure prevails close to the lower spacer grid, the highest near the upper stagnation point. So a driving pressure builds up in the wake in the upstream direction. This driving pressure is of course superimposed by the frictional pressure loss in the main stream. The velocity in the reverse flow region is determined by the resulting driving pressure and the frictional pressure drops in the wake region. The different flow paths for the reverse flow in Fig. 30 indicate a variety of transverse flow conditions (3) through the bundle structure. This illustrates one of the difficulties in predicting the frictional pressure drop.

As a result of the special device of the test section with variable blockages (see chapters 2.2 and 4.2) there is no flow contraction in the unblocked area at blockage level but a constant velocity distribution. Nevertheless, the general hydraulic behaviour of the wake region has been found to be nearly independent of the type of blockage, fixed or variable. A minor difference exists only with respect to the observed reverse flow velocities which are about 20% higher in case of the variable blockages. However, this does not explain why the measured maximum tempera-

tures behind fixed blockages are up to 3 times higher than for variable blockages.

The temperature profiles in the wake of the blockage are influenced by the mass, momentum and heat transfer between the main stream and the wake. The dominating region for mass and heat transfer was identified to be in the mixing zone (4) between the vortex and the main flow as shown in Fig. 30. The detailed development of the radial velocity profiles should dominate the mass and heat transfers between the main flow and the wake.

From the discussed hydraulic behaviour of the flow behind variable blockages it must be anticipated that the radial velocity gradient in the mixing region (4) is much steeper than in case of the fixed blockages. A steeper velocity gradient leads to higher mass and heat transfer coefficients. This agrees well with the lower temperatures measured in the wake of variable blockages. Further observations were made in experiments concerning gas accumulation and entrainment in the wake behind blockages /24/ which support this hypothesis. For a 21% blockage (variable blockage, test section) the gas entrainment rate was found to be higher (about 3 times) than for a fixed blockage of the same size. Because the gas entrainment rate is very much related to the heat and mass transfer coefficients the latter should be higher, too, compared with the fixed blockage case.

The preceding discussion illustrates some difficulties, which are responsible for the fact that 3 D-computer codes developed to predict the flow and temperature fields behind blockages in sub-assemblies have to overcome serious problems.

5.9 Summary of Experiments Performed under Single-phase Flow Conditions

The single-phase flow pattern and temperature distribution were investigated in a wide range of blockage configurations in water and in sodium. The main parameters were the size, the type, and the porosity of the blockages. The experimental results can be summarized as follows:

Flow pattern:

- In the range investigated a quasi steady-state recirculation flow pattern was developed downstream of the blockages.
- The recirculation zone is separated radially from the main flow by a transition zone (mixing region).
- The nature of the blockage was found to have an important feedback on the mixing region.
- The axial extension of the reverse flow region is influenced by the size of the blockage, the main flow velocity and, in case of large blockages, by the next grid downstream of the blockage. The ratio of the axial extension to the radius of the blockage is similar for the corner and the central blockage.
- The ratio of the reverse flow velocity and the mean main flow velocity was found to be dependent on the type of blockage but to be nearly independent of the size of the blockage.
- The different flow paths in the wake are subject to a variety of transverse flow conditions. This is one difficulty in predicting the frictional pressure drop.
- In the case of porous blockages the leakage flow greatly influences the reverse flow region. With increasing leakage flow the reverse flow velocity decreases.

- The distance between the blockage and the bottom of the recirculating flow increases with increasing leakage flow; however, little influence is exerted on the length of the wake region.
- The leakage flow causing the dissolution of the reverse flow increases with increasing blockage size but depends again on the nature of the blockage.

Temperature field:

- The temperature field in the wake is basically toroidal in form due to flow recirculation.
- In the case of fixed planar blockages the peak temperatures lie downstream of the blockage in the region of the vortex centre.
- Different blockage configurations influence mainly the level of the temperature field; however, to a minor extent, the flow field as well.
- Generally the temperatures increase to a maximum with increasing blockage size; it is reached when 45 to 55% of the flow area is blocked. A further increase in the blockage size causes a reduction of the temperatures in the wake.
- With the same operating conditions assumed, the maximum temperature rise behind a 21 % corner blockage is nearly twice that of a central blockage of 49%.
- Results of water experiments in terms of normalized temperatures can be well compared with those obtained in sodium, but this is valid for fixed blockages only.

- The mass and heat transfers between the wake region and the main flow and the resulting temperature profiles are dominated by the details of behaviour in the mixing region, whereas the mixing region is characterized by more or less steep radial velocity gradients between the main flow and the wake.

- The structure of the blockage and the radial velocity distribution in the unblocked part of the cross section may result in a tremendous feedback upon the temperature field in the wake. In this context, a factor of up to 3 was found in the maximum temperature for the same size of blockage.

- Plastic deformation of the pins (pin bowing) during repeated boiling tests may cause a change in the single-phase temperature fields. However, pin bowing had no influence on the results of subsequent boiling tests.

- In case of leakage flow the temperatures in the wake are generally higher compared to the case without leakage flow. The maximum temperatures appear always at a leakage flow close to the dissolution of the reverse flow.

- In case of natural convection with very low velocities the temperature distribution was changed compared with forced flow and only small temperature rises were measured.

6. Experimental Results Obtained under Boiling Conditions

Boiling experiments in sodium were carried out in the two bundle test sections described in Section 2.2 (49% central blockage and 21% corner blockage). A detailed description of the experimental results is given in /13, 17/. In this report only results of experiments are discussed in which permanent dryout occurred. Before details will be presented the general course of boiling will be outlined.

6.1 General Course of Boiling

The starting conditions (flow and power) of the boiling experiments were adjusted so that the peak temperature in the wake stayed only a few degrees below the saturation temperature. Boiling was initiated either by reducing the flow or by increasing the power level. The onset of boiling was indicated by the appearance of pressure spikes caused by bubble collapse. It starts in the region of high temperatures found in the single-phase experiments. If boiling is increased by a further change of power or flow the boiling region expands corresponding to the single-phase temperature distribution, i.e. the boundary of the boiling region follows the isotherms of the temperature distribution.

At the early stages of boiling the toroidal shape of the boiling region is not completely symmetrical with respect to the centre of the wake, but at later stages in boiling development these differences disappear. The recirculating flow and the temperature distribution of the surrounding liquid are hardly influenced by the boiling region.

Two boiling regimes have been found: a steady-state boiling regime in which the vapour region remained nearly constant, and an oscillatory boiling regime in which the vapour region varied between a minimum and a maximum value. Oscillatory boiling was mainly observed mainly in the experiments with the 49% central

blockage, and steady-state boiling in those with the 21% corner blockage.

Even if the oscillatory boiling regime is dominating for most of the parameter settings a steady-state boiling regime was always observed at the early stage of boiling. These two boiling regimes were also found in the local blockage experiments carried out at ECN in Petten /30/. In the experiments listed in Tab. 8 boiling increased until somewhere in the wake cooling was interrupted, i.e. dryout occurred. This was indicated by a steep temperature rise at the heater wall above the saturation temperature.

From thermocouple signals two kinds of dryout have to be distinguished. In the first case the temperature rises sharply above the saturation temperature, but falls again steeply after about 100 ms so that the peak clad temperature increase is of the order of 10 K. This is interpreted as the occurrence of a local dry patch on the pin which is rewetted after a short time; it is called here brief dryout.

In the second case the temperature rises steeply to the trip level (1000°C) of the pin protection system which trips the power to the pin. In this case it is assumed that the limits of pin cooling have been reached and the event is called permanent dryout.

For the two blockage cases the main parameters of experiments in which permanent dryout conditions were reached are listed in Tab. 8. This table includes also some experimental results which will be used in Section 7. The so-called excess temperature as defined in Annex A is used as a measure to characterize the degree of boiling and for comparing the various boiling experiments.

In the following sections some selected experiments, representing the two boiling regimes, will be described in more detail:

6.2 Oscillatory Boiling

To explain the oscillatory boiling behaviour mainly the results of test 32/2, run 58A to 58E, will be used. In this test boiling was initiated and intensified by a stepwise flow reduction until, finally, permanent dryout occurred. The pin power was kept constant. Typical boiling signals (temperature, void, pressure, flow and vapour volume) of each step of this test are given in Annex D. In Fig. 31 boiling signals are shown which were recorded in the last step (run 58E) during the time interval just before power switch off by dryout. The curves are marked with the number of the measuring point to identify the location. For instance, 7.10/120 is installed on the heater pin 7.10 (see Fig. 7) 120 mm downstream of the blockage. In the top part of Fig. 31 the amplitude of the temperature signal is found to be about 70 K at a frequency of about 5 Hz. This thermocouple is located downstream of the boiling region and it reveals a oscillating motion of the liquid in this region. Because of the temperature gradient in the liquid this temperature increases when the boiling region expands and reaches its maximum value at the time of maximum vapour volume.

The amplitude of the temperature (TC 12.6/40) measured in the heater wall corresponds well to the measured pressure oscillation in this region (P830, 3rd diagr. from bottom). However, the response time of the thermocouples embedded in the heater wall, compared to the pressure measurement, causes the amplitude of the measured temperature to be somewhat smaller and to have a small phase shift. From the fact that the temperature of the heater wall follows the amplitude of the saturation temperature it can be concluded that there is only a thin film of evaporating sodium left on the pin surface.

The 3rd diagram from top in Fig. 31 illustrates the dryout behaviour under oscillatory boiling conditions. The thermocouple is located in the same pin as in the diagram above, but nearer to

the blockage. The onset of dryout during each cycle occurs when the vapour volume is approaching its maximum value. Rewetting occurs as the vapour volume approaches its minimum value. It is observed that at the position of thermocouple 12.6/20 the time of rewetting eventually becomes too short to cool the clad down to the saturation temperature, and the peak temperature reached in successive cycles increases until the threshold of high temperature surveillance is surpassed and the power tripped. This event is called permanent dryout. It is evidently a local condition since at other thermocouple positions dryout with rewetting is still possible.

The void signal (V9.10/40) shows clearly the movement of the boiling region. At minimum vapour volume the signal reaches the base level indicating that the measuring point is completely immersed in liquid sodium during this period. As dryout conditions are approached this interval becomes shorter and shorter and finally disappears before the power is tripped by the high temperature surveillance system.

The flowmeter inlet and outlet signals, which are also shown in the figure, exhibit large sinusoidal variations. These are larger for the outlet flow as the outlet liquid column offers less inertial and frictional resistance to flow changes. The variations of vapour volume may be calculated by integrating the difference between the flowmeter signals. This provides an accurate measure of the amplitude of the vapour volume oscillations. However, vapour volume in the boiling region cannot be determined by this method, because the zero level of the vapour volume drifts over the time.

To illustrate the development of the oscillating boiling pattern the amplitude of the oscillatory vapour volume ΔV_v and the frequency are shown versus the normalized excess temperature in Fig. 32. The amplitudes were deduced from the flowmeter signals. The oscillating boiling pattern is first observed at an excess

temperature of $\Delta \theta_e = 0.15$ and 0.22 m, respectively. Below these values steady-state boiling prevails. The magnitude of the vapour volume oscillations depends on the boiling intensity in terms of the normalized excess temperature. The amplitudes of test series 32/1-2 with higher power are larger than those of series 17/1-2. However, under conditions of dryout the amplitudes are not very different. The frequency of the oscillation decreases from about 10 Hz near the onset of oscillations to a constant value of about 5 Hz for large amplitudes. The boiling behaviour, especially the transition from steady-state to oscillatory boiling, may be explained as follows /31/. When the boiling intensity and hence the size of the boiling region are increased, a point is reached at which the modified flow and temperature fields in the surrounding liquid can no longer sustain the increasing boundary heat flux required. A thermal balance becomes impossible under steady-state conditions. As a result, the boiling region grows creating more condensation surface than required to sustain the boundary heat flux. This leads to a subsequent contraction, thus initiating the oscillating motion which is governed by the need of preserving a thermal balance on average.

It is reasonable to assume that the amplitude of the oscillating motion increases steadily for conditions beyond the transition point from steady-state to oscillatory boiling. It is also to be expected that the transition conditions should be geometry dependent, as observed, since the geometry defines the flow/temperature field. Aside from the condition discussed above, the dynamic characteristics of the system have to be included to reproduce the pattern of development of the oscillation frequency and amplitude. It has been established /32/ that the periodic flow and pressure signals recorded during oscillatory boiling are consistent with the one-dimensional equations of motion of the inlet and outlet liquid columns of the KNS loop.

As an example of the development of the boiling region the max.

and min. boundaries from two runs of experiment 32/2 are reproduced in Fig. 33, run 58C, in which the first brief dryouts were observed, and run 58E in which permanent dryout occurred. The normalized excess temperatures were about 0.55 m and 0.61 m (312 K and 378 K), respectively. These boundaries are deduced from the thermocouple and void detection signals. The positions where dryout occurred are also indicated.

Although in run 58C the reverse flow path is partly constricted by the boiling region it remains open during all the oscillation cycles. In run 58E the main mass flow is 10% less than in run 58C which approximately doubles the size of the boiling region. In both runs the volume of the minimum boiling region is about 40% of that of the maximum. In run 58E the maximum and minimum boiling regions also include the centre of the wake; thus, the reverse flow is probably cut and finally causes the onset of a permanent local dryout. In this run one permanent and many brief dryouts were observed at many locations, but all within the minimum boiling region.

6.3 Steady-state Boiling

The steady-state boiling behaviour is very different from the oscillating boiling behaviour. The steady-state boiling pattern was found mainly in the experiments with the 21% corner blockage but also in some experiments with the 49% central blockage under low flow conditions ($v_0 \leq 1.5$ m/s). The typical behaviour during steady-state boiling is demonstrated by the results of experiment 216/2 with the corner blockage. In this experiment the pin power was increased in eight steps (run No. 478 to run NO. 485) from 62 to 107 W/cm^2 . In the last run a heater failed due to permanent dryout. The whole course of this test is given in Annex D.

Some typical signals recorded during run No. 485 just before power switchoff are shown in Fig. 34. The curves are marked in analogy to those in Fig. 31. None of the signals shows regular

oscillation. In the upper diagram the temperature, which was measured outside of the boiling region, shows a fluctuation with a maximum amplitude of about 25 K. This reveals that only small motions take place of the liquid vapour interface in this region. The temperatures reproduced in the second and third diagrams from top were measured inside the boiling region 50 and 30 mm downstream of the blockage. Both indicate a nearly constant saturation temperature in the boiling region and irregular temperature spikes above the saturation temperature. These are caused by local dryouts with rewetting after a short period of time. The temperature rise is about 40 K within 50 to 200 ms. Although this cannot be interpreted as a permanent dryout about 1 s later a heater failed without any change in the experimental conditions preceding this event. This heater was not instrumented so that dryout was not detectable.

Cooling in the boiling region seems to be disturbed irregularly by the occurrence of local dry patches with subsequent rewetting. It is observed that the onset of dry patches together with the highest temperatures are concentrated in the region of highest temperature which are deduced from the single-phase temperature field (e.g. Fig. 15). The void detector V11.2/50 located within the boiling region indicates the presence of liquid and vapour in an irregular sequence. The time intervals during which liquid is present are smaller than those when vapour was indicated. The pressure signal P828, third diagram from bottom, shows a fluctuation of about 0.05 bar without any specific frequencies dominating. The inlet and outlet flowmeter signals, first and second diagram from the bottom of Fig. 31, reflect small fluctuations, which are not very different from those without boiling.

In Fig. 35 the boiling regions are reproduced of run No.482, $\Delta \theta_e \approx 0.68$ m (147 K), and run No. 485, $\Delta \theta_e \approx 0.91$ m (229 K). The boiling volumes for run 482 and 485 were estimated at 48 cm³ and 67 cm³, respectively. The shape of the boundaries of the boiling region is similar to that of the isotherms in single-

phase temperature fields (Fig. 15). Run 482 shows the first appearance of brief dryout. The locations are also indicated. This distribution of dry patches with rewetting (brief dryout) was observed in most of the experiments. Brief dryouts appeared under much less intense boiling conditions than necessary for the onset of permanent dryout.

The general boiling behaviour in other experiments is similar to that in experiment 216/2. There is, however, an influence of the flow rate. At low flow rates ($v_0 = 2$ m/s) the boiling region reached the wall in the corner of the blockage before permanent dryout occurred. Under this condition the reverse flow is likely to be restricted and the actual boiling volumes become larger than that determined from the single-phase temperature field.

In experiment 224/3 with a flow rate of about 4 m/s steady-state boiling changed gradually to oscillatory boiling as soon as an excess temperature of $\Delta \theta_e = 0.7$ m was exceeded. The oscillating frequency was about 7 to 8 Hz and the maximum amplitude of the vapour oscillations about 20 cm^3 . The oscillatory motion of the boiling region improved cooling of the pins so that fewer brief dryouts appeared after the transition. Typical boiling signals of test 224/3 which show the transition to oscillatory boiling are given in Annex D.

6.4 Comparison of Measured and Estimated Boiling Regions

In Section 5.3 it was mentioned that the single-phase temperature distribution behind a wake can be used to predict the onset of boiling and with some restrictions the size and volume of the boiling region for a variety of conditions.

For the latter the single-phase temperature distribution in the form of normalized isotherms and the normalized excess temperature are used. The value of the normalized isotherm which should determine the boundary of the boiling region is calculated as the

difference from the normalized peak temperature in the wake and the normalized excess temperature, $\theta_i = \hat{\theta} - \Delta \theta_e$. This kind of determination is based on the assumption that the general temperature distribution does not change by the occurrence of boiling. As an example the boiling region of run 485 (see Fig. 35) will be estimated from the single-phase temperature field given in Fig. 15. With a peak temperature of 2.2 m and an excess temperature of about 0.9 m the isotherm representing the boundary conditions is $\theta_i = 1.3$ m. The next isotherm in Fig. 15 is 1.4 m and the region surrounded by this isotherm is therefore somewhat smaller than the boiling region in Fig. 35; however, it looks similar.

In Fig. 36 the minimum and maximum areas of the boiling regions determined from all runs of the two test series 17/1-3 and 32/1-2 for the central blockage with oscillatory boiling are compared with those estimated from the single-phase temperature distributions (solid line). The main difference in these series is the pin power which is 135 W/cm² in series 17 and 170 W/cm² in series 32. The experimental values of the test series 17/1-3 are considerably lower than predicted from the single-phase conditions. This result reveals an improved heat removal from the wake in oscillatory boiling due to the large motions of the wake fluid which do not occur under single-phase and steady-state boiling conditions. The maximum areas of test series 32/1-2 are close to those predicted, except for the value obtained under conditions of permanent dryout. In the latter case the maximum boiling region is larger than predicted. However, the areas of the regions of average or minimum values are again smaller, i.e. with some restriction made, the improved heat removal by oscillatory boiling holds also for test series 32/1-2. The size of the boiling region and the amplitude are approximately proportional to the normalized excess temperature, except for the dryout conditions. From the results shown in Fig. 36 it may be concluded that the boiling behaviour is markedly influenced by the pin power.

From the results of the experiments with the corner blockage in Fig. 37 the measured cross-section areas of the boiling regions together with those derived from single-phase isotherms (solid lines) are plotted against the normalized excess temperature. The area is defined as an axis symmetrical section through the blockage. In this figure the results of the boiling experiments for two inlet flow rates are shown as single points. For a sodium velocity of 4 m/s the areas of the boiling regions agree well with that derived from single-phase isotherms. For a sodium velocity of 2 m/s the cross-sectional areas agree well for normalized excess temperatures $\Delta \theta_e$ below 0.5 m. For larger values as explained above, the boiling region reached the wall in the corner of the blockage causing a deterioration in the cooling conditions. Nevertheless, the single-phase temperature distribution behind a blockage may be successfully used to estimate the size of the boiling region under steady-state boiling conditions. The volumes of the boiling regions used in Chapter 10 are estimated in a way similar to that explained before.

6.5 Experimental Conditions at the Onset of Dryout

As can be seen from Tab. 8 the experimental conditions are widely spread. Therefore, it is difficult to identify the influence of single parameters and to compare the dryout conditions of different experiments. During the experiments these difficulties still increased due to failures of heaters (see Tab. 8). To illustrate the dryout behaviour the excess temperatures of all experiments with permanent dryout are reproduced in Fig. 38 together with the boiling regimes observed. The flow, the power and the inlet temperatures are given, too. For the cases of central and wall blockages the following general behaviour can be deduced from the experiments:

49% Central blockage

Oscillatory boiling was prevailing. Steady-state boiling occurred only in the early stage of boiling with excess

temperatures $T_e < 50$ K and with low main flow velocities, $v_o < 1,5$ m/s. In the case of oscillatory boiling excess temperatures of $\Delta T_e \approx 330 - 430$ K were reached at the onset of permanent dryout. Brief dryouts were observed only just before the onset of permanent dryout.

In the experiments with steady-state boiling, $v_o < 1,5$ m/s, permanent dryout occurred already at excess temperatures of $\Delta T_e < 100$ K.

21% Corner blockage

In case of the corner blockage steady-state boiling was prevailing. Oscillatory boiling was observed in test 224/3 only. Permanent dryout occurred at excess temperatures of $\Delta T_e \approx 200$ K which is about half the value applicable to the central blockage and oscillatory boiling. Brief dryouts were observed much earlier than permanent dryout ($\Delta T_e \approx 50$ K). As soon as the boiling regime changed from steady-state to oscillatory boiling (test 224/3) much higher excess temperatures ($\Delta T_e \approx 330$ K) were reached until permanent dryout occurred than in the tests with steady-state boiling.

The dryout conditions certainly depend on the extension of the boiling regions and the local vapour velocities. Therefore, in Tab. 9 some characteristic data necessary to calculate vapour flow velocities are listed for each run in which dryout occurred. These data are: volume, boundary surface and axial extension of the boiling region, whereas the volume and surface include the pins. For oscillatory boiling the max. and the min. values are given.

The actual vapour velocities cannot be calculated without detailed knowledge of the turbulent thermal conductivity in the liquid adjacent to the condensation boundary. Therefore, two boundary vapour velocities, a radial and an axial one, have been calculated. For the radial velocity a uniform vapour flow to the

boundary surface (S_B of the boiling region) is assumed. This velocity is related to the gap between the last row of pins in the boiling region (v_{vR}) and is therefore about a factor 4 higher than the uniform velocity.

For the axial velocity it is assumed that there is only axial vapour flow, although in both directions, i.e. to the top and bottom of the boiling zone boundary. The length L_B are used to calculate the axial vapour velocities (v_{vA} in Tab. 9).

In the experiments with oscillatory boiling the mean value between the maximum and minimum is used for the calculation. In most of the experiments the axial flow velocity is about twice that of the radial one. In the experiments with oscillatory boiling both velocities are distinctly higher than those with steady-state boiling, except for the experiments 17/3 and 43/2. In spite of the scatter of values between the experiments these two velocities seem to be suitable as a measure for comparing different experiments. Furthermore, the vapour flow velocity must apparently stay within certain limits to avoid the onset of permanent dryout.

6.6 Summary of Boiling Tests

The KNS local boiling experiments as well as the experiments performed at ECN with two 60° bundle sections (K.J. Brinkmann et al. /30/) have revealed two boiling regimes with different dryout margins. At low boiling intensities boiling is steady-state, but a transition to oscillatory boiling occurs under conditions which are sensitive mainly to the bundle- and loop hydraulics and to blockage size and location. The margins between the conditions leading to the local onset of boiling and finally, to the onset of dryout are smaller for steady-state boiling than for the oscillatory boiling pattern. But in every case there is a distinct margin between the onset of boiling and the onset of dryout.

The knowledge of the single-phase temperature distribution and its dependence on the flow velocity and pin power allows an estimation to be made of the extension of the boiling region for a variety of boiling conditions. This means that reliable temperature and flow fields calculated with a well verified 3-D single-phase code constitute a sound basis to estimate the boiling regions to be anticipated behind different planar blockages without requiring further experiments. In steady-state boiling, the size of the boiling region can well be estimated from the single-phase temperature distribution. In oscillatory boiling extra cooling leads to smaller mean vapour volumes; however, a conservative upper limit can still be deduced from the single-phase temperature distribution.

The results from the two boiling experiments with the 49 % central and the 21 % corner blockages can be summarized as follows:

The boiling regimes, as explained before, are different for the two blockages, if normal operating velocity in the subassembly is assumed.

For the 49 % central blockage at flow rates of $1.5 < v_0 < 2$ m/s oscillating boiling is dominating. The margin between the start of boiling and the onset of dryout in oscillatory boiling corresponds to a 100 % increase of the power/flow ratio. This results in a rather high excess temperature (defined in Annex A) at the onset of permanent dryout.

At low flow rates ($\leq 1,5$ m/s) rapid development of the boiling region into a steady-state vapour cavity results in a small dryout margin (≈ 20 % increase in power/flow ratio) between the start of boiling and the onset of dryout.

The volume of pins at risk of melting at the onset of permanent dryout is estimated to be in the range of 50 to 100 cm³.

For the 21 % corner blockage the generally observed boiling pattern is steady-state. The margin between the onset of boiling and permanent dryout lies in a range corresponding to a 40 - 60 % increase in the power/flow ratio. However, brief dryout occurs much earlier. The excess temperature is only half that for the 49 % central blockage. This illustrates that the oscillating boiling regime is more efficient. The volume of pins at risk of melting is estimated to be in the range of 15 to 50 cm³.

Under normal SNR 300 Mk 1a operational power/flow conditions local boiling would occur only behind the 21 % corner blockage, but not behind the 49 % central blockage of the two types investigated.

With reference to the KfK and ENC local blockage experiments a transition to cross boiling in the subassembly can be excluded, which would constitute a necessary condition for a fast propagation of a local cooling disturbance into a subassembly fault. This consideration does not include the build up of a secondary blockage by a meltout of the first one after the occurrence of dryout. In case of the ECN experiments the most severe conditions were simulated by a 70 % blockage in a bundle section with all pins heated. The subcooled bulk flow appears to be hardly affected by local boiling of the coolant behind planar blockages.

7. Discussion of Dryout Conditions

The onset of local dryout with preceding intense boiling is attributed to an insufficient liquid sodium supply into the voided region. This means that more liquid sodium is vapourized than is fed to the heater walls locally. A transition to film boiling (critical heat flux) with subsequent dryout can be excluded because the specific heat fluxes applied are much below the critical heat flux. Heat fluxes nearly one order of magnitude higher would be needed, (R.C. Noyes /33/, Orrington, E. Dwyer /34/). The complex physical nature of boiling regions behind blockages makes it impossible to predict quantitatively the boiling behaviour and especially the onset of permanent dryout by application of suitable physical models. However, an attempt was made to find the governing physical parameters influencing the observed behaviour. In the next section the liquid supply mechanism will be considered; the vapour flow will be treated in the subsequent section.

7.1 Mechanisms of Liquid Supply to the Boiling Zones

General information of liquid supply to the voided region is drawn from different flow visualization experiments in water with fixed and variable blockages /20, 24/. In these experiments the void was generated by injection of gas into the wake. When the critical injection rate (see Chapter 8) was exceeded a gas voided region existed in the wake. By choice of the injection rate the size of the void could be adapted to that found in boiling experiments with permanent dryout. It was observed that a water film was draining down the pins (see Figure 39). The liquid-gas interface was not steady-state but subject to some random movement, especially in region "A" of Fig. 39. Waves were observed to move down the liquid film on the pins. It will be shown later that the injection rate is rather low in order to compensate the gas entrainment; therefore, the influence of gas velocity in the void can be neglected (see also Chapt. 8).

Two important mechanisms of liquid sodium supply into the voided zone shall be considered in detail:

- Draining film down the pins.
- Restoration of the sodium film by oscillation of the boiling zone or local fluctuations of the liquid-vapour-interface.

Draining film down the pins

There are two major forces supporting the liquid to enter into the void:

- Impingement of the liquid or two-phase stream on the pin surface.
- Gravity and, to some extent, pressure difference between top and bottom of the wake.

Clare has shown /27, 31/ that at the point of impingement (Fig. 36, region B) of the liquid stream on a pin surface at the void boundary conservation of momentum implies a significant momentum flux of liquid along the pin into the void. Liquid entering at the top will be further accelerated by gravity, whilst liquid entering from below will be rapidly decelerated and penetration is therefore very small (≈ 1 cm). This means of liquid supply into a gas void was observed and its magnitude investigated by Clare and Board /35/. Their experiments in water with pins of a size similar to those of interest here suggest that a liquid supply rate of about $1-3 \text{ cm}^3\text{s}^{-1}$ per pin may be expected at coolant flow rates at the void boundary in the range of 2-4 m/s.

It may be stated that this supply mechanism would call for a dryout limit much higher than that observed. Therefore, to explain the onset of permanent dryout additional effects, e.g. the superimposed vapour flow have to be included.

Restoration of the sodium film by movement of the liquid- vapour- interface

As outlined in Section 6.2, there exists an oscillatory form of boiling. The boiling zone varies between a minimum and a maximum value. Under these conditions the removal of heat from the wake by boiling is higher than in every other case observed under steady-state boiling conditions. In the major part of the boiling zone a vapour-liquid interface passes back and forth at a frequency of 5-7 Hz always restoring the liquid film on the pins.

It can easily be estimated that a film of 0.1 mm thickness is sufficient to account for pin cooling by evaporation within the period considered. A film thickness of this size is left behind a moving liquid vapour interface, H. Kottowski /36/, A.J. Brook et al. /37/.

The boiling zone, however, does not collapse completely. There is always a minimum boiling zone left (see Fig. 36). It was found from the experiments that dryout starts within this minimum boiling zone. Therefore, the conditions for the onset of dryout are controlled by the supply mechanism of liquid into the minimum boiling zone and the competing mechanism of entrainment. In the case of steady-state boiling it is likely that there are also dynamic effects superimposed to the steady-state behaviour. For example, very local fluctuations of the liquid-vapour interface, as deduced from the measured characteristic of temperature and void signals, may cause an additional liquid supply to the row of pins close to the interface.

7.2 Dryout Mechanisms

In the previous section it was seen that liquid, which enters the void, by whatever mechanism, is likely to form draining films on the pins which are able to dissipate heat by evaporating liquid.

The quantity of liquid alone was estimated to be so large, that the conditions observed for the onset of permanent dryout cannot be explained unless other limiting conditions are included like the influence of the vapour flow which may vary between counter-current and perpendicular to the draining film. Therefore, the influence of an axial vapour counterflow on the draining liquid film will be estimated next. Earlier experiments (A. Kaiser et al /38/, W. Pepler /39/) in sodium-cooled bundle test-sections, which were completely blocked at the inlet, were performed to measure the remaining decay heat removal capacity. Under these conditions cooling was effected by a draining film along the pins from the top being driven by gravity alone. The film evaporated nearly completely during draining giving rise to a vapour flow countercurrent to the draining film. The experimental results were reproduced by a simple model /39/ calculating the film mass flow with counter vapour flow for the cross-section close to the upper liquid vapour interface in the vapour region.

This model was applied to the tests listed in Table 9 and the ECN tests /40 p. 85/. The model predicts a maximum vapour velocity in the critical cross-section of about 29 m/s at a saturation pressure of about 1.5 bar. This is about 30 % higher compared to the values estimated from the experiments listed in the last column of Tab. 9. In other terms, the model predicts a 30 % too high heat flux at which permanent dryout would occur first. The sodium film thickness and velocity at the cross-section of entrance into the voided region was also estimated with the model to be 0.36 mm at an average film velocity of 0.05 m/s.

However, it has to be kept in mind that the boiling region is surrounded by condensation surfaces, i.e. the local vapour velocities must have axial and radial components as well. Assuming radial flow only the velocities related to the row of pins close to the interface of the voided region are listed in the next to the last column of Table 9. These values are only about half those with axial flow assumed. Clare /13/ also considered the

possibility of liquid entrainment under cross flow conditions. From an experiment with gas and water it is estimated that a vapour cross flow of 15 m/s would be needed to start entrainment. The values from the experiments in the range of dryout conditions are generally lower than 15 m/s. Therefore, entrainment does not seem to be very likely.

The preceding considerations are valid only under steady-state conditions. However, this does not correspond to the experimental evidence. In the boiling process always oscillations or at least local fluctuations of the liquid-vapour interface are involved. During these periodically local vapour velocities much higher velocities may arise than the average values reported. Therefore, entrainment in the pin rows close to the interface cannot be ruled out completely.

The considerations concerning dryout will be summarized as follows:

The simple model based on axial flow seems to reproduce rather well the experimental values with respect to the onset of dryout if the calculated values are lowered by about 30 %. So, the model may be used to estimate the dryout conditions behind a wake based on a known temperature field under single-phase conditions (see also Chapt. 5). It must be kept in mind, however, that the real physical behaviour of the boiling region is much more complex and that several feeding and entrainment mechanisms may exist which are superimposed.

8. Experiments with Gas Injection

Due to the possibility of pin failure combined with fission gas release into the recirculating zone behind the blockage, the behaviour of gas and its influence on cooling of this zone were investigated in water (Fukuzawa /20/) and in sodium (F. Huber et. al. /18/). In these experiments the following aspects were studied with respect to the influence of gas:

- Behaviour of gas in the wake.
- Effects on the temperature distribution
- Effects on local boiling.

8.1 General Behaviour of Gas in the Wake

In order to establish the behaviour of gas in the recirculation zone, tests were carried out with and without power. The main parameters were the inlet flow velocity, the gas injection rate, and the position of gas injection. Gas was injected both into the recirculating flow and into the main flow upstream of the blockage. In the case of gas injection into the main flow only part of the injected gas is transported into the recirculating flow region by the mass exchange between the main flow and the recirculating flow.

In the water experiments the behaviour of injected gas was observed directly through the window (see Fig. 4) and recorded by high-speed cine photography (see Chapt. 4.4). In the sodium experiments the information about the gas distribution was obtained from the void detectors and the influence of the gas on cooling from the temperature measurements.

The main result of the experiments is that under specified conditions the injected gas collects in the recirculating zone leading to a gas cavity which may occupy almost the whole recirculating zone.

Figure 40 illustrates exemplary gas accumulation found in the water experiments for the 21 % corner blockage and the 49 % central blockage. In these cases nearly the whole recirculating zone was voided. It is obvious that in such a case cooling of the wake is disturbed considerably.

For a given blockage the main parameters influencing gas accumulation are the gas injection rate and the main flow velocity. They will be treated in detail in the following paragraphs.

8.2 Conditions Leading to Gas Accumulation

All experiments, in water and in sodium /14, 18, 20, 24/ as well, showed same general behaviour under conditions of gas accumulation. These are:

- Below a minimum main flow velocity gas does not accumulate.
- At flow velocities higher than this threshold the gas rate necessary to produce gas accumulation increases exponentially with increasing main flow velocity.

As an example of this behaviour Fig. 41 shows the conditions under which gas accumulates for the 21 % impermeable corner blockage in sodium. The gas was injected into the recirculating zone. The gas accumulates in the hatched region. In this case the minimum main flow velocity is about 2.2 m/s and the minimum gas injection rate about 3 cm³/s.

Generally it was found that the minimum main flow velocity is dependent on the type and size of the blockage but nearly independent of the gas injection rate and the position of injection.

It was observed that in the water experiments /20/ at main flow velocities lower than the minimum velocity the gas bubbles rise up through the wake due to buoyancy without forming a gas cavity.

Since the behaviour of gas in the wake certainly depends more on the recirculating flow than on the main flow the reverse flow velocity is used for comparison. In Fig. 42 the minimum reverse flow velocities found in different experiments are entered. In all experiments the minimum reverse flow velocities are similar and nearly independent of the size and type of the blockage. The mean value is $v_{Rmin}=0.55$ m/s.

This minimum flow velocity below which there is no gas accumulation can be explained physically. The reverse flow velocity in the recirculating flow has to be at least of the same size as the rising velocity of the gas bubbles due to buoyancy; otherwise the gas bubbles disappear downstream without the possibility to collect. At reverse flow velocities higher than the rising velocity gas bubbles are transported towards the blockage and reach the wake center by centripetal forces. There a gas cavity is formed.

This general behaviour is also valid in the case of permeable blockages in which the reverse flow velocity is influenced by the leakage flow through the blockage (see Fig. 12). The boundary conditions concerning the minimum main flow velocity have been calculated as outlined in Annex C. The dependence of this velocity on the size of the blockage was determined for the two types of blockages with the leakage flow through the blockage as the parameter. These results show that in the case of porous blockages the field of conditions for gas accumulation is as smaller as the leakage flow will be.

The gas injection rate which is necessary for gas accumulation increases exponentially with increasing main flow as can be seen in Fig. 41. This can be explained by entrainment of gas bubbles from the cavity into the main flow. To describe this behaviour Fukuzawa /41/ developed a semiempirical model based on the assumption that gas bubbles are entrained into the main flow due to pressure fluctuations and turbulences on the surface of the gas

cavity. Since the entrainment rate increases with increasing main flow velocity a correspondingly increasing gas injection rate is needed to maintain gas accumulation. This behaviour explains also why the residence time (time from the termination of gas injection to the disappearance of the cavity) decreases with increasing main flow.

Whenever the conditions for gas accumulation are given, the extension of the gas cavity and the region of cooling disturbance are of interest. In the experiments it was observed that the size of the gas cavity depends again on both the main flow velocity and the gas injection rate. It increases with increasing gas injection rate and decreases with increasing main flow velocity. As an example the dependence of the cavity size on the main flow velocity is shown in Fig. 43 for various gas injection rates (injection into the wake or main flow). The results are obtained from experiments in water /20/ with a 21 % impermeable corner blockage. The largest gas cavity was found at a main flow velocity near the threshold for cavity formation. As shown in Fig. 40, the cavity may occupy the whole wake under these conditions.

The time to build up a gas cavity is dependent on both the injection rate and the main flow velocity. In the experiments values of about one to few seconds were found.

In the experiments with a permeable blockage /21/ it was found that with increasing leakage flow

- the minimum main flow velocity increases because the reverse flow is reduced by the leakage flow;
- the size of the cavity decreases as a result of the shortened length of the reverse flow region;
- the residence time hardly changes.

To simulate a sudden fission gas release caused by pin failure some experiments were carried out in which gas was injected in short pulses with constant flow rate or with release characteri-

stics (decreasing flow rate). From these experiments two boundary conditions were derived:

- An accumulation will take place if the injection rate is higher than the minimum rate known from the experiments involving continuous injection.
- The time of accumulation corresponds to the residence time after termination of the injection rate also known from experiments involving continuous injection.
- At a given injection rate the injection time evidently must be sufficiently long to deliver the quantity of gas necessary to build up the cavity.

With the information found in the experiments, especially the boundary conditions, it is possible to estimate whether an accumulation will take place and what extension it will have, provided the flow conditions are known experimentally or theoretically.

8.3 Influence of Gas on Cooling

The influence of gas on cooling of the wake was investigated under single-phase conditions with low and high power levels and under boiling conditions /12-14, 17, 18/. In these experiments gas was injected continuously and in the form of gas pulses. The gas injection rate and the main flow velocity were varied in a wide range of conditions with and without gas accumulation. The degree and the extension of the cooling disturbance were derived from the temperature measurements.

An important result of these experiments is that under conditions not leading to gas accumulation the temperature field in the wake was only slightly influenced, partly increased and partly decreased. This behaviour was found under single-phase and boiling conditions. In the experiments with gas cavity formation cooling of this region was disturbed markedly and interrupted in most cases.

As described in Sect. 7.1 a liquid film is draining down the pins within the voided region caused by boiling or gas accumulation. If the liquid mass flow of this draining film is sufficient to remove the heat generated the temperature will only increase until a new equilibrium is reached. This phenomenon is confined to low powers and small cavities.

In the experiments with high power and cavities comparable with those of the boiling experiments the temperature rose continuously to the saturation temperature, finally causing local dryouts. As an example, in Fig. 44 a temperature signal is shown of an experiment with the 49 % central blockage. The pin power was 135 W/cm^2 and the main flow velocity 2.8 m/s . Gas was injected into the main flow. Before the gas injection the peak temperature was about 850° C . One second after injection the temperature increased nearly continuously to the saturation temperature. There it stayed for a time interval of about 0.3 s until, due to dryout, the temperature rose further leading to a power trip. Other temperature signals from measuring points within the gas cavity showed a similar behaviour. From these results it is supposed that with cavity sizes and pin powers comparable with those under boiling conditions local dryout will occur.

The extension of the region with disturbed cooling was investigated in low power experiments because with high power the power had to be switched off immediately after a local dryout occurred somewhere in the disturbed region. As an example, Fig. 46 shows the region with disturbed cooling in the case of the 21 % corner blockage for different gas injection rates. In this case the power was only 5 W/cm^2 . With high power local dryout would occur in every case. From this figure it is clear that the region with disturbed cooling is comparable with the size of the boiling region.

A typical result of an experiment with pulswise gas injection and release characteristics is shown in Fig. 45. In this case cooling

was interrupted locally for about 10 s. The volume of the gas tank was 14 cm^3 and the pressure 22.5 bar.

Boiling experiments with gas injections were carried out with the 49 % central and 21 % corner blockages. The main parameters were: the main flow velocity, the boiling intensity, and the gas injection rate. In all cases boiling conditions were chosen so that dryout was not to be expected without gas injection. The injection rate was increased stepwise close to the boundary conditions of gas accumulation. In the experiments the following phenomena were observed:

- Gas injection rates well away from the conditions of accumulation hardly influenced the boiling region and the boiling behaviour. In the experiments with the 21 % corner blockage the boiling intensity was even reduced at such injection rates.
- Gas injection rates close to or above the minimum conditions for accumulation generally led to an increase of the boiling region and in most experiments to permanent dryout. This behaviour was similar for both blockages.
- In the case of the 49 % central blockage the oscillations became irregular and much smaller in amplitude; as a result brief dryout occurred earlier.

The effects of gas in bundles with local blockages were also investigated by K. Haga et.al /56/ using wire and grid spaced bundles with different planar blockages. Generally their results are similar. In the case of wire spacer the temperature rise was somewhat higher than that with grid spacer.

8.4 Summary of Tests with Gas Injection

To investigate the influence of gas cooling experiments with gas injection were carried out under single-phase and boiling conditions. The main results can be summarized as follows:

Single-phase conditions

- Under specified conditions gas injected into the coolant accumulates in the recirculating zone and forms a gas cavity.
- For a given blockage the main parameters influencing the condition are: the main and the reverse flow velocities, the location of the gas injection, and the injection rate.
- Below a minimum reverse flow velocity equivalent to the velocity of gas bubble rise due to buoyancy gas accumulation does not take place independent of the injection rate and the type of the blockage.
- A gas cavity can occupy almost the whole recirculating zone.
- The time from the termination of gas injection to the dissolution of the cavity by gas entrainment depends on the main flow velocity. It can last for a few seconds.
- Gas not leading to an accumulation does not have a significant influence on the temperature field.
- In the case of gas accumulation cooling in the voided region is disturbed considerably. Dependent on the size of the voided region dryout can occur.

Boiling conditions

- Gas injection rates well away from the conditions of accumulation hardly influenced the boiling region and the boiling behaviour.
- Gas injection rates close to or corresponding to conditions of accumulation generally led to an increase of the boiling region and in most experiments to permanent dryout.

9. Comparison of Experiments with 3-D Code Calculations

The temperature distribution downstream of blockages is of great importance for the definition of the starting conditions for subsequent failure propagation in a subassembly. Several codes have been developed which are capable of predicting for a variety of blockages the single-phase flow and temperature distribution in the wake. Some of these codes are: SABRE (UK), ASFRE (Japan), CAFCA (France) and BACCHUS (French-German cooperation).

The basic features of the codes are rather different: SABRE and ASFRE are three-dimensional subchannel codes whereas BACCHUS and CAFCA are porous body codes. Details on the codes have been published elsewhere /42-47/.

In the frame work of collaboration between KfK and UKAEA some of the experiments in sodium (49 % central blockage and 21 % corner blockage) were calculated with SABRE /48, 49/. In the case of the central blockage there was good agreement between the experiments and the calculations but in the corner blockage case large deviations were stated.

Within the LMBWG (Liquid Metal Boiling Working Group) - an unofficial international cooperation of scientists in the field of liquid metal thermal-hydraulics - benchmark calculations were performed with some of the codes /50-54/. To compare the calculated results of different codes special experiments were selected and recalculated (see Tab. 10). Only with SABRE all specified cases are treated.

As examples of the calculations the results of the SABRE code from two experiments in sodium with impermeable blockages (49 % central blockage and 21 % corner blockage) and the experiment in water with a permeable blockage will be reproduced and compared with the experimental results. In the output of the calculated data the flow distribution was given as vector diagrams and the

temperature field as radial temperature profiles and isotherms. For comparison with the experimental results the radial temperature profiles are mostly used.

49 % Central Blockage in Sodium (Tab. 1 Blockage No. 9)

Figure 47 shows the measured and calculated (SABRE) radial temperature profiles of different measuring levels from run No. 1. In this run a main flow velocity of 4 m/s was used.

Good agreement can be found between the experiments and the calculations. The shape of the radial temperature profiles is predicted rather well. The amount of temperature rise is mostly calculated to be somewhat too high. In the case of lower main flow velocity (run No. 6, not shown here) the inverse was found.

In addition, the isotherms calculated for run No. 1 are presented together with the measured ones in Fig. 49. In general, the calculated results agree well with those deduced from the experiments. Also the maximum temperatures are the same. There is some minor deviation in the position of the highest temperature region. For the SABRE results this region is shifted downstream from measuring plane 50 to plane 70.

21 % Corner Blockage in Sodium (Tab. 1 Blockage No. 10)

In Fig. 48 three of the measured and calculated radial temperature profiles from run No. 287 are shown. The main flow velocity is again 4 m/s. In the 70 and 100 mm measuring planes large deviations occur between the measured and calculated data.

In Fig. 50 the isotherms of run 287 are shown. Comparing the experimental and calculated results the code predicts a maximum temperature too low by 100° C and the range of high temperatures too small although the trend of the values is in agreement with the experiment. Considering the velocity field not shown here it

seems that the code predicts the length of the wake too short compared with the experiments.

This discrepancy in case of the 21 % corner blockage indicates the difficulties which may arise with code predictions in the field of complex thermal-hydraulic behaviour. It can not be considered as a specific outcome of the selected SABRE code. The calculations with ASFRE showed a similar behaviour.

21 % Corner Blockage in Water with Leakage Flow

(Tab. 1 Blockage No. 15)

Remark: In this experiment the scatter of the experimental results is larger than in the sodium experiments. Possible reasons are: less accuracy of the temperature measurement because of the small temperature rises, the thermocouples from different azimuthal positions, effects of the glass wall of the half bundle, and inhomogeneous distribution of the leakage flow over the blockage cross section.

Figure 51 shows the measured and calculated radial temperature profiles for two measuring planes and three leakage flow rates (1, 5 and 7 %). At a leakage flow rate of 1 % the measured temperature profiles are similar to those obtained in sodium (Fig. 48). In the 35 mm plane the calculated profile agrees well with the measured one. At 75 mm level there is about the same difference as in the sodium experiments. With increasing leakage flow the temperature profile near the blockage (35 mm) becomes flatter whereas in the calculations the peak temperature in this plane increases. In the 75 mm plane the relative maximum found in the experiments is missing in the calculations.

For comparison, the measured and calculated peak temperatures in the wake are reproduced in Fig. 52. Below a leakage flow of 5 % the measured peak temperatures are roughly constant. A further increase of the leakage flow rate causes a rapid decrease of the

temperatures. At about 7 % leakage flow recirculating flow disappears.

The weak dependence on the leakage flow between 1 and 5 % is not predicted by the calculations. SABRE predicts a peak temperature, which is generally too high and located at shorter distances from the blockage than observed experimentally. In the experiment the temperature in this region strongly decreases by the cold leakage flow. The temperature decrease at leakage flow rates above 5 % is, in principle, predicted. In general, also in the case of a porous blockage the wake region calculated is too short.

Summarizing Remarks

Impermeable Blockages

In spite of some deviations between calculations and experiments with respect to detailed phenomena in the recirculating zone, it can be stated that the major features of this type of blockages are described adequately by the codes available. The degree of agreement which has been obtained seems to be sufficient to allow the application of the codes in the safety analysis of LMFBRs as far as impermeable blockages are concerned.

Permeable Blockages

Large differences exist between code results and experiments in the case of porous blockages. These differences are not only related to the peak temperature in the wake but also to its dependence on the leakage flow rate. It seems that the interactions between the leakage flow and the wake characteristics (length of the recirculating zone, its separation from the blockage, recirculating velocity) are not yet adequately modeled in the code.

However, the importance of these deficiencies should not be overestimated. The experiments with the variable blockage have shown that the wake temperature can sensitively react to minor modifications of the nature of the blockage. One should be aware of the

large spectrum of possible blockage configurations under reactor conditions even at a given size (shape and position of the blockage, degree and distribution of the porosity, shape of the leading edge, etc.) which leads to a large variety of possible consequences. In this discussion of the quality of the codes one should have in mind this category of uncertainties.

10. Application of Results to Reactor Conditions

10.1 SNR 300, MkIa Fuel Element Design

In this chapter the behaviour of blockages of different sizes and porosities is predicted mainly from experiments. The prediction is confined to planar blockages, the implications with respect to axially extended blockages /1-4/ are not treated.

Most of the experiments were performed in MkIa subassembly geometry. Therefore, the general behaviour of blockages is characterized primarily for this case. However, in spite of a lot of supporting experiments, the numerical results presented in the following chapters must not be considered as very reliable in quantitative terms. These restrictions are based on the observations made in series of experiments, e.g. that details in the area of the blockage proper and the distribution of coolant flow can change the numerical results remarkably, however, not the general tendency.

To assess the implications of a variety of blockages the process of growth has to be included. For instance, during blockage build up the porosity may change from very high to smaller values in time intervals of hours or even days. Therefore, it is impossible that an impervious blockage arises suddenly. With respect to the growth of blockages it is referred to /5/.

Given the present status of 3D computer codes the single-phase flow- and temperature fields furnished by codes are not reliable in every case as proved by comparison with experimental results (see Chapter 9).

Therefore in the following paragraphs the behaviour of various blockages conceivable has to be estimated mainly from experimental results.

10.1.1 Flow and Temperature Fields under Single Phase Conditions

Estimated Maximum Temperature Rises

To find out the behaviour of local blockages under sodium cooling conditions two test series were performed with a full bundle /12, 16/ and two with a bundle section /30, 38/. These experiments are characterized by the use of impermeous blockages. Therefore these test data are not sufficient to generate a complete picture of the temperature fields to be anticipated behind blockages varied in size and especially porosity. Therefore, other series of tests /19, 23, 24, 25, 26/ were performed in water to cover the possible fields of temperatures behind blockages. These results, however, cannot easily be applied to sodium conditions because the flow distribution mainly near the edge of the blockage is different for the water experiments where various blockage sizes were simulated, compared to the sodium-experiments with a fixed blockage. This has been explained in detail in Chapt. 5.

Comparison of the results in sodium and water for the same size of blockage yields that the reverse flow velocity is only about 20 % higher in case of the water experiments /23, 25/. Nevertheless, a discrepancy was found to exist between the normalized temperature fields in sodium and water. The normalized max. temperatures for the sodium case are 2 to 3 times higher. In these water tests the flow velocity profiles in the area downstream of the edge of the blockage are different from those in the sodium experiments, e.g. the radial velocity profile is steeper. This may lead to a more intense mass- and heat transfer in the mixing zone. This is accepted as the main reason for the differences in the normalized temperature fields although the flow fields are very similar. Based on these considerations the results obtained from these water tests were transferred to sodium conditions as follows:

The max. norm. temperatures from the experiments with the impervious 21 %-corner and 49 % central blockage in sodium were related to test results in water with main flow velocities of 3 and 4 m/s. This led to two factors. One for the central, the other for the wall blockage case. These factors were used to transfer the results of the tests with the variable blockage to sodium conditions. This coarse estimate is the basis for the Figs. 53a and 54 a. They show the field of possible max. normalized temperatures depending on the blockage size for the corner and central blockage cases with 75 % power. The field is confined within two lines. The upper line corresponds to the maximum normalized temperature at leakage flow, the lower line to that at leakage flow zero. With respect to the upper limit a specified leakage flow belongs to every blockage size.

In these figures three horizontal lines are drawn in addition. The lowest line marks the boiling temperature of 1000°C , the next two the fictitious temperatures of 1200°C and 1400°C corresponding to excess temperatures (see Annex A) of 200 K and 400 K at which a very local dryout might occur in a steady-state or oscillatory boiling regime. The normalized temperatures in Figs. 53a and 54a are based on the assumptions of a blockage inlet temperature of 500°C and an axial temperature gradient of 300 K/m corresponding to the conditions in the upper third of the core for the highest rated subassembly.

In the case with leakage flow the boiling temperature in the wake is reached earliest, however, still locally only for a 10 % corner and a 25 % central blockage.

Information furnished by the two figures will be discussed in more detail.

Growth of Blockage

In reality during growth a blockage must start from high porosity passing gradually to lower porosity, i.e. the temperature maximum determined by the upper limiting curves in the two figures will be applicable initially.

It is rather improbable that a blockage starts to grow right from the wall. Therefore and this should be true at least for smaller blockages up to 25 % the behaviour corresponds more closely to the central blockage case. This means that the upper limiting line in Fig. 53a up to a blockage size of 25 % is considered to be the more probable course of the maximum normalized temperatures. With these assumptions made the boiling temperature is just reached locally for a 25 % blockage.

Detection of Primary Blockages by Passing the DND Threshold

From an analysis of the blockage growth /5/ it must be assumed that the blockage consists primarily of fuel from the subassembly proper. There are no plausible circumstances that the blockage could be caused by foreign matter. To build up a blockage of a certain size some minimum amount of material is necessary /5/. Because this material is primarily fuel it was possible to estimate /54/ under very conservative assumptions the minimum size of a blockage to be detected safely by the DND system. This size is close to 9 % for the corner and 12 % for the central blockage case. If it is assumed that blockages in the range up to 25 % behave more like central blockages a large margin exists between the detection of a blockage (12 %) and the onset of boiling (25%).

10.1.2 Cooling under Boiling Conditions

Limits of Cooling

On the assumption that the DND system and the cover gas monitoring system does not respond the blockages may grow further. If one keeps to the conservative example mentioned before, the boiling temperature will be reached locally in the wake of a 10% corner or a 25% central blockage. Even if the blockage grows further cooling in the boiling region is still very effective until a fictitious temperature of 1200°C is surpassed. This threshold is determined by the boiling temperature at 1000°C together with an observed excess temperature of $\Delta T_e = 200$ K, as explained in Chapter 6.5. Above this fictitious temperature local regions in the wake may no longer be cooled by evaporation so that dryout may occur with subsequent melting of the clad and fuel. In Figs. 53a, 54a this threshold is also traced. It will be surpassed for a 15 % corner and a 43 % central blockage. This second threshold is deduced from the measured results of the 21 % corner blockage experiment in sodium where the dryout condition at a fictitious max. temperature of 1200°C was reached. The boiling regime in these tests was primarily steady state. This regime is associated with the lowest cooling capability as observed in the tests.

A second threshold at 1400°C for the onset of dryout is also entered in Figs. 53a and 54a. It is based on the 49 % central blockage experiments in sodium. The boiling regime observed in these tests was primarily oscillating boiling. This regime lead to very efficient cooling of the wake, i.e. the dryout conditions are reached for much larger blockage sizes compared to those in the steady state boiling regime. In the example under consideration the dryout conditions are attained behind a 33 % corner and a 50 % central blockage.

Volumes at or above Boiling Temperature and Amounts of Involved Fuel

Knowledge of the maximum normalized temperatures and the dryout threshold is not sufficient to estimate the propagation potential of blockages of different size and porosities. The maximum volumes in the wake above a specified temperature (boiling temperature or dryout threshold) should be known, too. They are estimated from the isotherms derived from the experiments in water /23, 25/ (see also chapter 5.4) which are transferred to sodium conditions. The course of these volumes versus blockage size are reproduced in Figs. 53b and 54b. The curves start from a blockage size at which the boiling temperature (V_w above $\theta = 1.67$) or the fictitious dryout temperature (V_w above $\theta = 2.33$) is attained locally. With increasing blockage size the volume involved increases exponentially up to a certain blockage size. With further increasing blockages the volume diminishes again. This behaviour corresponds to the course of the estimated max. normalized temperatures in Figs. 53a and 54a. The case of zero leakage flow is not treated for either blockage of any size. In case of central blockages boiling is never reached; in case of corner blockages the anticipated volumes at boiling are not conservative compared to the porous blockage case.

To estimate the propagation potential of a blockage the following assumption are made:

Loss of cooling in the wake occurs as soon as the first dryout threshold is reached, which is defined by a fictitious temperature of 1200°C . Consequently a total melt out of the boiling region occurs. The molten material (steel and fuel) is swept out and deposits completely at the downstream spacer grid thus forming a secondary blockage. These assumptions, however, are very conservative because experiments have shown that loss of cooling is confined to a very local area in the wake. Therefore, a total melt out of the boiling region must not be anticipated. Further-

more, in-pile experiments /6/ have shown that part of the material, which was molten before, remained in the wake and that only part of the material swept out did deposit at the next spacer grid.

With respect to the build up of secondary blockages the maximum amount of material involved during the melt out of the wake behind a primary blockage is yet estimated.

In the case of the central blockage the first dryout threshold is surpassed for a blockage size of 43 %. The related volume of the boiling region (V_w above $\theta = 1.67$) including the coolant is about 19 cm^3 as can be taken from Fig. 53b. For the assumption that the secondary blockage is 10 mm thick and has a porosity of 50 % the material in this volume corresponds to that enclosed in a blockage of about 43 %, i.e. a blockage of the same size as the original one.

For the corner blockage the results are similar to that in the central blockage case. The first dryout threshold is surpassed for a blockage size of 15 % (see Fig. 54a). For this blockage the volume of the boiling region is about 8 cm^3 (see Fig. 54b). The material in this volume corresponds to that enclosed in a blockage of about 18 %, i.e. a blockage somewhat larger than the original one (thickness and porosity as above).

As discussed before only part of the material during melt out of the primary blockage may contribute to build up a secondary blockage. Therefore, secondary blockages will be markedly smaller than the original one and cannot lead to an escalation of a local cooling disturbance. This statement, however, does not include the possibility of gas accumulation in the wake (see chapt. 10.1.3) and is valid only for planar type blockages.

If loss of cooling (dryout) occurs when the second threshold is reached which is defined by a fictitious temperature of 1400° C only part of the boiling region is assumed to melt out. This is based on the facts that dryout is a local event and the second threshold can be reached only if the cooling disturbed region can be cooled sufficiently under boiling conditions. Therefore, it is assumed that the volume of loss of cooling will not be larger as in the case when the first threshold is surpassed.

Detection of Secondary Blockages by Passing the DND Threshold

Another consideration referring to the detection of secondary blockages also marked at the top of Figs. 53a and 54a, will be added here. Experiments /3, 4, 6/ and calculations /54/ have proven that 1 cm³ of highly heated or molten fuel is enough to be safely detected by the DND system. This means that even in the hypothetical case that the blockage would consist of foreign matter without any fuel the DND system would give a reliable signal as soon as a very small amount of fuel had been overheated or molten. Under these assumptions a corner blockage of 15 % and a central blockage of 43 % would be detected last. In both cases a dryout threshold of $\theta = 2.33$ is assumed.

10.1.3 Implications of Gas Release

Field of Conditions under which a Gas Cavity could Exist

The blockage growth from higher to lower porosities has to be considered to assess the possible influence of fission gas on cooling. The fission gas could be released from damaged pins. It has been discussed in chapt. 10.1.1 that the material to build up a blockage should come mainly from damaged pins of the subassembly proper. It is further known /5/ that the radial displacement of e.g. fuel particles from one subchannel to the other between two grid spacers is rather small as long as there is no remarkable flow diversion in front of the blockage itself. Therefore,

it is very probable that, the pins in the center of a growing blockage are at least damaged to such an extent that the fission gas will have been released before the blockage has grown to a condition under which a wake with reverse flow could exist. The latter is an essential condition for gas accumulation (see Chapt. 8).

It has been shown that cooling of the wake behind a blockage is remarkably impeded only if a gas cavity builds up for some time (see Chapt. 8.3). This condition roughly exists for a reverse flow velocity above 0.55 m/s, i.e. a velocity somewhat higher than the buoyancy velocity of the gas bubbles. For corner and central blockages in Annex C the equations (C8, C9) have been deduced from experimental results with the variable blockage. They correlate the necessary minimum main flow velocity $v_{o,min}$ in the undisturbed cross section of the subassembly with the blockage size B . The parameter is the leakage flow L through the blockage. The results are reproduced as a field of curves in Figs. 55 and 56 together with some results of other experiments shown as single points. These single points fit the related curves rather well. The field is limited towards the top by the maximum flow velocity in the subassembly, $v_{o,max}$, and towards the bottom by the curve related to zero leakage flow through the blockage. For a given leakage flow all data below the specified lines would not lead to a build up of gas cavity.

The information which can be taken from these two diagrams will be illustrated by two examples:

A 15 % corner or central blockage is chosen assuming full load conditions $v_{o,max}$ (upper line). In the corner blockage case the leakage flow through the blockage must be lower than 6 %, in the central blockage case lower than 12,5 % until the conditions for a build up of a gas cavity are met, i.e. all pin failure occurring during the densification process of the blockage before the specified values are reached, cannot cause a build up of cavities. When the power is lowered to 2/3 power the same leakage flow

condition assumed, a 38 % or 20 % blockage respectively would be necessary to fulfil the conditions of cavity buildup. These figures show that leakage flow generally reduces the field of conditions for gas accumulation. At a given blockage size the minimum main flow velocity increases with increasing leakage flow. A further limitation exists by the relation between blockage size and leakage flow. In the case of planar blockages build up by particles there is a relation between blockage size, porosity and driving pressure. Therefore, not all conditions shown in Fig. 55 and 56 are possible.

To complete the picture of the conditions of a gas cavity buildup, the maximum temperatures in the wake to be anticipated during blockage growth have to be included. In Fig. 57 the dependance of the leakage flow upon the very dissolution of the reverse flow region is shown versus the blockage size (two dashed lines) for the central and corner blockage cases. The two solid lines determine the limits above which a gas cavity cannot exist, because the reverse flow velocity is too low as explained before. The dashed lines define the limit for zero reverse flow. In addition, the conditions for the observed maximum temperatures in the wake are indicated for the 3 and 4 m/s velocity cases. Most of the test results are found to be within the two regions determined by the two pairs of lines. It follows that there is a clear tendency that the maximum temperatures are reached in the wake before the conditions of any gas accumulation are met. If however there is still an undamaged pin in the blockaged area, this pin has to withstand the high temperature during further decrease of the porosity of the blockage a nearly constant size of the blockage presumed during this process and then to fail to meet the condition for gas cavity buildup.

Maximum Sizes of Gas Cavities

Disregarding the preceding considerations the maximum size of the volumes have been estimated enclosed by the isotherms above boi-

ling or dryout of the mentioned tests performed in water and sodium (Figs. 53b and 54b). These volumes, however, are not identical with the anticipated sizes of gas cavities. The most conservative upper limit of gas cavity volumes for porous blockages at a minimum reverse flow velocity of $v_R = 0.55$ m/s is determined by a different procedure. The volumes for the central and corner blockages in Fig. 58 are taken from the measurements by Decker /24/. They are based on high speed photography. In the central blockage case the volume of the gas cavity is about three times larger than that of the boiling region. In the corner blockage case the difference is smaller. It should not be derived from the larger volumes that also a larger propagation potential exists because the build up of a gas cavity is restricted by several conditions as discussed in this chapter.

Fission Gas Release and Entrainment

About 200 cm^3 of fission gas corresponding to an ambient pressure of 3 bars could be released from one pin under maximum burn up conditions /18/. For the buildup of a gas cavity it is very important at which location in the subassembly the gas is injected, roughly either into the main stream or into the center of the vortex proper. If the gas is released into the main flow only part of it reaches the center of the vortex and therefore the gas inventory of one or even several pins is probably not sufficient to build up a gas cavity even under adverse injection conditions. Further more this case is very unlikely because as a result of the higher temperature a pin will fail mainly within the wake. Therefore only the case involving gas release into the wake will be discussed further.

The model of Fukuzawa /41/ concerning the behaviour of gas cavities behind blockages has been used to estimate the rate of entrainment from the gas cavity dependent on the blockage size. Again the porous blockage conditions for a reverse flow of $v_R = 0.55$ m/s are used. The course of the entrainment rate for the two

types of blockages is shown in Fig. 59 for a main flow velocity of $v_0 = 4$ m/s. For lower main velocities the entrainment rate is somewhat lower, however, $v_0 = 4$ m/s is still the worst case, because the time interval until melt out of the subassembly region in a gas cavity is the shortest under full power conditions.

The entrainment rates for central blockages are of course higher than for the corner blockages. Up to blockages of 40 % and 60 %, respectively the entrainment rates increase only moderately. For large blockages the increase is steeper. In the case of the central blockage there is a maximum at about 65 %. Using these entrainment rates the time can be estimated during which a gas cavity is maintained with the gas inventory of one pin injected directly into the vortex under the most adverse characteristic of release for a specified case. This time decreases exponentially with increasing blockage size.

Influence of Gas on Cooling

Disregarding the preceding considerations concerning blockage detection and growth the buildup of a gas cavity is yet postulated. Considering full power conditions the implications of a sustained gas cavity would be that the pins start to melt locally after some time depending on the temperature field prior to the injection. Because the outer regions of the cavity will still be cooled by penetrating sodium the actual volume which can melt out, will be much smaller than the upper limiting values represented in Fig. 58.

In case of blockages up to 15 - 20 % the volume of the gas cavity remains small enough, so that the involved material which could melt does not give rise to a fast escalation of the failure. In case of larger blockages the pins in the center of the blocked area should have failed prior to reach a critical blockage size. Therefore gas could only be injected from the outer pins into the wake and only part of it may go into the center the other is

swept away in the main flow. On the other hand the entrainment increases remarkably with the blockage size. So also the actual volume of the gas cavity volume should be smaller than reproduced in Fig. 58. Nevertheless a mild failure propagation by fission gas release has to be taken into account.

10.2 Application of Results to Different Subassembly Designs of the SNR 300, e.g. Change of p/d Ratio

Experimental results from one subassembly geometry with grid spacers to another should be transferred with validated 3-D codes. But the results of such codes used for parametric calculations such as blockage size and porosity are not satisfactory in every case as shown in Chapt. 9.

Nevertheless, with a very simple model, parameter calculations were performed to better understand the influence e.g. of the p/d ratio. Therefore, tendencies indicated below, have to be considered with restriction. The model considers the flow in the unblocked cross-section, the resulting flow constriction, a typical flow path in the wake region for the case of leakage flow zero. The model was applied to a Mk Ia subassembly and a Mk II subassembly with a p/d ratio of 1.31 and 1.16 respectively. The resistance along the reverse flow path is very important for the development of the temperature fields. Comparing the results of the parameter calculations of the two types of blockages the following tendencies should exist.

For the same power operating conditions (see Table 2) and a ratio of v_R/\bar{v} assumed to be 0.5 (see central blockage case Mk Ia, chapt. 5.2) the pressure drop in the wake, especially across the pins of the Mk II subassembly, was determined to be much higher than for Mk Ia. In reality this will be compensated partly by the higher driving pressure available for the reverse flow in the wake due to the higher main flow velocity in the Mk II subassembly and a reduction of the ratio v_R/\bar{v} . Therefore the behaviour of blockages in case of the Mk II geometry should generally be the same with something elevated max. temperatures in the wake.

If the gap between the pins is narrowed further below the 1.16 mm value of the Mk II design the flow resistance across the pins will increase steeply as the parameter calculations have shown.

It has to be anticipated that the temperatures go up too and cooling even of smaller blockages, may get insufficient. It seems to be feasible to transfer the results also to subassemblies with wire wrapped spacers, of course again for the planar blockage case only. This is based on the consideration that although the flow resistance across several pins locally can become very high because of the wire the averaged flow resistance is only a little different from that in grid spacer type design. However, the influence of the locally different rotational flow in pin clusters is rather difficult to estimate. Therefore the transfer of results is subjected to severe restrictions.

It must be kept in mind that the preceding considerations are valid only as long as the width over the flats of the subassembly and the distance between the grid-spacers are not very different from the Mk Ia design.

Whenever the subassembly geometry is changed towards smaller p/d ratios compared to the Mk II design a reliable method to estimate the anticipated behaviour would be to measure the single-phase temperature distribution in water behind one or two different blockages. Based on these results all other available data, e.g. the boiling behaviour could then more reliably be transferred to the new subassembly considered.

10.3 Conceivable Tendencies of Changes of the Size of the Subassembly

The anticipated influence on cooling behind blockages of a subassembly with an enlarged size of the subassembly was estimated too. The enlarged bundle corresponds thermal-hydraulically to the SNR 300 Mk Ia bundle design with two rows of pins added so that the considered bundle has 271 pins and a bundle cross section increased by 55 %. It is assumed that the distance between the spacers is also increased by about the same percentage. Using the same relative blockage sizes the driving pressures for the re-

verse flow are estimated to be nearly the same for either bundle size. The path for the reverse flow, however, is about 25 % longer in case of the 271 pin bundle. Because the driving pressure remains the same, the reverse flow velocity has to change to an approximately 15 % lower velocity compared to the Mk Ia design. From a very rough estimate the temperatures in the wakes behind a specified blockage should go up by about 40 % compared to a blockage of the same relative size in a Mk Ia subassembly. If results are available of temperature fields behind blockages in a bundle of the Mk Ia size these can be transferred in a first crude estimate to a larger bundle size by the following relation:

$$\Delta T_2 = \Delta T_1 \cdot \left(\frac{A_2}{A_1} \right)^{0.75}$$

where A_1 is the cross section of the measured bundle and A_2 of the enlarged bundle. ΔT_1 is the measured temperature increase in centigrade.

Concluding the preceding considerations it can be said that the cooling capability of blocked regions in larger bundles is generally smaller than in small bundles the same ratio of blocked area assumed. In every new subassembly design this has to be taken into account appropriately.

11. Conclusion

Cooling disturbances in rod bundles caused by local blockages were investigated in a wide range of blockage configurations in water and in sodium. From the experimental results the following general conclusions can be drawn:

Single-phase flow pattern and temperature distribution

- The effects of the type and the size of the blockage on the flow pattern and the resulting temperature field in the wake of blockages are very complex. Therefore the nature of the blockage was found to have an important feedback on the flow pattern and, consequently, also on the temperature field. Under normal operating conditions of the SNR 300 a recirculating flow always exists behind planar impermeable blockages of any size, except very small ones, ($< 5\%$ of the cross section). As a result of the recirculating flow a vortex and a temperature field basically toroidal in shape are produced in the wake.
- Aside from parameters like size, position and porosity of the blockage, the temperature field is influenced by the local thermal-hydraulic conditions, such as mass and heat transfer prevailing in the mixing zone between the wake flow and the main flow. At low recirculating flow velocities and high power levels the flow and temperature field is influenced in addition by buoyancy forces.
- The temperature rise in the wake of a corner blockage is generally higher than that of a comparable central blockage. Dependent on the flow pattern, the peak temperature in the wake can occur in the region of the vortex centre or at the end of the longest flow path close to the edge of the blockage. With increasing blockage size the peak temperature increases up to a maximum. Depending on the type of blockage this maximum arises for blockages between 40-60 %.
- In the case of porous blockages the leakage flow through the blockage influences the recirculating flow in the wake and, consequently, the temperature field. With increasing leakage

flow the reverse flow velocity decreases. Consequently the peak temperature increases. The maximum temperature in the wake has to be anticipated close to the dissolution of the recirculating flow.

- A detailed knowledge of the single-phase temperature fields and their dependence on the main physical parameters allows to predict the conditions for the onset of boiling and to estimate the extension of the boiling region for specified boiling intensities. Results of water experiments in terms of normalized temperatures can well be compared with those in sodium provided that the hydraulic conditions are similar.

Boiling and dryout behaviour

- Boiling starts in the region of the single-phase peak temperature and expands correspondingly to the shape of the surrounding isotherms. It can well be detected by monitoring the acoustic noise.
- Two local boiling regimes were identified: steady-state boiling and oscillatory boiling with the boiling region changing periodically between a maximum and a minimum value. Boiling always started as steady-state boiling. A transition to oscillatory boiling occurred under conditions which are sensitive to the blockage size and location and to the boiling intensity. There was always a distinct margin between the conditions prevailing at the onset of boiling and those at the onset of dryout. For a given bundle design the margin depends mainly on the boiling pattern. It was markedly smaller for steady-state boiling than for oscillatory boiling.
- In case of the 49% central blockage oscillating boiling was dominating. The margin between the onset of boiling and the onset of dryout corresponds to roughly a 100 % increase of the power to flow ratio. In case of the 21 % corner blockage steady-state boiling was observed generally. The margin between the onset of boiling and permanent dryout corresponded to a 40 - 60 % increase of the power to flow ratio.

- It is deduced from the experimental results that cooling of the boiling region is sustained by a liquid film draining down the pins into the voided region. Aside from evaporation the flow of this film is influenced by the vapour flow towards the surrounding condensation surface. If the boiling zone has grown to a given size, feeding and the evaporation and entrainment mechanisms are no longer balanced so that local loss of cooling occurs.
- With increasing boiling intensity, the boiling region grew to some extent; however, it was confined always within the recirculating zone. This result is also supported by the results of the ECN experiments with a 70 % blockage. Therefore, a transition to cross boiling as a consequence of the local boiling process in the subassembly which would constitute one mechanism for a fast propagation of a local cooling disturbance into a cross subassembly fault, can be excluded. This consideration does not include building up of a secondary blockage by molten and relocated material from the first one.

Behaviour of injected gas

- Gas released into the coolant accumulates under certain conditions in the recirculating zone. A gas cavity can extend over nearly the whole recirculating zone. In the voided region cooling is considerably disturbed and local dryout can occur. Gas injection not leading to an accumulation does not have a significant influence on the single-phase temperature field and on the boiling behaviour.
- For a given blockage the parameters influencing gas accumulation are mainly the flow velocities in the bundle and in the wake and the rate and location of gas injection. Below a minimum reverse flow velocity in the wake, which was found to be about 0.55 m/s, gas does not accumulate independent of the gas injection rate and the blockage size. This behaviour restricts the possibility of gas accumulation, especially in the case of porous blockages because their density must reach a specified level before reverse flow establishes. It must increase further

so that conditions for gas accumulation are met.

- A gas cavity can also be formed by a sudden gas release, if the conditions for accumulation are given. The time from termination of gas injection to the dissolution of the cavity depends on the main flow velocity and the rate of gas entrainment into the main flow. It can last a few seconds.

Results applicated to reactor condition

Mainly based on the performed tests but also on calculations with simple models the safety implications of planar blockages in subassemblies were estimated. Because blockages formed by particles may build up from high to smaller porosity in time intervals of hours or even days the process of growth is included, too.

Detection of blockages and limits of cooling

The material for the blockage buildup is mainly fuel from the subassembly proper. If the DND System operates appropriately a blockage can be detected before boiling conditions are reached.

On the assumption that the DND- and the cover gas monitoring system does not respond the blockages may grow further. The boiling temperature (about 1000°C) will than be reached locally in the wake of a 10 % corner or a 25 % central blockage. Even if the blockages grow further cooling in the boiling region is still very effective until specified sizes of the two types of blockages considered are surpassed.

Using the different fictitious peak temperatures (1200°C and 1400°C) found for the dryout conditions in the two boiling regimes dryout, i.e. the local interruption of cooling with subsequent melting of clad and fuel, is reached in the case of steady-state boiling with a corner blockage of 15 % and a central blockage of 43 %. If the oscillatory boiling regime is prevailing the dryout conditions are attained behind a 33 % corner and a 50 % central blockage.

Volumes of the wake and propagation potential

From the single phase temperature fields volumes of the wake at or above a specified temperature, e.g. boiling temperature, were determined. With increasing blockage size the volume increases exponentially up to a maximum at a certain blockage size then it diminishes again. This behaviour corresponds to the course of the normalized peak temperatures. In case of the SNR 300 subassembly the maximum volume above the boiling temperature was determined to be $\approx 200 \text{ cm}^3$ for a central blockage of 77 % and $\approx 160 \text{ cm}^3$ for a corner blockage of 55 %.

The amount of fuel and clad material in the volume above a specified temperature level is taken as the basis for the propagation potential. Very conservatively it was assumed that whenever the first dryout threshold (fictitious temperature of 1200°C) is reached, all the material in the boiling region melts out and part of it deposits at the downstream grid spacer thus forming a secondary blockage. In that case the secondary blockage would always be smaller than original one. Therefore, in the absence of a fission gas release into the wake an escalation of local cooling disturbances can be excluded.

Implications of gas release

Gas released into the coolant exhibits a remarkable effect on cooling only when the conditions of an accumulation are met in the wake of a blockage. Taking into account the blockage growth and pin failure phenomena the field of possible conditions is narrowed remarkably. In case of small blockages ($\leq 20 \%$) an escalation of the local cooling disturbance may be excluded. In case of larger blockages, as improbable they may be, a slow propagation has to be taken into account if one does not credit the consideration that all pins in the blocked region have failed and released the fission gas until the blockage has reached a critical size.

Application to different subassembly designs

It is assumed that the widths over flats and the spacer grid design are not changed. For this case the results gained in SNR 300 Mk Ia subassembly geometry ($p/d=1.31$) were transferred to the subassembly of the Mk II design with a p/d of 1.16 by the use of a simple model. It is estimated that the maximum temperatures in the wake would increase by about 30 % compared to MKIa. Consequently boiling inception and dryout will be shifted to smaller blockages. If the p/d ratio is decreased further the model predicts a steep increase in the pressure drop in the reverse flow path and hence also a steep increase in the maximum temperatures to be anticipated. Therefore it is not recommended to go below the $p/d = 1,16$ value. However, it has to be kept in mind that the preceding considerations are based on a rough estimate only. A more reliable method would be to measure the single-phase temperature distribution in water behind one or two different blockages in the bundle geometry considered. Based on these data all other results gained in the Mk Ia geometry, as the boiling and dryout behaviour could more reliably be transferred.

In case the size of the subassembly is increased, keeping the subchannel geometry and relative blockage size constant the simple model predicts also a steep increase in the maximum temperatures in the wake. Again as mentioned before a reliable basis would be to measure the single-phase temperature distributions in the wake in some tests in water.

For the future it would be very desirable that the analysis of anticipated implications of blockages is strongly supported by 3D computer code calculations. However, at present the single-phase flow and temperature fields furnished by these codes are not yet reliable in every case compared with experimental results.

12. Nomenclature

A_B	area of the boiling region enclosed by the saturation isotherm (axial cross section)
B	blocked flow area
c_p	specific heat
d_i	inner diameter of a tubular test section
d_h	hydraulic diameter of the central subchannel
d_p	pin diameter
D	diameter of a central blockage
l_B	heated length upstream of a blockage
L_R	length of the reverse flow region
L_B	length of the boiling region
L	leakage flow through the blocked flow area in percent of undisturbed flow
L_K	leakage flow through the blocked flow area leading to the disolution of reverse flow
m_O	total mass flow rate of the bundle
m_L	mass flow rate of the leakage flow
P	pin pitch
q	mean surface related pin power density

R	radius of a corner blockage
S_B	surface of the boundary of the boiling region
t	time
$t_{0.5}$	half-time
T	temperature
T	peak temperature
T_{sat}	saturation temperature
T_{in}	inlet temperature
ΔT_e	excess temperature
v_o	flow velocity in the undisturbed bundle cross section (main flow velocity)
v_B	flow velocity in the unblocked cross section at the blockage level
v	mean main flow velocity $1/2 (v_o+v_B)$
v_R	reverse flow velocity without leakage flow through the blockage
v_{RL}	reverse flow velocity with leakage flow through the blockage
$v_o \text{ min}$	minimum main flow velocity necessary for gas cavity formation

$V_{R \min}$	minimum reverse flow velocity necessary for gas cavity formation
v_{va}	axial vapour flow velocity in the boiling region
v_{vr}	radial vapour flow velocity in the boiling region
V_B	total volume of the boiling region (including the pins)
V_w	volume of the wake enclosed by isotherms
ΔV_V	oscillating vapour volume
\dot{V}_{GM}	rate of gas injection into the main flow
\dot{V}_{GR}	rate of gas injection into the recirculating flow
\dot{V}_{EC}	rate of gas entrainment from the gas cavity
V_{GR}	amount of gas injected into the recirculating flow
z	axial coordinate
ρ	density
θ	normalized temperature rise
$\hat{\theta}$	normalized peak temperature
$\Delta\theta_e$	normalized excess temperature

13. References

- /1/ K. Gast:
Ausbreitung örtlicher Störungen im Kern Schneller natrium-
gekühlter Reaktoren und ihre Bedeutung für die Reaktorsi-
cherheit
KfK 1380, May 1971
- /2/ K. Gast, D. Smidt:
Cooling Disturbances in the Core of the Sodium Cooled Fast
Reactors as Causes of Fast Failure Propagation
Nucl. Eng. Design 14 (1970), pp 12-22
- /3/ D. Smidt, K. Schleisiek:
Fast Breeder Safety against Propagation of Local Failures
Nuclear Engineering and Design 40 (1977) P. 393
- /4/ K. Schleisiek:
Accommodation of Subassembly Faults in SNR 300
LMFBR Safety Topical Meeting, Lyon, France, July 1982
- /5/ G.F. Schultheiß:
Analyse der Bildung lokaler Kühlungsstörungen in schnellen
natriumgekühlten Brutreaktoren
KfK 2331, September 1976
- /6/ W. Kramer, K. Schleisiek:
Mol 7C-Schlüsselexperiment zur Problematik lokaler Kühlstö-
rungen bei schnellen Brutreaktoren
KfK-Nachrichten 1/82, pp. 51-63

- /7/ J.D. Macdougall, Lillington:
The SABRE Code for Fuel Rod Cluster Thermohydraulics
Nuclear Eng. and Design, Vol. 82, 1984, Pages 171-190
- /8/ K. Schleisiek:
Natriumexperimente zur Untersuchung lokaler Kühlungsstörungen
in brennelementähnlichen Testanordnungen
KfK 1914, February 1974
- /9/ D. Kirsch:
Untersuchungen zur Strömungs- und Temperatur-Verteilung im
Bereich lokaler Kühlkanalblockaden in Stabbündel-Brennelementen.
KfK 1974, May 1973
- /10/ P. Basmer:
Unveröffentlichter Bericht, 1975
- /11/ P. Basmer, D. Kirsch, G.F. Schultheiß:
Phänomenologische Untersuchungen der Strömungsverteilung
hinter lokalen Kühlkanalblockaden in Stabbündeln
KfK 1548, January 1972
- /12/ F. Huber, K. Mattes, W. Peppler, W. Till:
Unveröffentlichter Bericht, 1980
- /13/ A.J. Clare, F. Huber
Unveröffentlichter Bericht, 1980
- /14/ F. Huber, K. Mattes
Unveröffentlichter Bericht, 1980

- /15/ P. Basmer:
Unveröffentlichter Bericht, 1977
- /16/ F. Huber K. Mattes, W. Pepler, W. Till:
Unveröffentlichter Bericht, 1981
- /17/ A.J. Clare, F. Huber:
Unveröffentlichter Bericht, 1980
- /18/ F. Huber, K. Mattes:
Unveröffentlichter Bericht, 1981
- /19/ J. Hannappel:
Phänomenologische Untersuchungen der Strömung um lokale
Kühlkanalblockaden
Diplomarbeit am Lehrstuhl für Reaktortechnik, Karlsruhe,
September 1976
- /20/ Y. Fukuzawa:
Observations of the Behaviour of Gas in the Wake behind a
Corner Blockage in Fast Breeder Reactor Subassembly Geo-
metry
KfK 2820, July 1979
- /21/ Y. Fukuzawa:
Influence of Leakage Flow on the Behaviour of Gas behind a
Blockage in LMFBR Subassembly Geometry
KfK 2969, July 1980
- /22/ Y. Fukuzawa:
Unveröffentlichter Bericht, 1979

- /23/ E. Reuter:
Ermittlung der Temperaturverteilung hinter einer porösen
Blockade in einem simulierten Schnellbrüter-Brennelement
Diplomarbeit an der Fachhochschule für Technik, Mannheim,
July 1980
- /24/ G. Decker
Ermittlung der Strömungsverteilung hinter Blockaden.
Studienarbeit am Institut für Reaktortechnik, Universität
Karlsruhe, December 1982
- /25/ P. Adamski:
Ermittlung der Temperaturverteilung hinter Blockaden
Studienarbeit am Institut für Reaktortechnik, Universität
Karlsruhe, April 1983
- /26/ F. Huber, W. Pepler:
Influence of Size and Porosity of a Blockage in a Bundle
Geometry on the Flow and Temperature Distribution in the
Wake
10th Meeting of the LMBWG in Karlsruhe, October 1982
- /27/ A.J. Clare:
Pin Cooling and Dryout in Steady Local Boiling
KfK 2944, April 1980
- /28/ F. Huber, R.A. Müller:
The Karlsruhe Sodium Tank Test Facility
KfK 1203, July 1970
- /29/ F. Huber, E. Jenes, K. Mattes:
Beschreibung der Teststrecken zum lokalen Sieden im kompak-
ten Natriumsiedekreislauf
KfK 2475, April 1978

- /30/ K.J. Brinkmann, B. Dorr, J.E. de Vries:
Survey of local boiling investigations in sodium at ECN-
Petten
Paper presented at the Fast Reactor Safety Technology
Meeting, Seattle, August 19-23, 1977
- /31/ A.J. Clare, F. Huber:
Boiling and Dryout in the KNS Local Blockage Experiments
LMBWG, 9th Meeting, Rome, 4-6 June 1980
- /32/ F. Huber, D. Roberts:
An Evaluation of the Boiling Oscillations Observed in the
49 % Central Blockage KNS Experiment
LMBWG 7th Meeting, Petten, 1977
- /33/ R.C. Noyes:
An Experimental Study of Sodium Pool Boiling Heat Transfer
Trans. ASME, Series C, B. Heat Transfer, 85:125 (1963)
- /34/ O.E. Dwyer:
Boiling Liquid Metal, Heat Transfer
American Nuclear Society, 1976
- /35/ A.J. Clare, S.J. Board:
A study of gas/vapour cavities and the implications for
boiling propagation
LWBWG 6th Meeting, Risley, 1975
- /36/ H. Kottowski:
Über die Ausbildung einer Restschicht beim Sieden von Alka-
limetallen in Kanälen
ATKE 15-28 (131-137), 1970
- /37/ A.J. Brook, A. Kaiser, W. Peppler:
Flow Rundown Experiments in a Seven Pin Bundle
Nucl. Eng. and Design 43, 177, 273-283

- /38/ A. Kaiser, W. Pepler, M. Straka:
Decay Heat Removal from a Pin Bundle
International Meeting on Fast Reactor Safety and Related
Physics, Chicago, October 5-8, 1976, Conf. 76-1001
1578-1586
- /39/ W. Pepler:
Experimentelle Untersuchungen der Siedevorgänge mit Natrium
in engen Kanälen und deren Anwendung auf schnelle Reaktoren
Kernforschungszentrum Karlsruhe, Externer Bericht 8/72-1
- /40/ J.E. de Vries, B. Dorr, J.-R.C. Marleveld:
Final Report of the ECN-KfK Local Boiling Experiments in
the 500 kW Sodium Loop at Petten
ECN-83-202, December 1983
- /41/ Y. Fukuzawa:
Model of Gas Cavity Breakup behind a Blockage in Fast
Breeder Reactor Subassembly Geometry
KfK 2953, May 1980
- /42/ J.D. MacDougall:
SABRE 3B - A version of the SABRE computer programme for
the calculation of flow in rod clusters
AEEW - M 1850, June 1981
- /43/ H. Yoshikawa et al.:
ASFRE - A computer code for single-phase subchannel thermal-hydraulic analysis of LMFBR single subassembly
PNC N941 81-74 (1981)
- /44/ H. Ninokata:
ASFRE-IIP: Upgraded ASFRE computer code für single-phase
subchannel thermal-hydraulic analysis of LMFBR single
subassembly; in preparation

- /45/ M. Bottoni, B. Dorr, Ch. Homann, D. Struwe:
BACCHUS 3D/SP, A computer program for the three-dimensional description of sodium single-phase flow in bundle geometry
KfK 3376, July 1983
- /46/ B. Basque et al.:
Thermohydraulic analysis of LMFBR subassemblies with the BACCHUS programme
ANS/ENS Int. Topical Meeting on LMFBR safety, and related design and operational aspects, Lyon, 1982
- /47/ J. Olive, Ch. Simon, J.M. LeGouez:
Calculations of Flow and Temperature in a Partially Blocked Heated Channel (Type SNR 300)
9th LMBWG-Meeting 4-6 June 1980 Rome, Italy
- /48/ J. Adamson, A.J. Brook, W. Pepler, M.G. Staniforth:
Comparison of SABRE Predictions with Results from the KNS Tests
7th LMBWG Meeting, Petten, the Netherlands, June 1977
- /49/ A.A. Cooper, M.G. Staniforth:
SABRE Code Validation Studies Using KfK Cluster Experiments
8th LMBWG Meeting, Mol, Belgium, October 1978
- /50/ A.A. Cooper, M.G. Staniforth, J.M. Jenkins:
The Application of SABRE to the LMBWG 1980 Bench-Mark Test
9th LMBWG-Meeting 4-6 June 1980, Rome, Italy
- /51/ I. Ishimarn, H. Yoshikawa and M. Hori:
A Verification Study of the ASFRE Code through Experimental Analysis of Local Flow Blockage Tests
9th LMBWG-Meeting 4-6 June 1980, Rome, Italy

- /52/ A. Fels:
Analytical Studies on Obstruction Effects in Large Pin
Bundles
9th LMBWG-Meeting 4-6 June 1980, Rome, Italy
- /53/ H. M. Kottowski, W. Pepler:
Proceedings of the 10th Meeting of the LMBWG, Karlsruhe
October 27-29, 1982, Part II pp. 1102-1123
- /54/ K. Schleisiek:
Unveröffentlichter Bericht, 1979
- /55/ B. Dorr:
Unveröffentlichter Bericht, 1978
- /56/ K. Haga, K. Yamaguchi, F. Namekawa:
Temperature Rise due to Fission Gas Release in Locally
Blocked LMFBR Fuel Subassembly Simulations
International Topical Meeting on Liquid Metal Fast Breeder
Reactor Safety and Related Design and Operational Aspects,
Lyon, pp. IV-291-300, July 1982










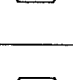






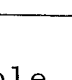
Blockage			Bundle Design	Coolant	Investigations	Ref.	
No	Type	Size					
1	 Ring impermeable	67%	Ring channel with sub-channels $d_i=12\text{mm}$, $d_h=4.42\text{mm}$	Water	- single-phase temperature distribution	8	
				Sodium	- single-phase temperature distribution and boiling behaviour		
2	 Ring impermeable	75%	Ring channel with sub-channels $d_i=21\text{mm}$, $d_h=3.96\text{mm}$	Water	- single-phase temperature distribution	8	
				Sodium	- single-phase temperature distribution and boiling behaviour		
3	 Central impermeable	15%	169 pin bundle $d_p=6\text{mm}$ $p=7.9\text{mm}$ $d_h=5.47\text{mm}$ heated length 700mm max. heat flux 27W/cm^2	Water	- dimensions of the wake - mass exchange between wake and main flow - single-phase temperature distribution	9	
4	 Central impermeable permeable	41%			- dimensions of the wake - mass exchange between wake and main flow - single-phase temperature distribution	9	
	 permeable					- single-phase temperature distribution	10
5	 Wall impermeable	47%			- dimensions of the wake - mass exchange between wake and main flow - single-phase temperature distribution	9	
					- single-phase temperature distribution	10	
6	 Central impermeable permeable	41%	Half of a 169 pin bundle $d_p=6\text{mm}$, $p=7.9\text{mm}$ $d_h=5.47\text{mm}$ unheated	Water	- phenomenological study of the flow in the wake - influence of the pins and the grid on the flow in the wake	9 11	
7	 Wall impermeable	47%					
8	 Central impermeable	66%	169 pin bundle $d_p=6\text{mm}$, $p=7.9\text{mm}$ $d_h=5.47\text{mm}$ Water: heated length 700 mm max. heat flux 27W/cm^2	Water	- single-phase temperature distribution	10	
9	 Central impermeable	49%		Water	- single-phase temperature distribution	10	
				Sodium	- single-phase temperature distribution - boiling behaviour up to dryout - influence of gas in the wake	12 13 14	
				Water	- single-phase temperature distribution	15	
10	 Corner impermeable	21%		Sodium: heated length 300 mm max. heat flux 17W/cm^2	Sodium	- single-phase temperature distribution - boiling behaviour up to dryout - behaviour of gas in the wake	16 17 18
11	 Corner impermeable permeable	21%	Half of a 169 pin bundle $d_p=6\text{mm}$ $p=7.9\text{mm}$ $d_h=5.47\text{mm}$ unheated	Water	- phenomenological study of the flow in the wake - influence of the porosity of the blockage - influence of a grid in the wake	19	
12	 Central impermeable permeable	66%					
13	 Central impermeable	49%					
14	 Corner impermeable	21%				- behaviour of gas in the wake	20
15	 Corner permeable with variable leakage flow	21%	Half of a 169 pin bundle heated length 700mm max. heat flux 27W/cm^2	Water	- influence of leakage flow on the behaviour of gas in the wake - influence of leakage flow on the wake structure	21 22	
						- influence of leakage flow on the single-phase temperature distribution	23
16	 Blockage variable in size and porosity	10-70%	Half of a 169 pin bundle $d_p=6\text{mm}$, $p=7.9\text{mm}$ $d_h=5.47\text{mm}$ heated length 700 mm max. heat flux 27W/cm^2	Water	- phenomenological study of the flow in the wake - influence of size and porosity of the blockage - influence of leakage flow - influence of main flow velocity - influence of a grid in the wake - conditions of gas accumulation	24 26	
						- single-phase temperature distribution dependent on the size and porosity of the blockage	25 26

Table 1 Survey of the Blockages Investigated

		KNS-Test Section 1/2	SNR 300 Fuel Element	
			Mk I a	Mk II
Number of pins	-	169	169	127
Pin diameter	mm	6	6	7.6
Pin pitch	mm	7.9	7.9	8.8
Number of heated pins	-	88/90	166	124
Heated length	mm	290	950	950
Unheated length				
inlet	mm	385	1070	1070
outlet	mm	455	455	455
Width of hexagonal tube	mm	104.8	105.1	102.2
Type of spacer grid	-	honey comb	honey comb	honey comb
Max. heat flux	W/cm ²	170	187	188
Max. coolant velocity	m/s	4.3	4.3	5.6

Tab. 2: Technical Data of the KNS-Test Sections 1 and 2 and the Fuel Elements of the SNR 300

Coolant	Water		Sodium				
	Classification						
Parameter	F	S	S	B	G	S/G	B/G
Blockage No. 1)	13	9	9	9	9	9	9
q $[W/cm^2]$	-	27	9..200	42..200	-	5..135	76..135
v_o $[m/s]$	0,9..5,8	2,35..4,7	0,5..4	1..4,5	1..4	1..4	2..4
T_{in} $[^{\circ}C]$	20	18..21	400..580	530..590	400..590	400..580	530..590
\dot{V}_{GM} $[cm^3/s]$	-	-	-	-	90..1000	24..1000	130..1000
T_{Sat} $[^{\circ}C]$	-	-	-	890..930	-	-	920..930

1) see Tab. 1

Table 3 Range of Experimental Parameters with a 49 % Central Blockage in Water and Sodium

Coolant	Water		Sodium				
	Classification						
Parameter	F	S	S	B	G	S/G	B/G
Blockage No. 1)	11	10	10	10	10	10	10
q $[W/cm^2]$	-	27	3..110	27..173	-	5..74	47..127
v_o $[m/s]$	4	2,35..4,7	0,6..4,5	1..4	2..4,3	2..4	2..4
T_{in} $[^{\circ}C]$	20	22..28	400	420..625	400	400..590	580..590
\dot{V}_{GR} $[cm^3/s]$	-	-	-	-	5..18	5..19	1,4..7,2
\dot{V}_{GM} $[cm^3/s]$	-	-	-	-	50..1000	50..160	-
v_{GR} $[cm^3]$	-	-	-	-	-	50..200	-
$t_{0,5}$ $[s]$	-	-	-	-	-	0,4..6	-
T_{Sat} $[^{\circ}C]$	-	-	-	904..930	-	-	930
L $[\%]$	0-24	-	-	-	-	-	-

1) see Tab. 1

Table 4 Range of Experimental Parameters with a 21 % Corner Blockage in Water and Sodium

Classification Parameter	Classification			
	G	F	G	S
Blockage No.	14	15	15	15
q [W/cm]	-	-	-	2,5..26
v _o [m/s]	1,2..4,5	1,2..5,9	1,2..5,9	0,6..5
T _{in} [°C]	20	20	20	15..23
\dot{V}_{GR} [Ncm ³ /s]	1..20	-	1..20	-
\dot{V}_{FM} [Ncm ³ /s]	10..230	-	10..230	-
V _{GR} [cm ³]	150	-	150	-
L [%]	-	0..8	0..8	0..9

Table 5 Range of Experimental Parameters with a Porous 21 % Corner Blockage in Water

Classification Parameter	Classification					
	F	G	S	F	G	S
Type of Blockage	Central			Corner		
Blockage Size %	4..69	10..69	10..69	2..74	2..74	9..64
q [W/cm ²]	-	-	27	-	-	4..27
v _o [m/s]	0,5..6	1..4	1..4	0,5..6	1..6	1..4
T _{in} [°C]	20	20	20..36	20	20	20..36
\dot{V}_{GR} [cm ³ /s]	-	1..200	-	-	0..112	-
L [%]	0..33	-	0..45	0..17	-	0..18

Table 6 Range of Experimental Parameters with a Variable Blockage in Water

Run No	Blockage		Coolant	Main Flow Velocity	Heat Flux	Inlet Temp.	Ref.
	Size	Type		m/s	W/cm ²	°C	
278	21%	Corner	Sodium	4	101	397	16
20A	49%	Central	Sodium	3.8	129	589	13
21.23	21%	Corner	Water	3.5	28	25	10
21P72	21%	Corner	Water	4.0	2.6	16	23
49.05	49%	Central	Water	3.5	27.5	20	10
21E01D	21%	Corner ¹⁾	Water	3.0	27.4	24	26
49201D	49%	Central ¹⁾	Water	3.0	27.5	28	26

1) Test section with variable blockage

Table 7 Conditions of the Experiments Represented in Figure 19

Type of blockage	Expt. No.	Run No.	v_o	q	T_{in}	T_{sat}	dT/dz	ΔT_e	$\Delta \theta_e$	Heated pins
			m/s	W/cm ²	°C	°C	K/m	K	m	
49 % Central blockage	17/3	*	3,68	131,9	587	922	257	0	0	88
		22A	1,91		587	914	495	319	0,644	
		22B	1,81		584	914	524	355	0,677	
		22C	1,71		583	913	554	394	0,711	
		22D●	1,63		583	913	580	427	0,763	
	17/7	56A	3,47	134,2	579	921	277	-8	0	88
		*	3,38		579	921	285	0	0	
		56B	3,34		577	921	288	3	0,012	
		56D								
		56E	2,83		577	919	339	66	0,196	
		56F	1,93		579	914	496	262	0,529	
	56G●	1,68		578	913	570	351	0,617		
	32/2	58A	4,04	170	577	925	300	-4	-0,013	88
		*	4,00		577		303	0	0	
		58B	2,33		579	917	519	257	0,495	
		58C	2,14		580	916	555	312	0,552	
		58D●	1,96		579	916	596	346	0,581	
	43/2	98A	1,50	67,5	574	916	323	-33	-0,101	85
		*	1,50	75,4	571		360	0	0	
		98B	1,50	79,9	571		381	20	0,052	
98C		1,50	90,2	570		431	66	0,153		
98D●		1,50	97,3	571		464	98	0,212		
44/1	116A	1,03	50,0	588	912	349	-40	-0,114	83	
	*		58,3	581		406	0	0		
	116B		59,4	585		414	10	0,024		
	116C		64,7	581		449	34	0,077		
	116D●		69,7	581		483	62	0,128		
21 % Corner blockage	214/1	*	4,00	120,5	426	928	204	0	0	90
		390		121,6	425		206	5	0,024	
		391		152,3	424		258	132	0,513	
		392		157,1	422		266	150	0,564	
		393●		165,0	422		279	182	0,652	
	214/2	396	3,00	91,6	429	928	207	-17	-0,080	90
		397*		95,1	427		215	0	0	
		398		105,2	425		237	49	0,208	
		399		115,7	426		261	106	0,407	
		400		120,3	425		272	131	0,481	
		401		126,3	429		286	167	0,585	
		402		131,9	428		298	194	0,652	
		403●		135,0	427		305	210	0,688	
	215/1	451	3,02	81,5	500	928	189	-11	-0,056	89
		*		84,2	499		194	0	0	
		452		85,4	498		197	5	0,025	
		453		95,8	498		222	60	0,271	
		454		105,2	498		243	107	0,439	
		455		111,7	498		258	140	0,541	
		456		116,3	498		269	164	0,610	
		457		123,7	499		286	203	0,708	
	458●		128,2	498		296	224	0,755		
	215/2	459	2,01	60,9	504	930	212	-18	-0,085	89
		*		63,7	505		221	0	0	
		460		64,6	504		224	5	0,022	
		461		72,1	504		250	55	0,220	
		462		79,1	503		275	102	0,371	
		463		84,1	505		292	137	0,469	
464			88,3	504		307	165	0,536		
465			93,0	505		323	196	0,608		
466●		97,0	505		337	227	0,673			
216/2	478	3,03	61,7	584	929	146	-12	-0,081	89	
	*		64,8	582		152	0	0		
	479		66,0	583		156	10	0,064		
	480		75,1	582		178	59	0,333		
	481		85,6	582		203	116	0,573		
	482		91,5	581		217	147	0,678		
	483		96,9	580		229	174	0,758		
	484		102,7	581		243	207	0,850		
	485●		106,8	581		253	229	0,907		
	216/3	486	2,02	46,6	590	928	166	-15		-0,089
*			49,3	588		175	0	0		
487			64,1	588		228	104	0,456		
488			68,3	588		243	133	0,548		
489			71,3	588		253	153	0,603		
490			75,0	587		266	177	0,665		
491●			79,1	588		281	207	0,737		
224/3	*	3,82	74,1	629	929	141	0	0	86	
	642		76,2	628		145	8	0,054		
	643		81,3	629		155	30	0,195		
	644		133,2	626		253	236	0,932		
	645●		155,4	627		296	328	1,110		

* Conditions at the start of boiling

● Conditions at the onset of permanent dryout

Tab.8 Conditions of Experiments in which Permanent Dryout Occurred

Type of Blockage	Expt. No	Run No. in which dryout occurred	Flow	Power	Geometry of the Boiling Region						Vapour Flow	
			v_o	q	V_B [cm ³]		S_B [cm ²]		L_B [cm]		v_{vr}	v_{va}
			m/s	W/cm ²	max	min	max	min	max	min	m/s	m/s
49 % Central Blockage	17/3	22D	1.63	132	220	90	258	140	7.5	3.7	10.4	19
	17/7	56G	1.68	134	270	183	280	208	8.5	7	12.9	26.7
	32/2	58E	1.96	170	338	132	301	299	8	7.5	13.7	33.9
	43/2	98D	1.5	97	243	70	196	104	9	3	10.4	15
	44/1	116D	1.0	70	173		161		10		7.9	18
21 % Corner Blockage	214/1	393	4	165	19		55		5.1		5.8	21.7
	214/2	403	3	135	45		72		6.1		8.7	21.2
	215/1	458	3	128	52		68		6.2		10.0	20.4
	215/2	466	2	97	72		73		8		10.0	20
	216/2	485	3	107	67		89		6.7		8.3	18.4
	216/3	491	2	79	62		73		8		7.1	16.3
	224/3	645	3.8	155	97	54	93	69	7.4		15.0	29.5

Table 9 Experimental Dates During Dryout Conditions

	Blockage	KfK				ECN		
		Central 49 %		Corner 21 %		Corner 21 % (permeable)	Central 34.4 %	Central 68.5 %
Experiments	Medium	Sodium		Sodium		Water	Sodium	
	Inlet temp. [$^{\circ}\text{C}$]	≈ 400		≈ 400		≈ 17.5	493	494
	Run No.	1	6	282	287	21P 32-37	250	72
	Flow velocity [m/s]	4	1	1	4	5	1.86	1.5
	Leakage flow [%]	-	-	-	-	7-1	-	-
Codes and Calculations	ASFRE (PNC)	x	x	x	x	x		
	SABRE (UKAEA)	x	x	x	x	x	x	x
	BACCHUS (KfK)	x						
	CAFCA (EdF)	x	x				x	x
	MICHELLE (CNEN)	x						

Table 10 Benchmark Calculations with Local Blockages (9th and 10th Meeting of the LMBWG)

Type of Blockage		Corner Blockage						Central Blockage				
Blockage Size	%	9	10	15.5	30	33	45	12	25	43	50	70
DND Signal safely to be detected	1.*	x	x	x	x	x	x	x	x	x	x	x
	2.*	-	-	x	x	x	x	-	-	x	x	x
Boiling temperature reached first locally	°C	-	x	-	-	-	-	-	x	-	-	-
Max. fictitious temperature reached locally	°C	-	-	1200	1325	~1400	~1880	-	-	1200	1370	1490
Vol. at boiling	cm ³	-	~0	5	20	30	140	~0	0	18	31	140
Vol. at boiling during the local onset of dryout	cm ³	-	~0	5	20	30	~140	0	0	18	31	140
Vol. at risk of melting	cm ³	-	0	0	<1.4	17.5	~60	0	0	~0	8	85
Fuel involved in the wake above boiling temp.	g	-	0	25	100	150	~700	0	0	90	155	700
Fuel involved in the wake above fictitious dryout temp. of 1200°C	g	-	0	~0	<7	87	~300	0	0	~0	40	425

1.* Blockage mainly consisting of fuel

2.* Blockage consisting of foreign matter without fuel, the cooling disturbed region partly molten

Tab.11 Summarized Values from the Discussion of the SNR 300 MkIa Subassembly Case

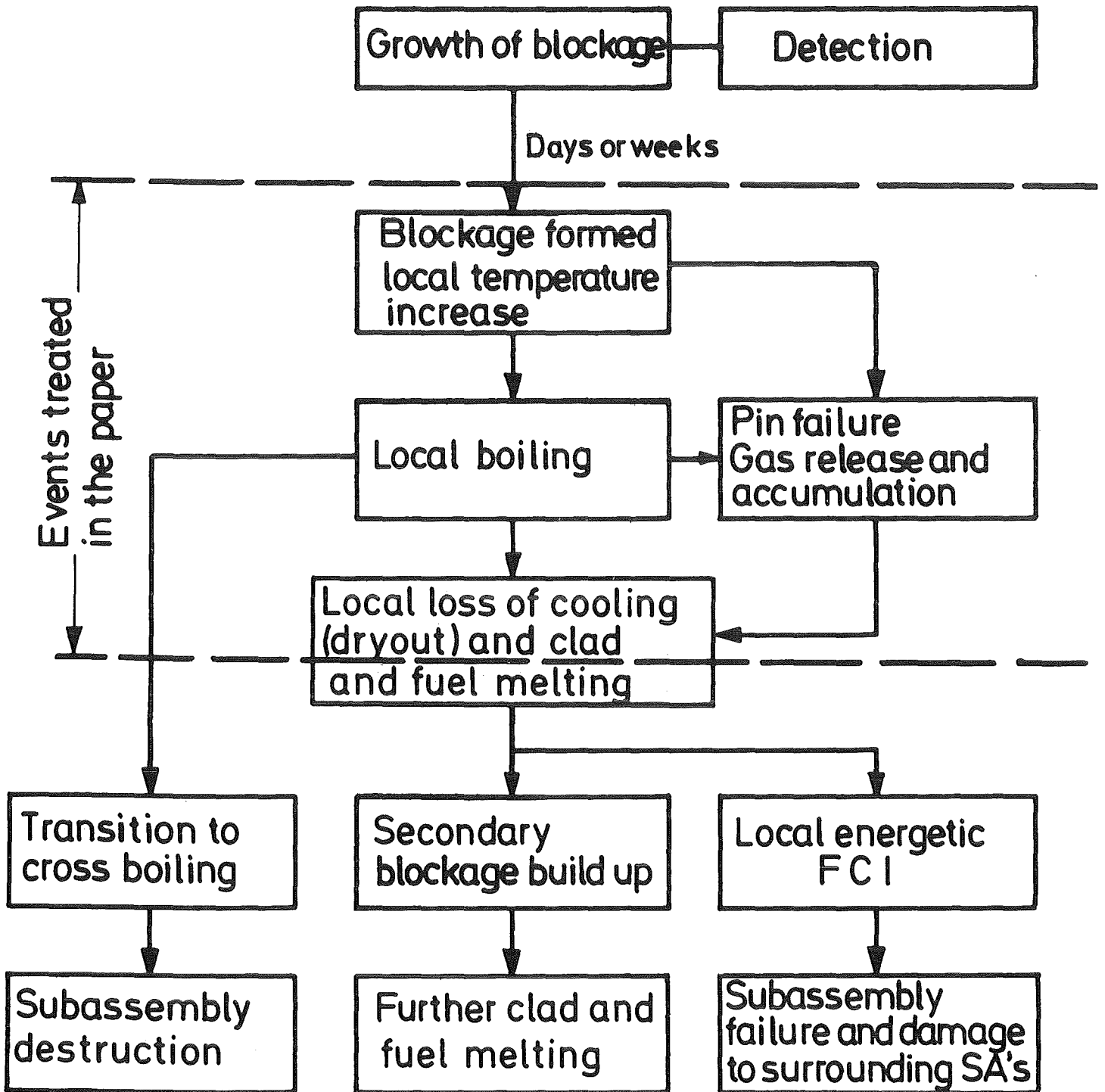
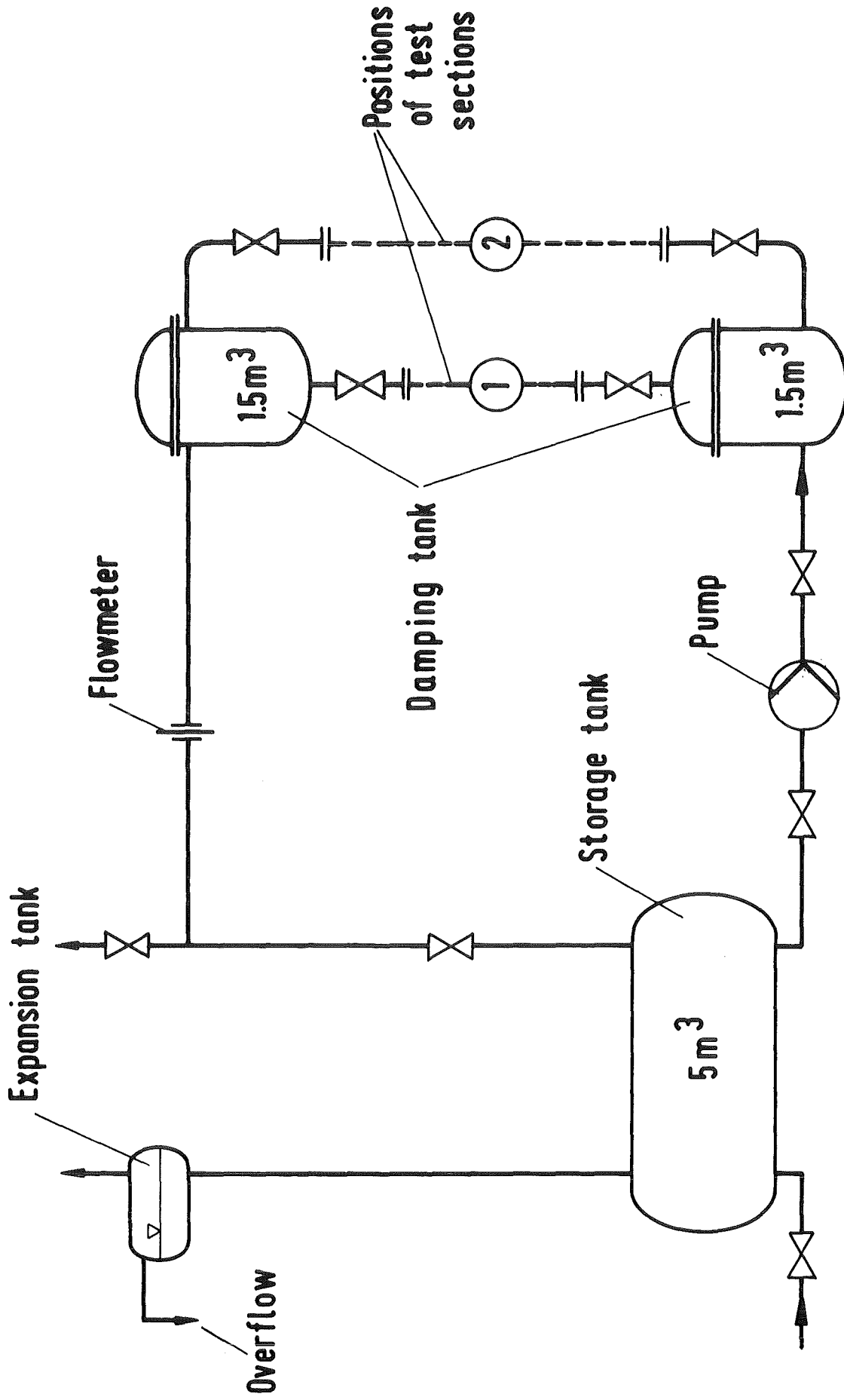


Fig.1 Local Blockages in Subassemblies: Chain of Events



KJK
KJIRE 847863

Fig. 2 Schematic Diagram of the Water Loop

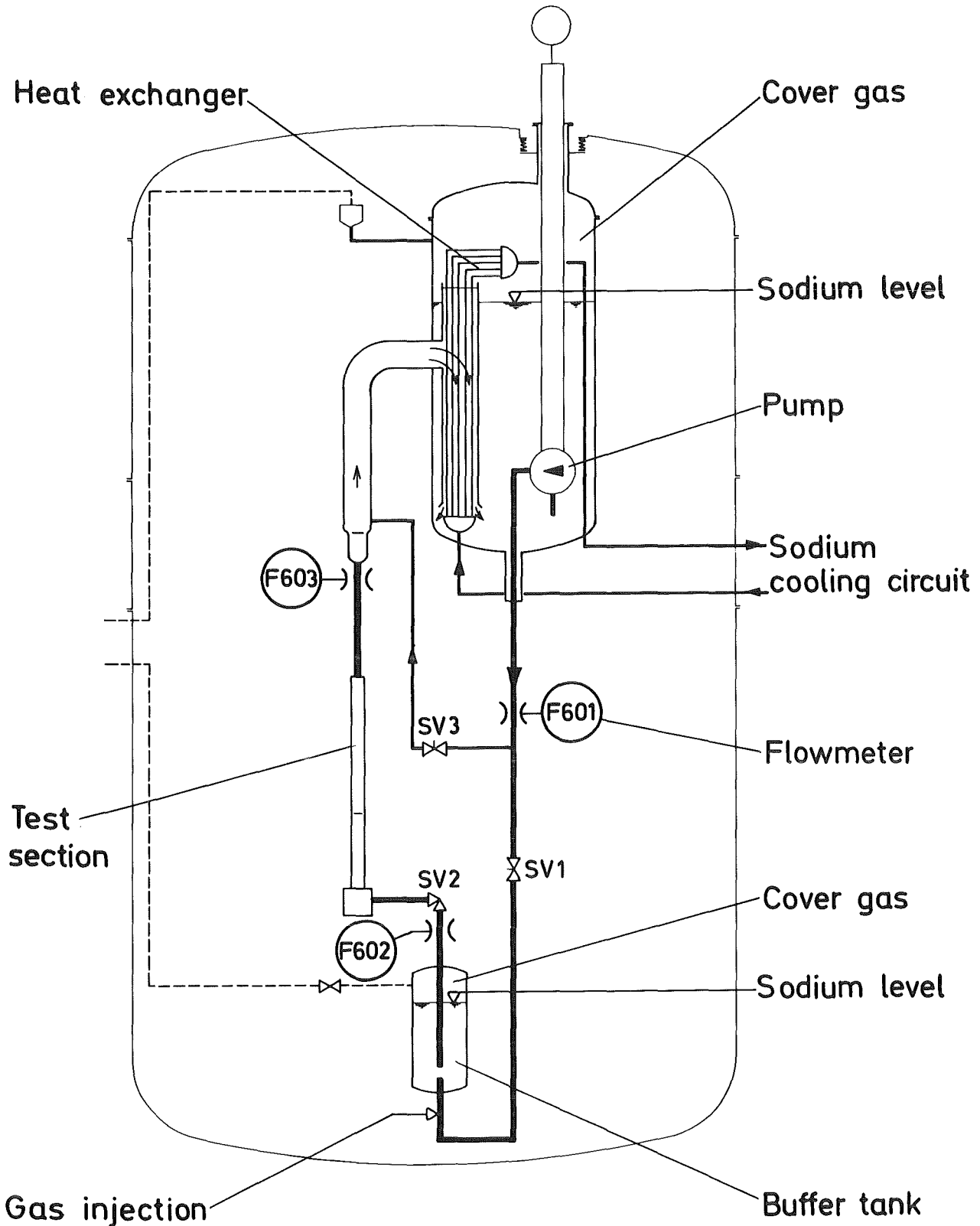


Fig.3 Schematic Diagram of the KNS Sodium Loop

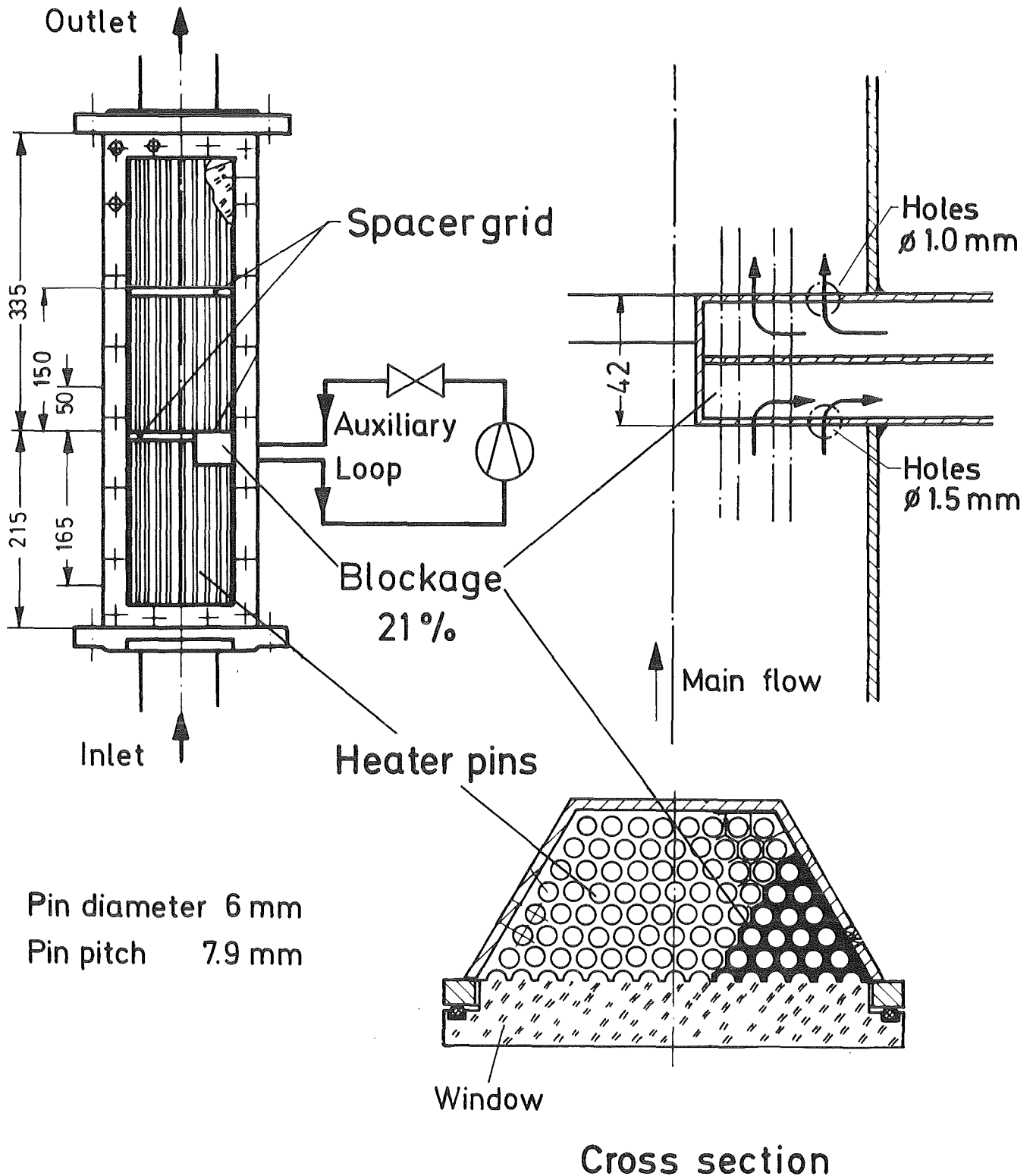
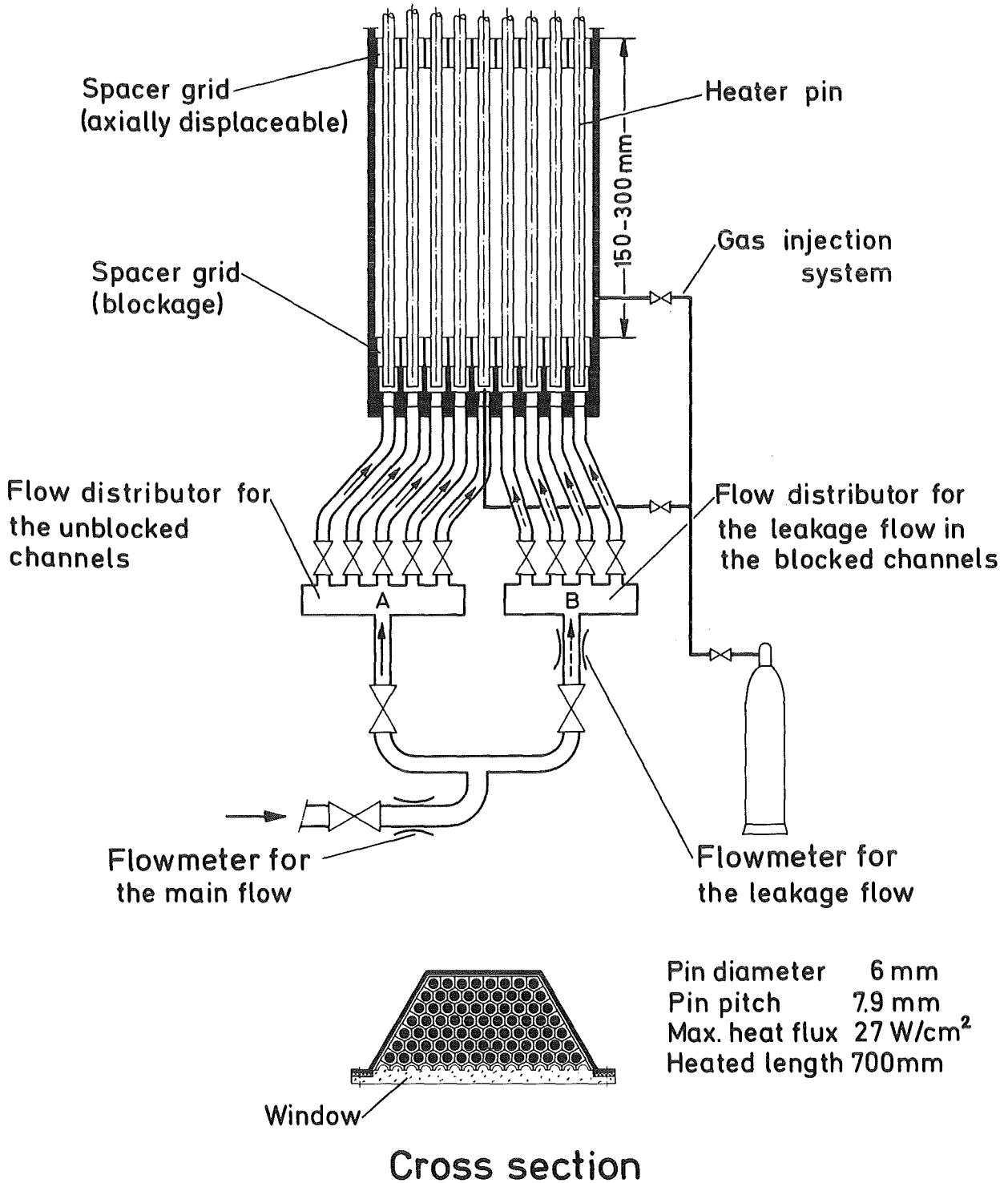


Fig.4 Water Test Section with a 21% - Corner Blockage of Variable Porosity



KIK IRE847860

Fig.5 Schematic Diagram of the Test Section with Variable Blockage

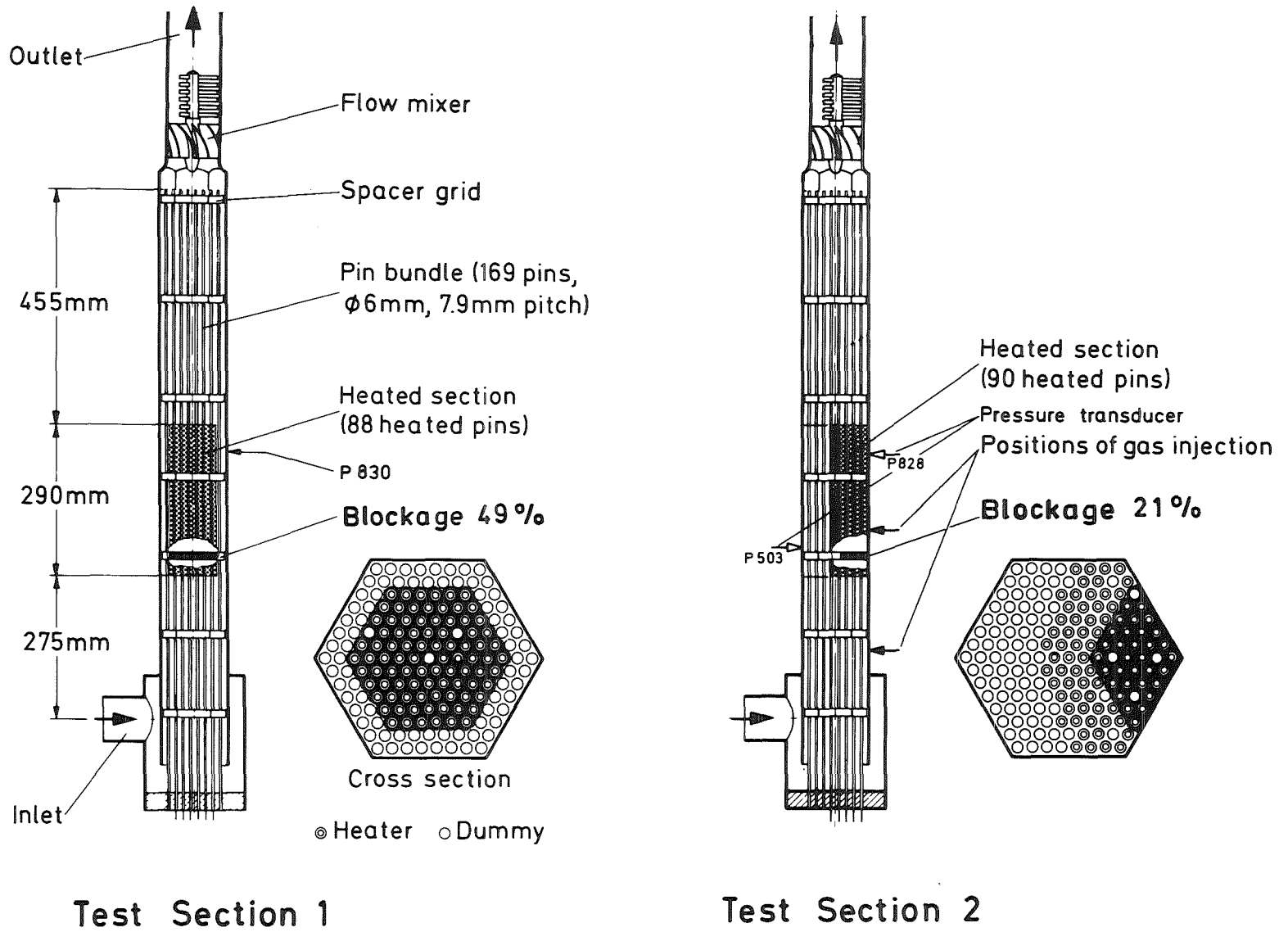


Fig.6 KNS - Test Sections 1 and 2

49% - Central blockage

21% - Corner blockage

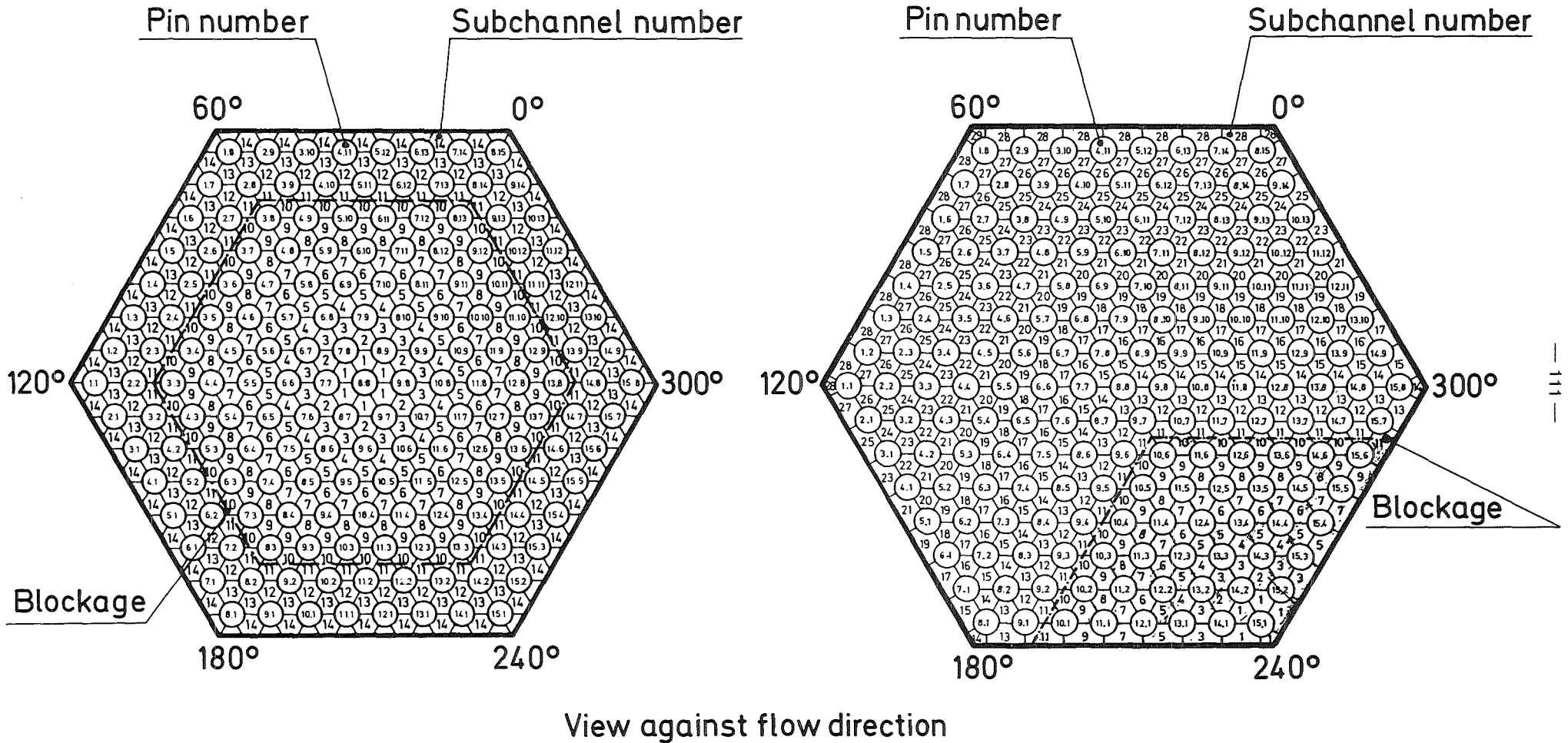


Fig.7 Subchannel and Pin Reference Identification

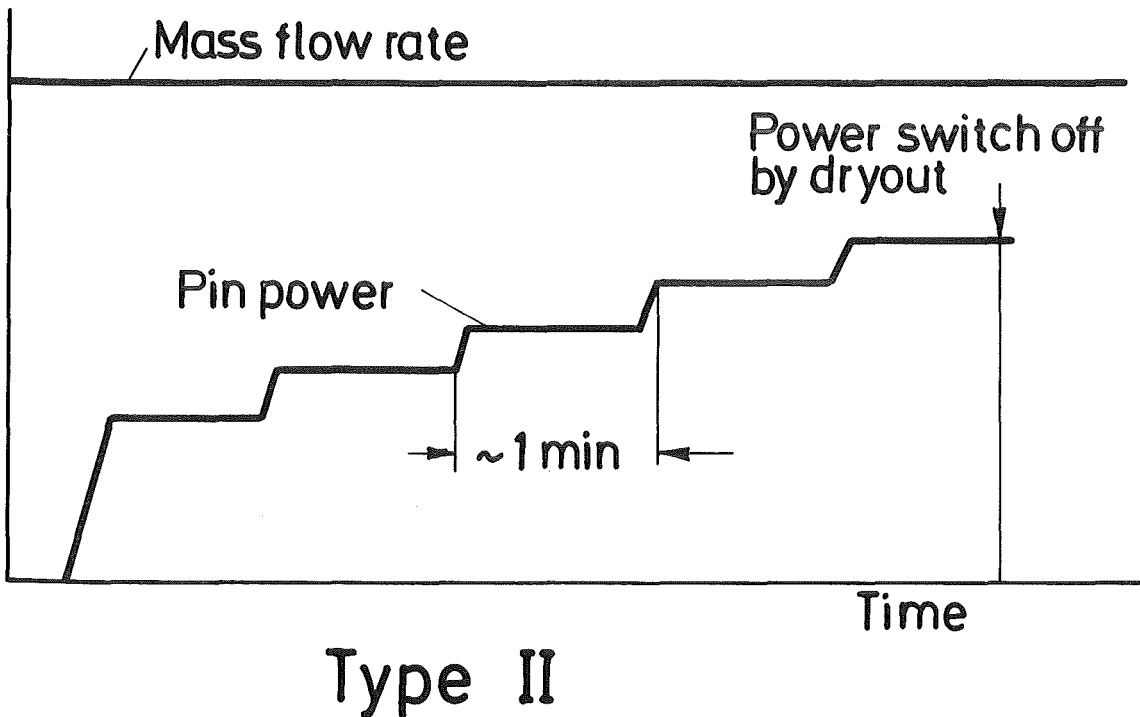
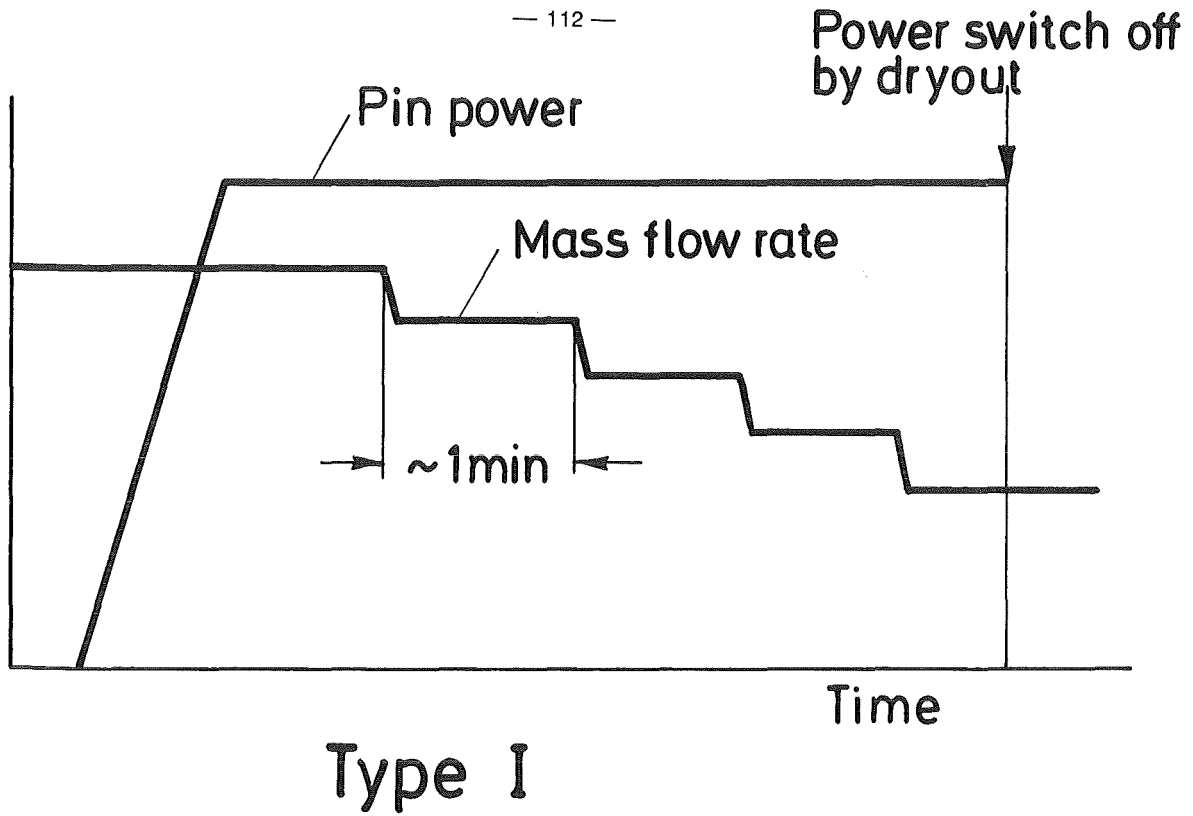
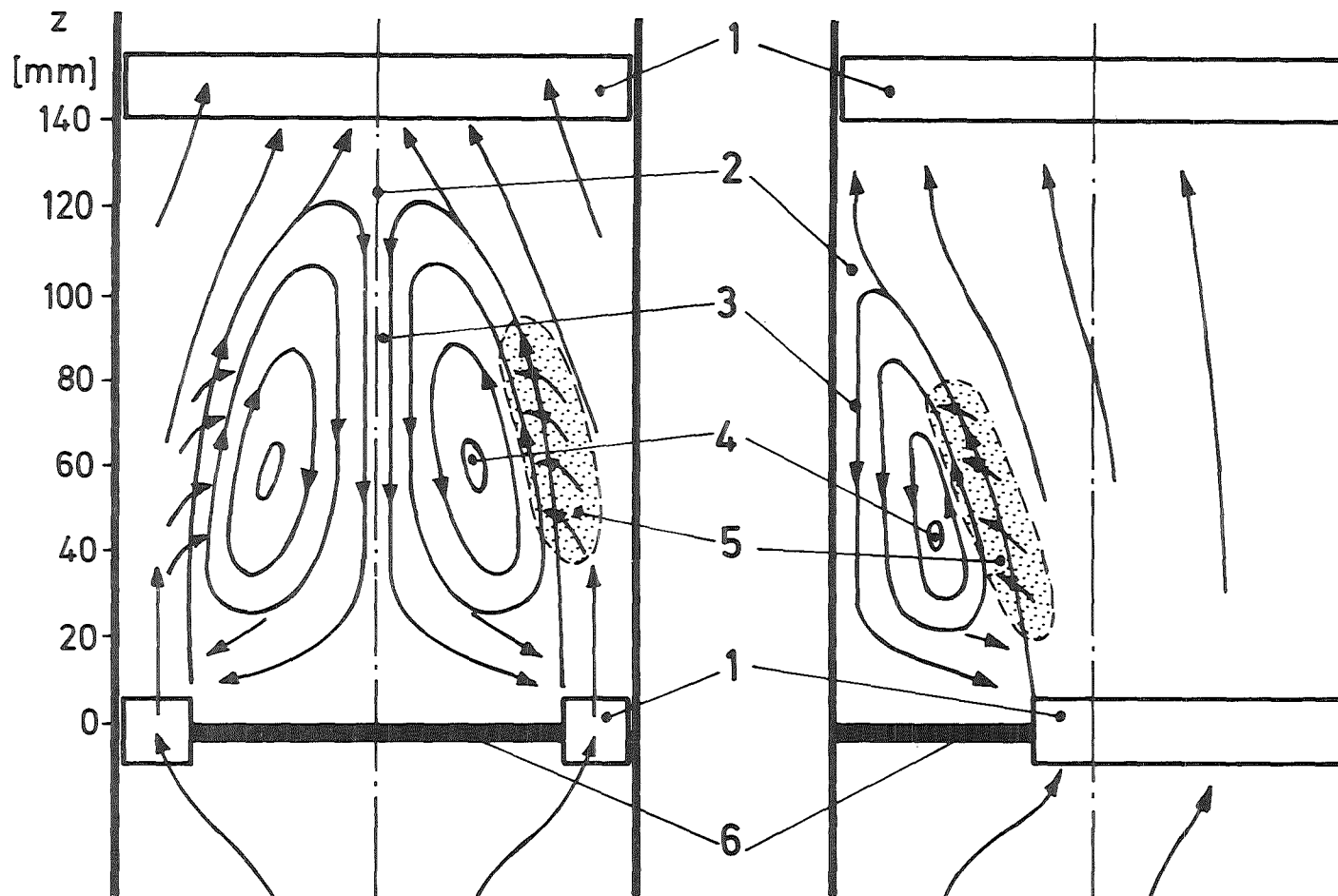


Fig.8 Local Boiling Experiments
Experimental Procedures



49%-Central blockage

1 Spacer grid

2 Upper stagnation point

3 Reverse flow

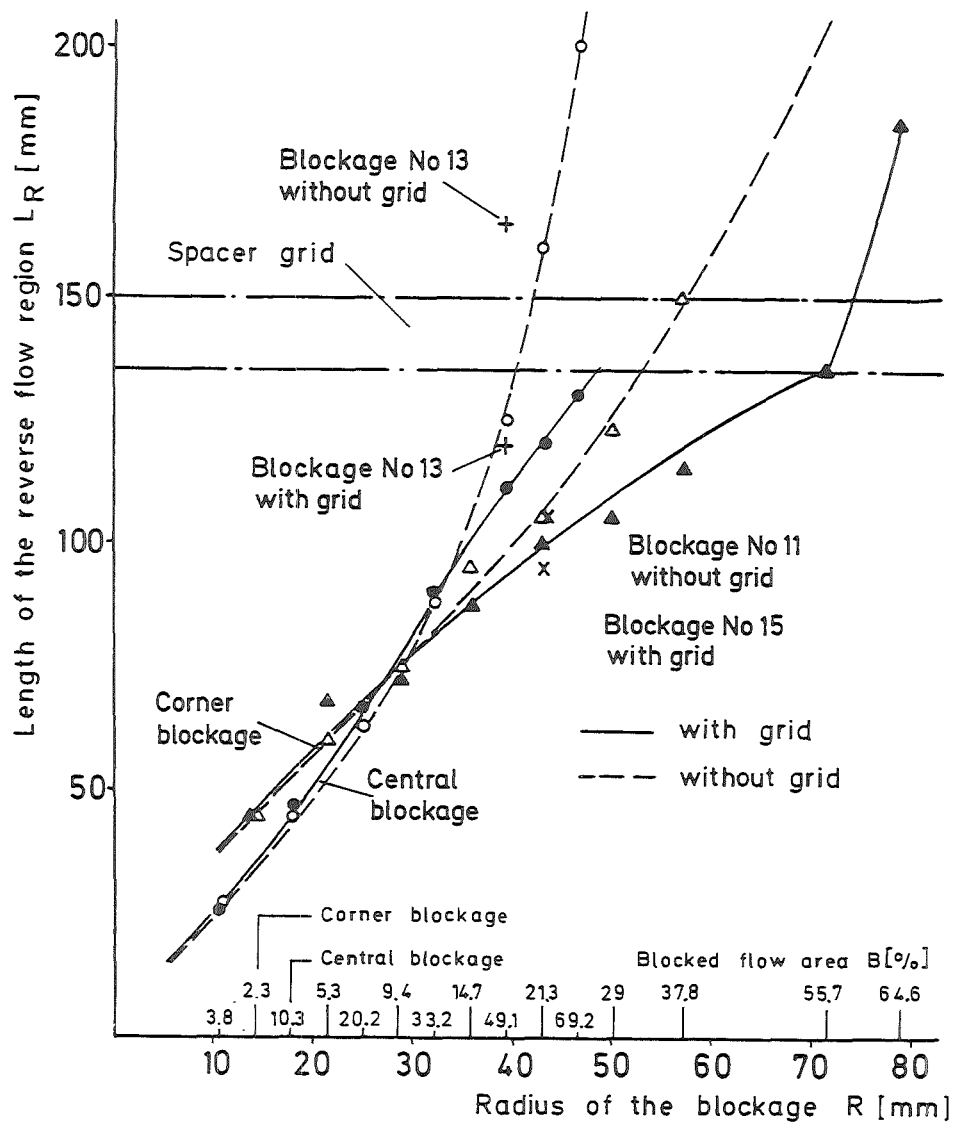
21%-Corner blockage

4 Centre of the vortex

5 Mixing zone between main flow and recirculating flow

6 Blockage

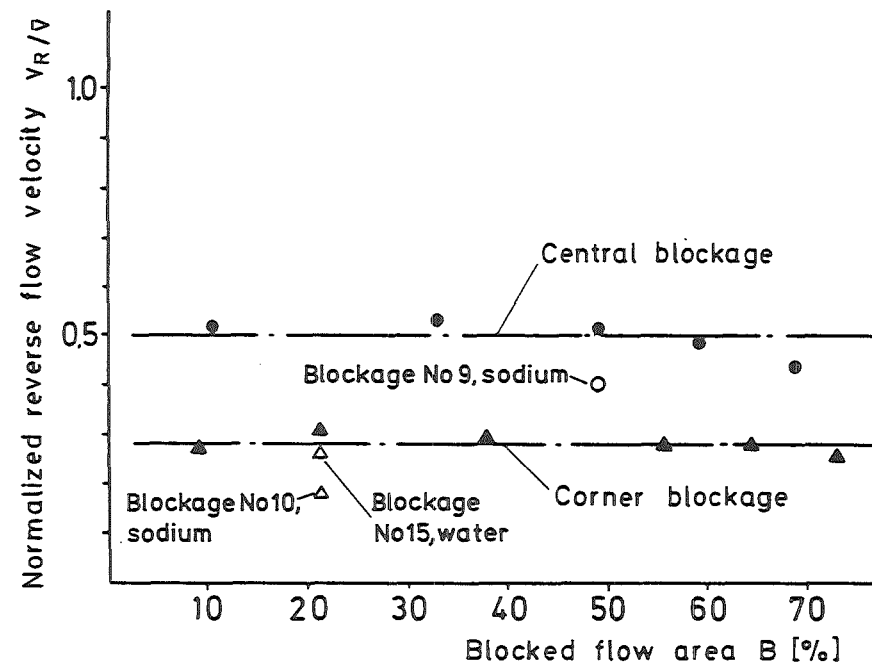
Fig.9 Typical Flow Pattern Behind a Central Blockage and a Corner Blockage



Results from blockage No 16 at $v_0 = 3\text{m/s}$

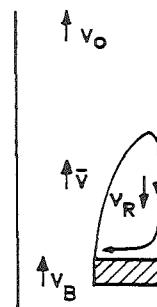
IRE 847857

Fig.10 Length of the Reverse Flow Region Dependent on the Blockage Radius



$$\bar{v} = \frac{v_0 + v_B}{2} = \frac{v_0}{2} \cdot \frac{200 - B}{100 - B}$$

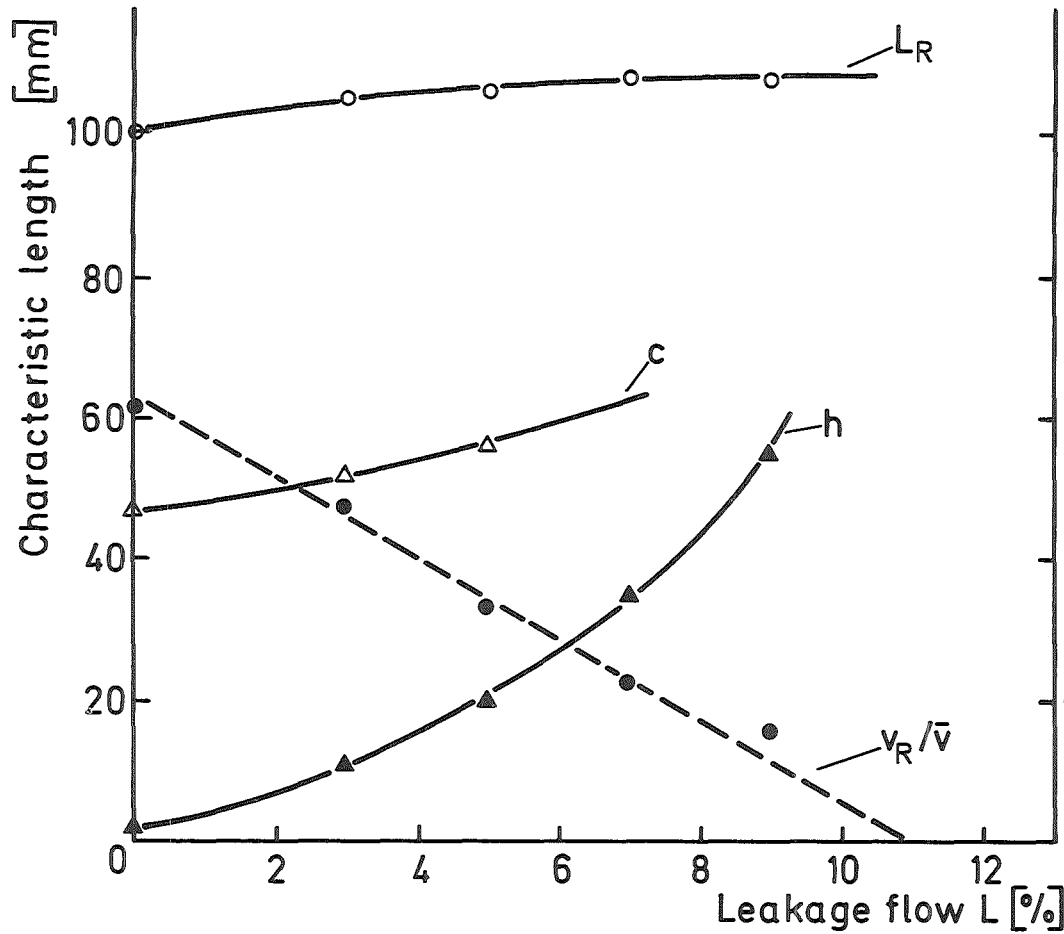
$$\frac{v_R}{\bar{v}} = \frac{v_R}{v_0} \cdot \frac{2(100 - B)}{200 - B}$$



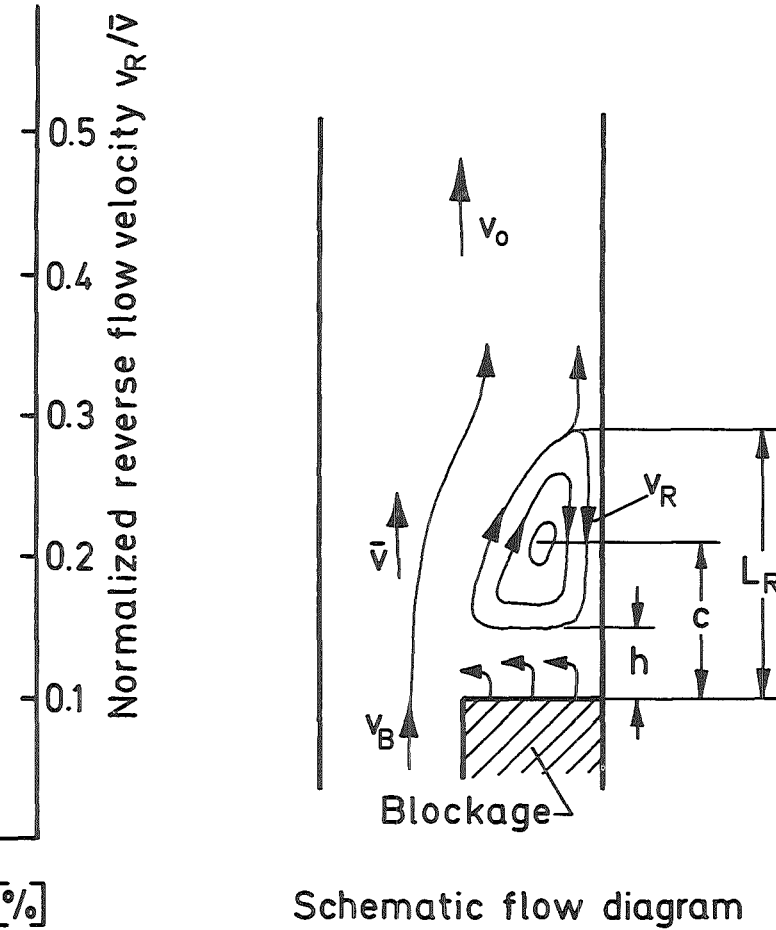
Results from blockage No 16

IRE 847856

Fig.11 Influence of the Size of the Blockage on the Reverse Flow Velocity



Main flow velocity $v_0 = 3\text{m/s}$
 21% -Corner Blockage



Schematic flow diagram

Fig.12 Influence of the Leakage Flow on the Wake Geometry and Reverse Flow Velocity

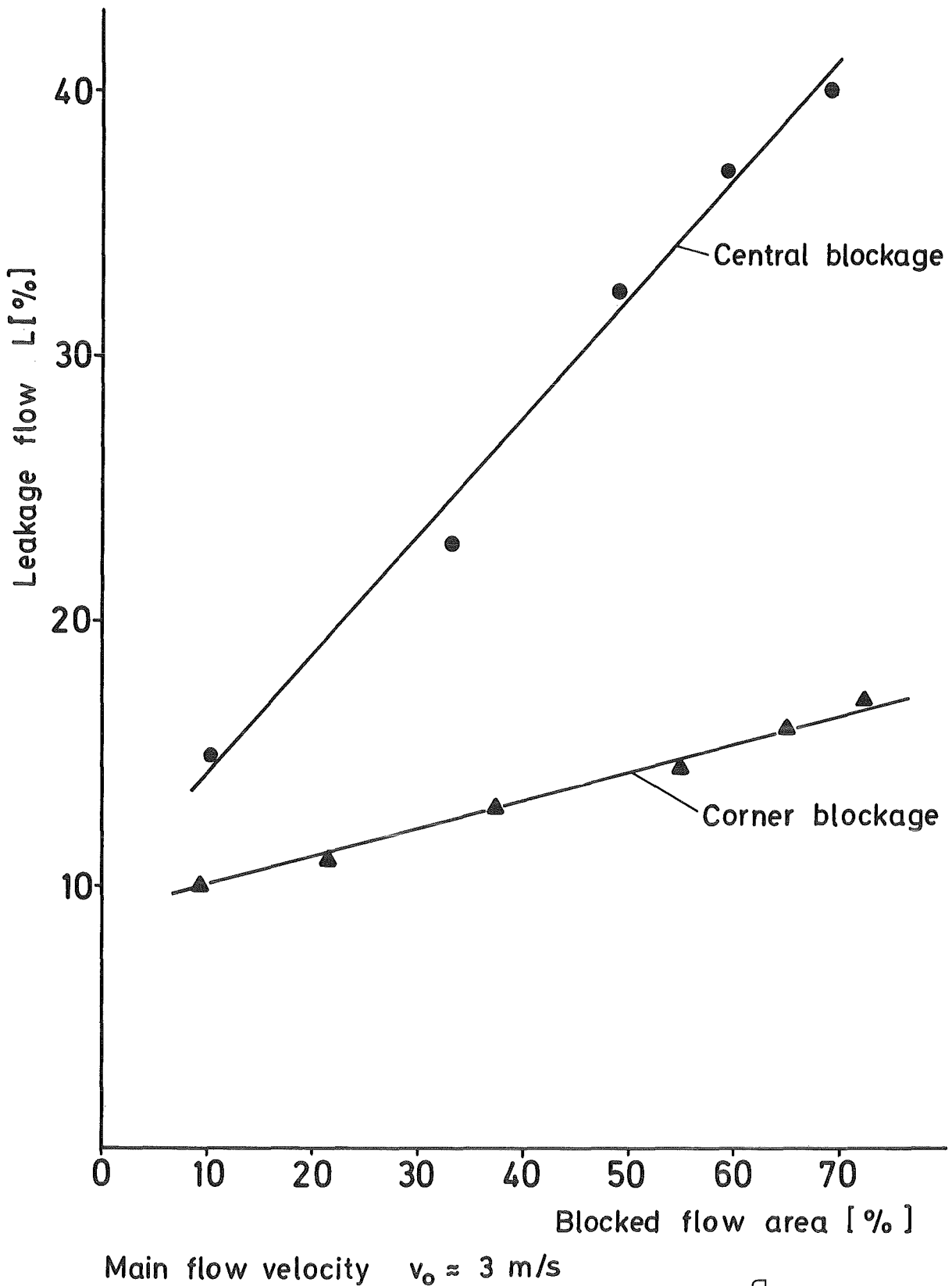
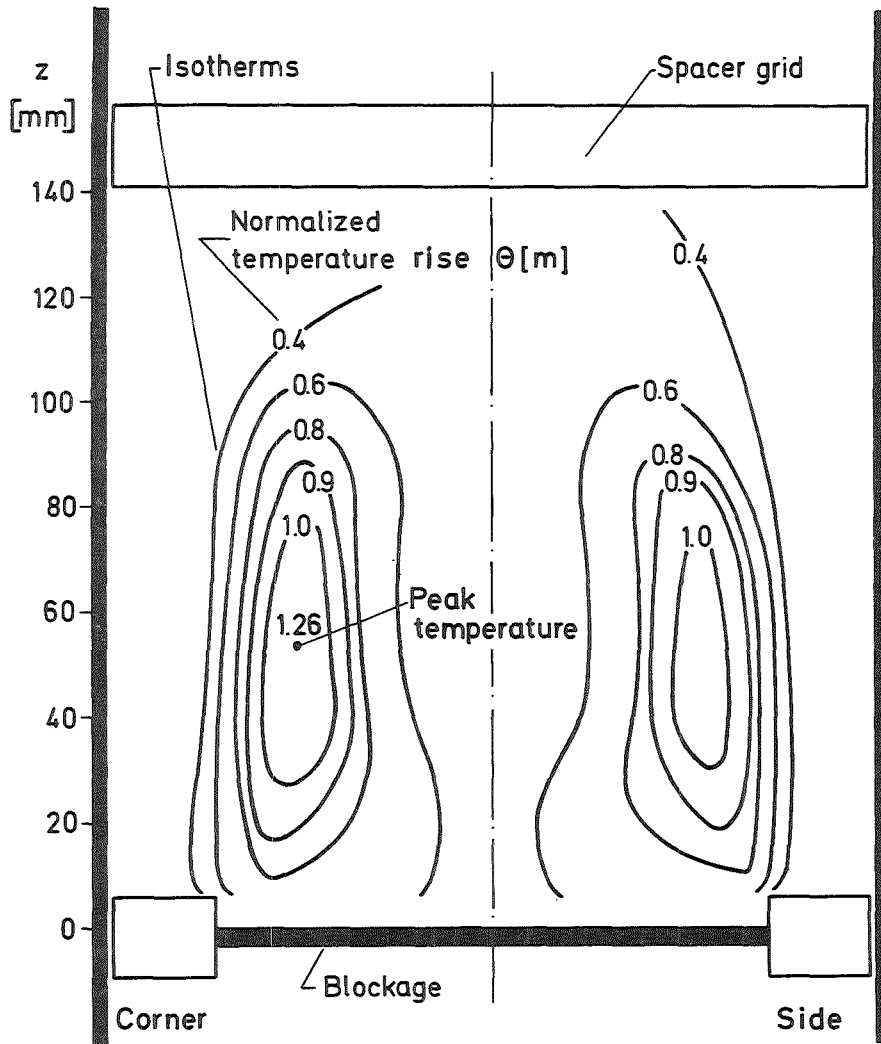
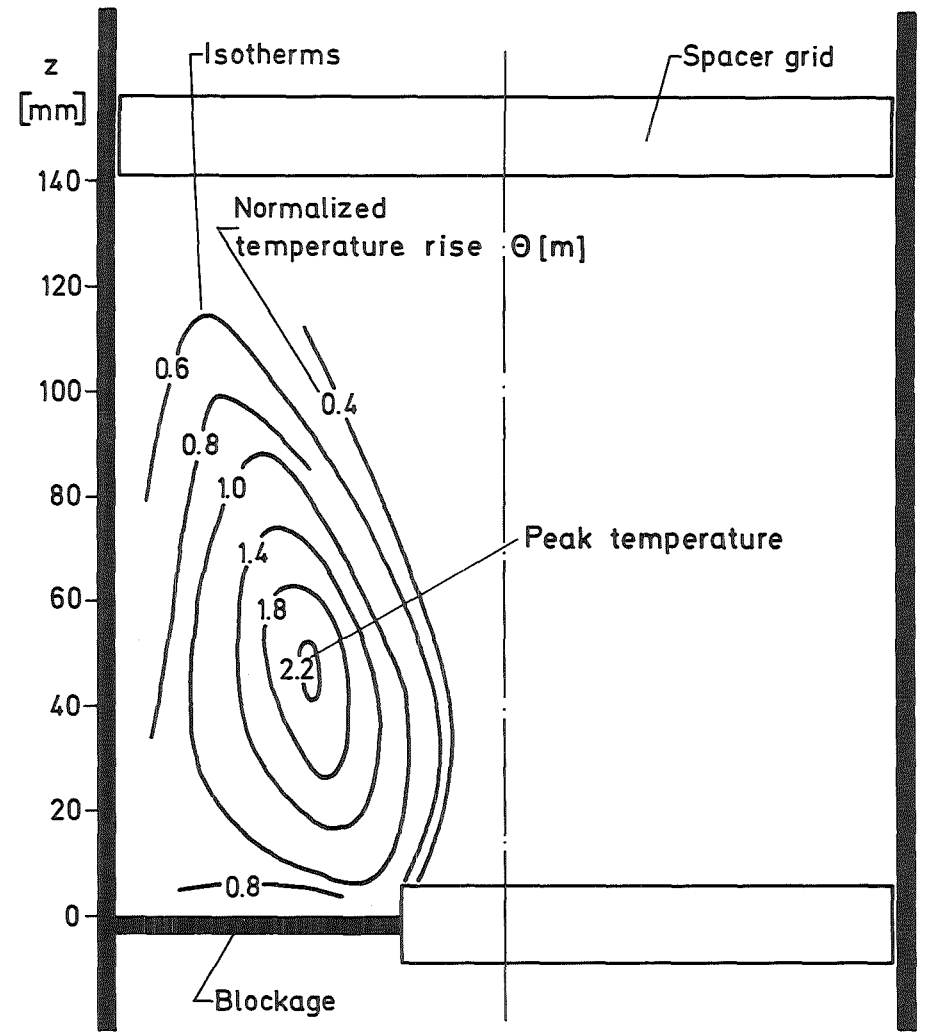


Fig.13 Leakage Flow Causing the Dissolution of the Reverse Flow



IRE847853

Fig.14 Normalized Temperature Field behind the 49% Central Blockage

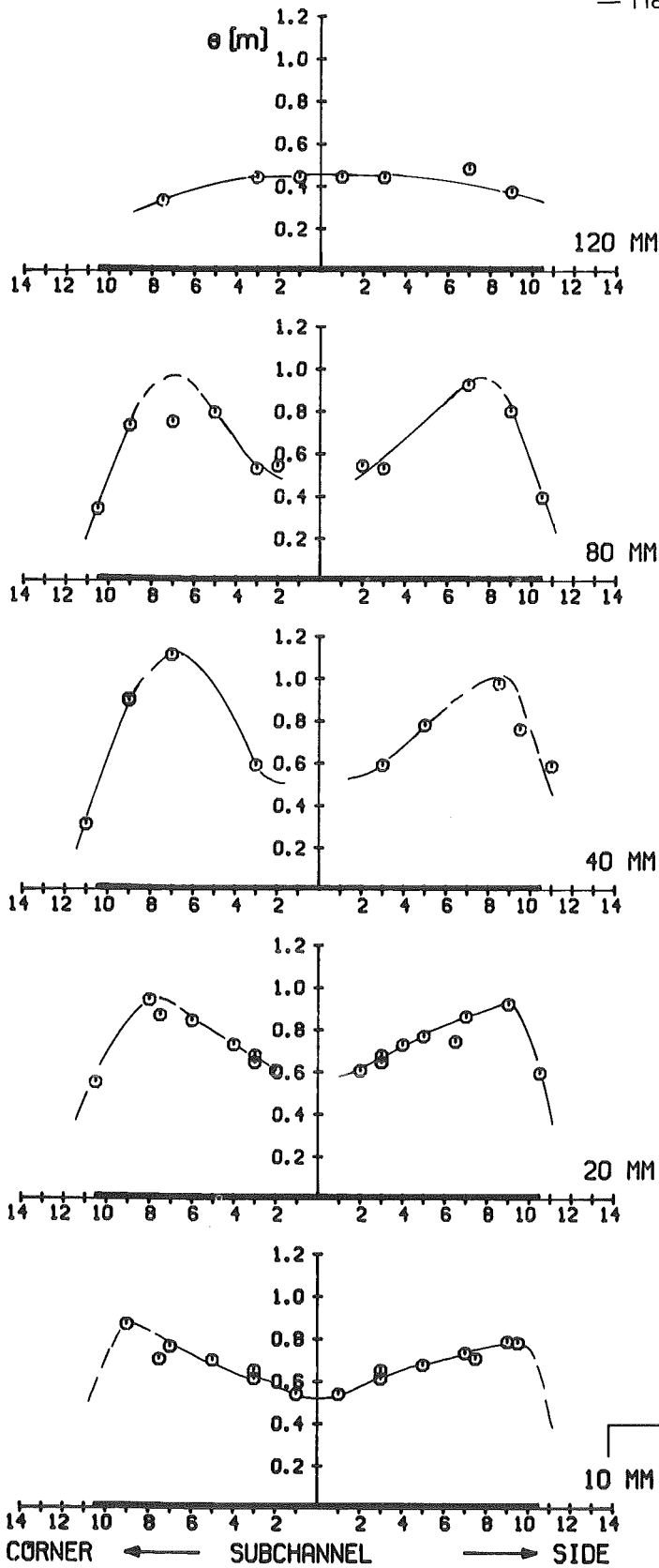


IRE847852

Fig.15 Normalized Temperature Field behind the 21% Corner Blockage

TEST 17/1
RUN 20A

HEAT FLUX: 129.28 W/CM²
INLET TEMP.: 589.34 DEG C
FLOW VELOCITY: 3.80 M/S
TEMP. GRADIENT: 244 K/M



49% Central Blockage
Fig.16 Normalized Temperature Profiles just before Boiling

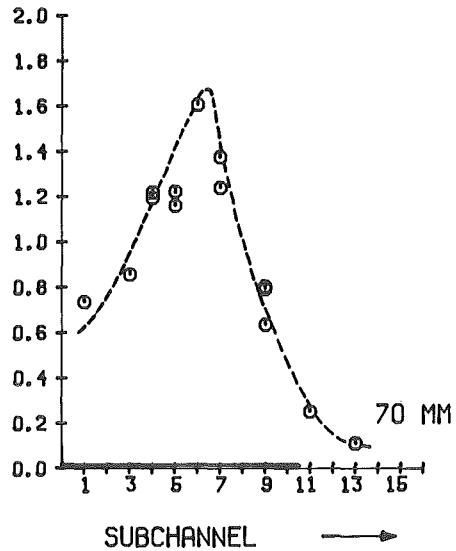
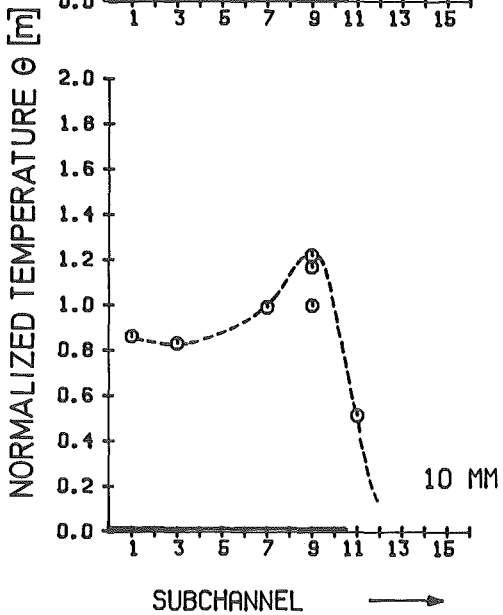
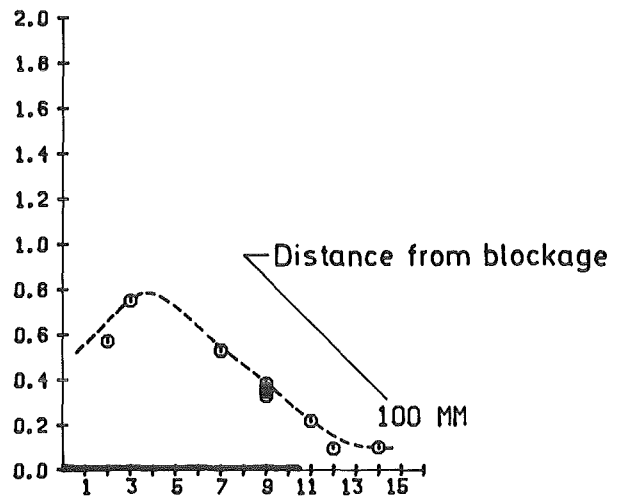
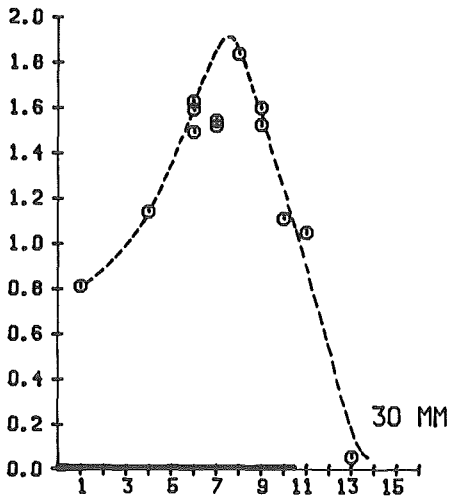
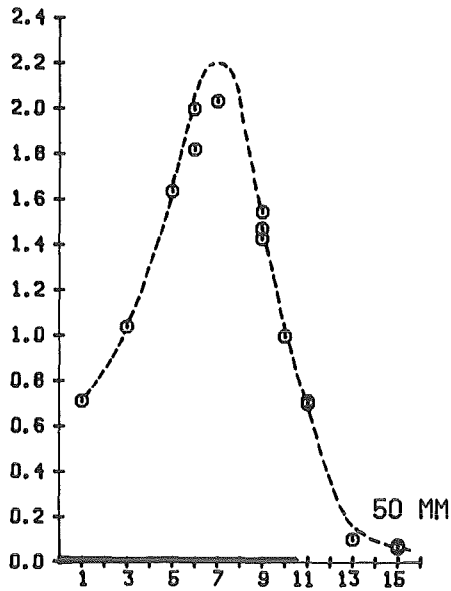
TEST 208/6F2 RUN 278

HEAT FLUX: 100.75 W/CM²

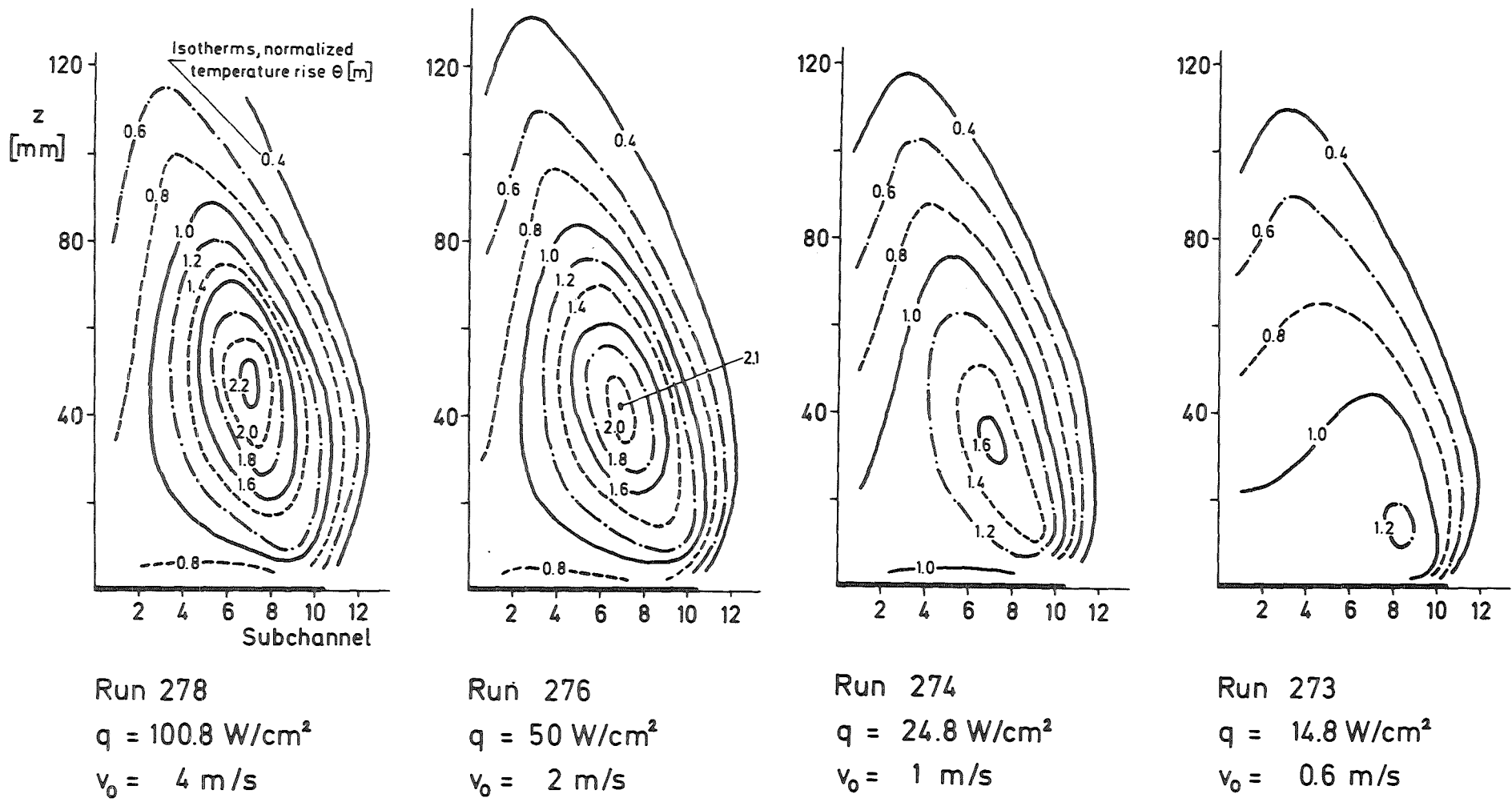
INLET TEMP.: 396.5 DEG C

FLOW VELOCITY: 4.00 M/S

TEMP. GRADIENT: 168.57 K/M



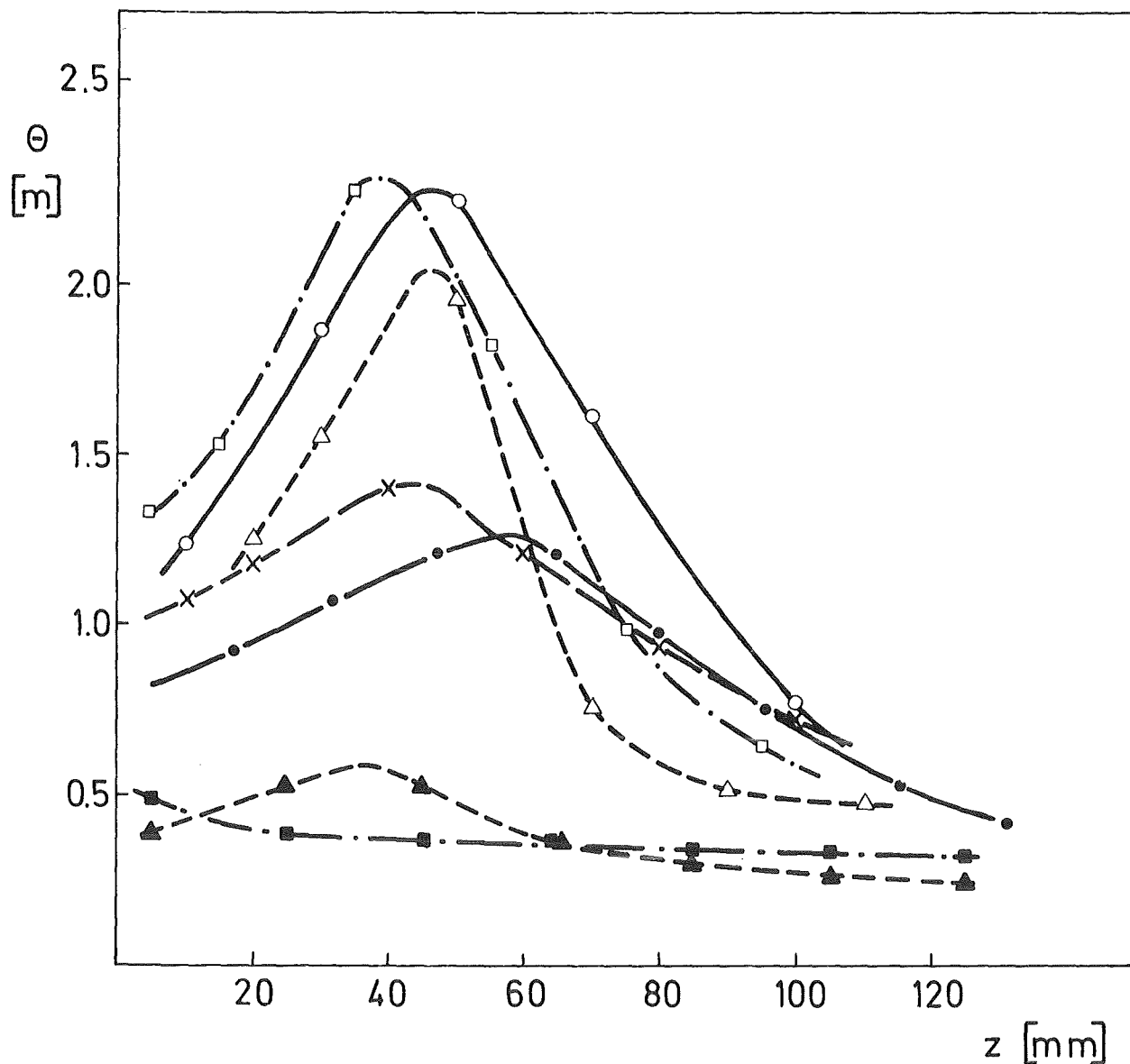
21% Corner Blockage
Fig.17 Normalized Radial Temperature Profiles



KNS-Test Section 2

KfK IRE 847849

Fig.18 Influence of Main Flow Velocity on the Temperature Field



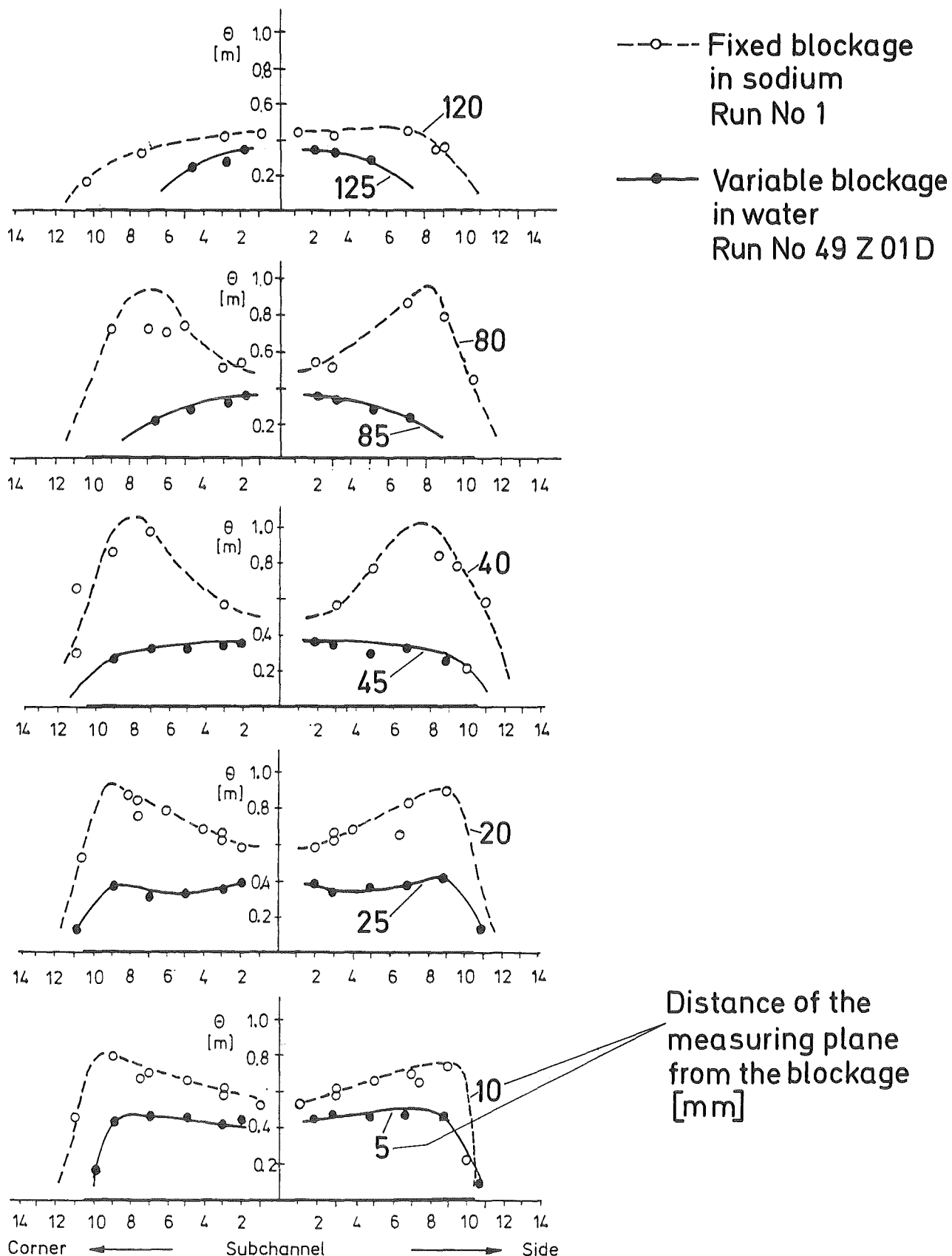
21% Corner Blockage

49% Central Blockage

- Blockage No 10, Sodium
- △ Blockage No 10, Water
- Blockage No 15, Water
- ▲ Blockage No 16, Water

- Blockage No 9, Sodium
- × Blockage No 9, Water
- Blockage No 16, Water

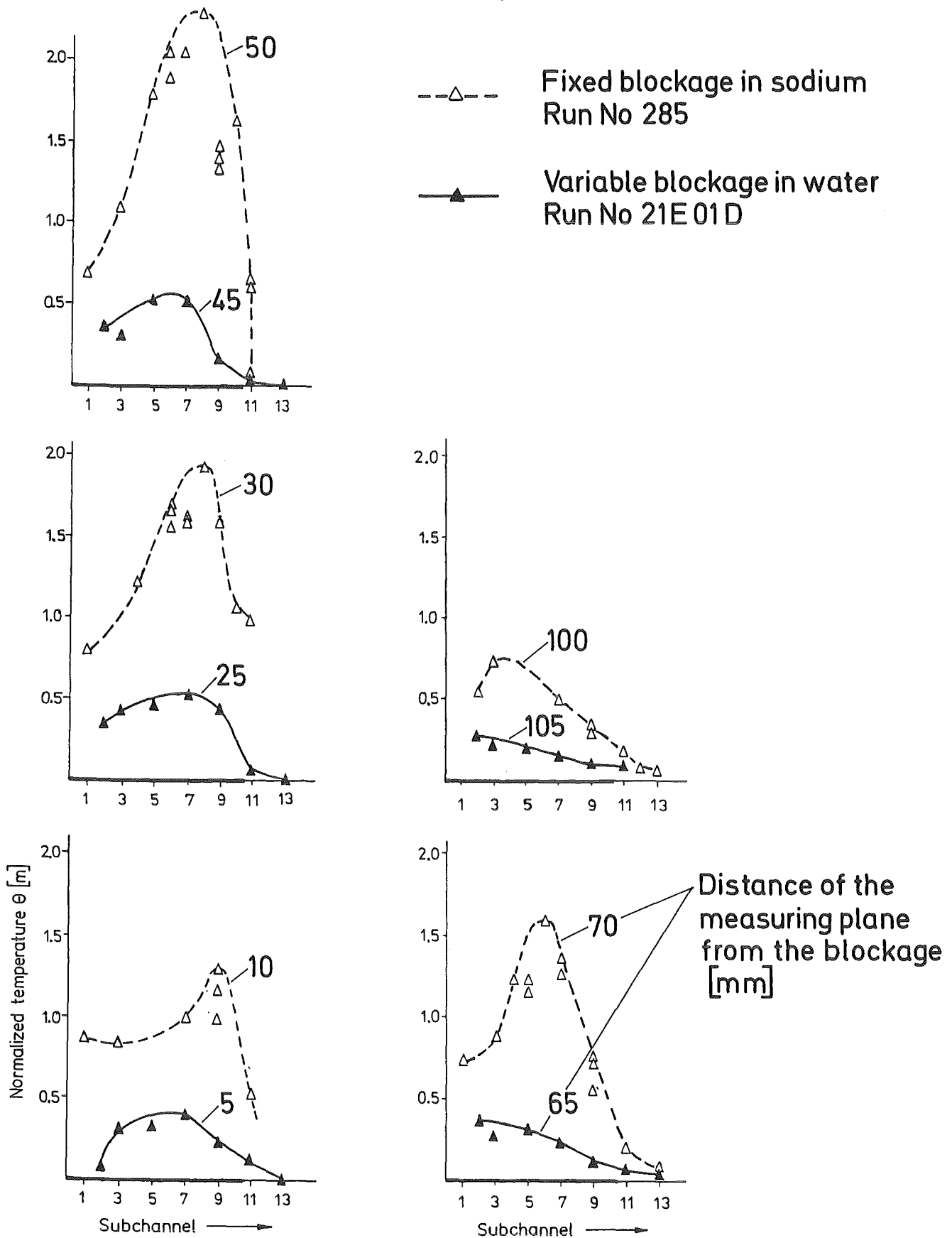
Fig.19 Axial Peak Temperature Distribution Comparison of Different Blockages



49% Central Blockage, Fixed and Variable

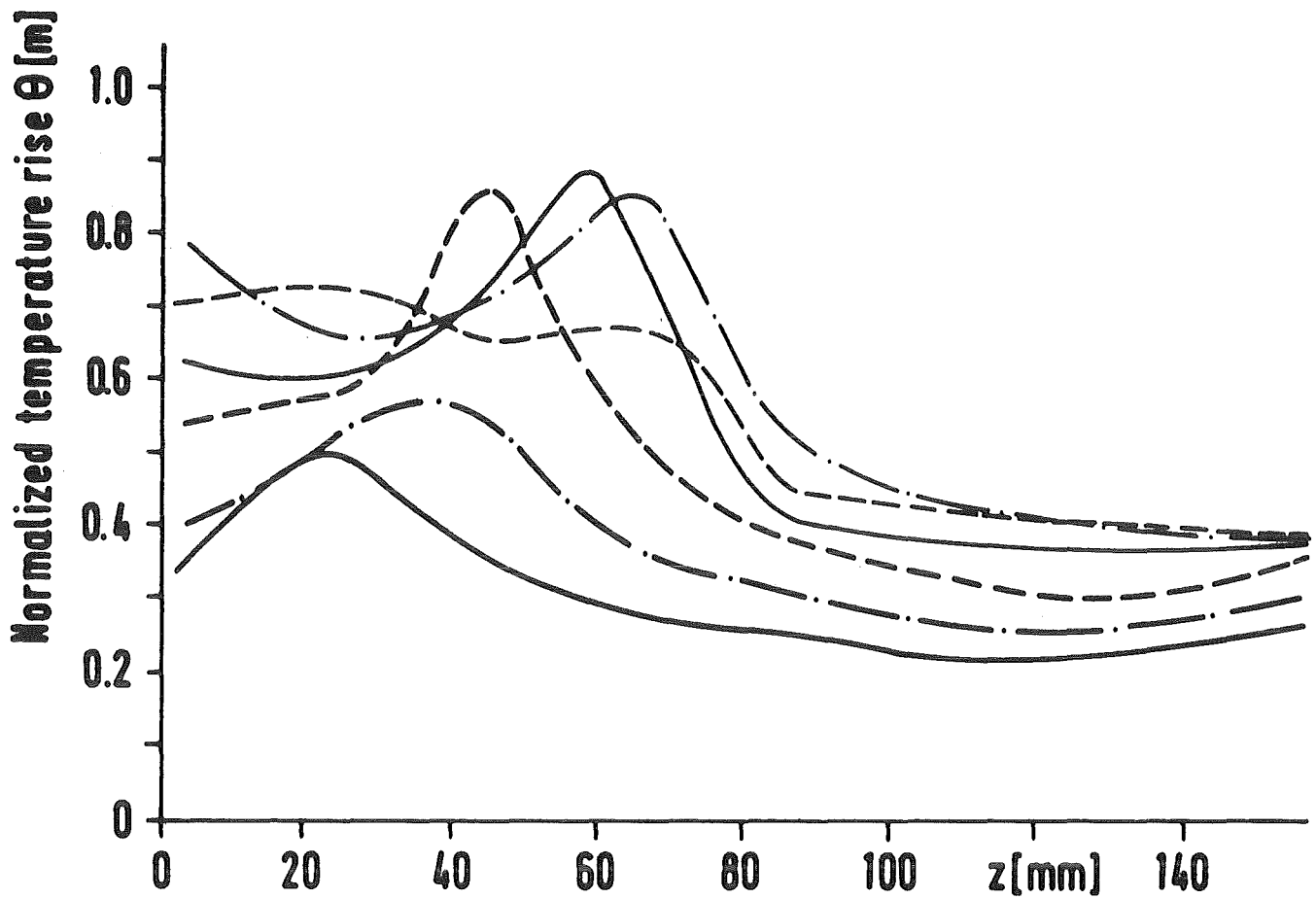
KIK IRE 847847

Fig.20 Radial Temperature Profiles



21% Corner Blockage, Fixed and Variable

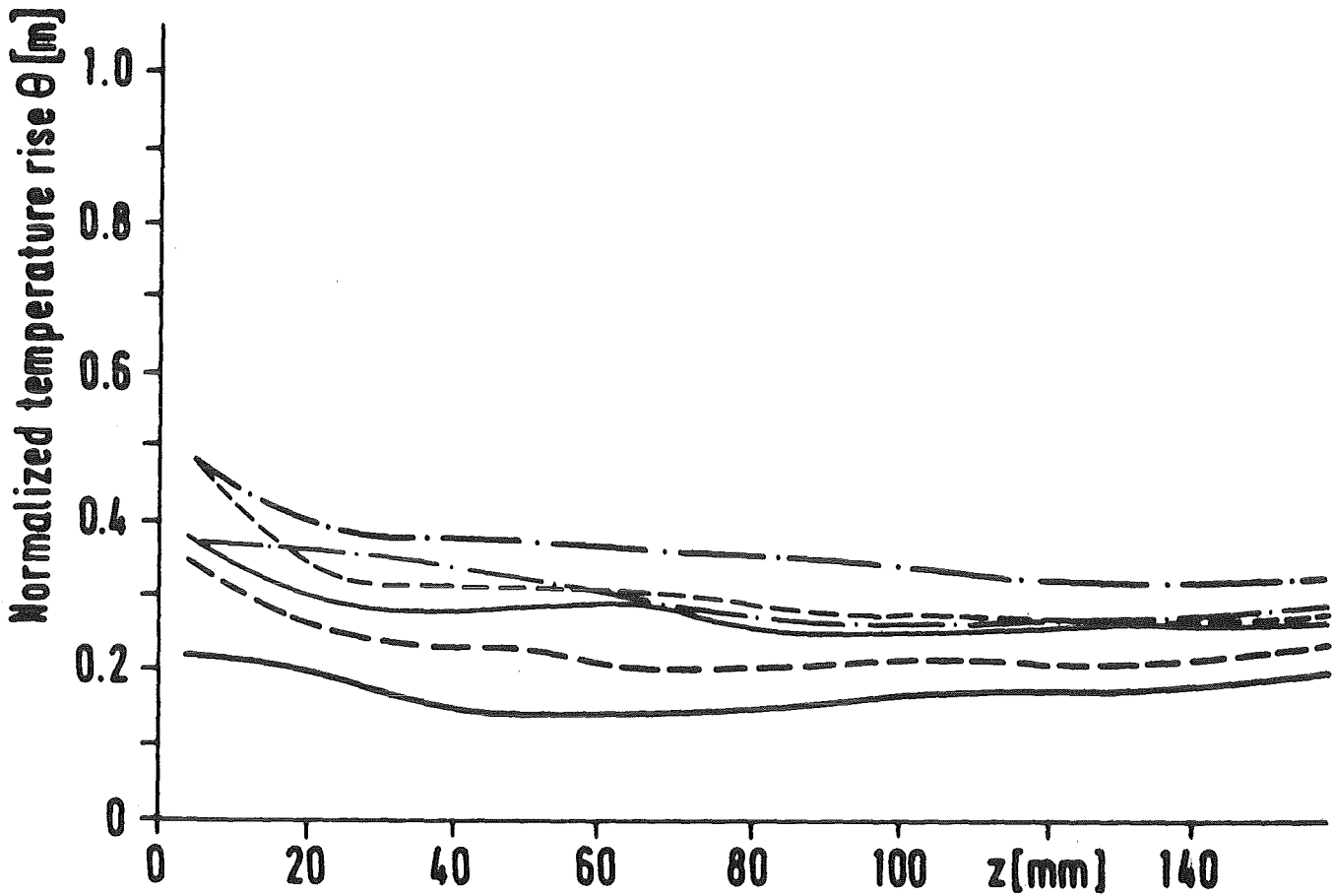
Fig.21 Radial Temperature Profiles



Line	Blockage Size	Run No.
————	14 %	14 E 01
- · - · -	21 %	21 E 01
- - - -	29 %	29 E 01
————	37 %	37 E 01
- · - · -	55 %	55 E 01
- - - -	64 %	64 E 01

$v_0 = 3 \text{ m/s}$ $q = 27 \text{ W/cm}^2$

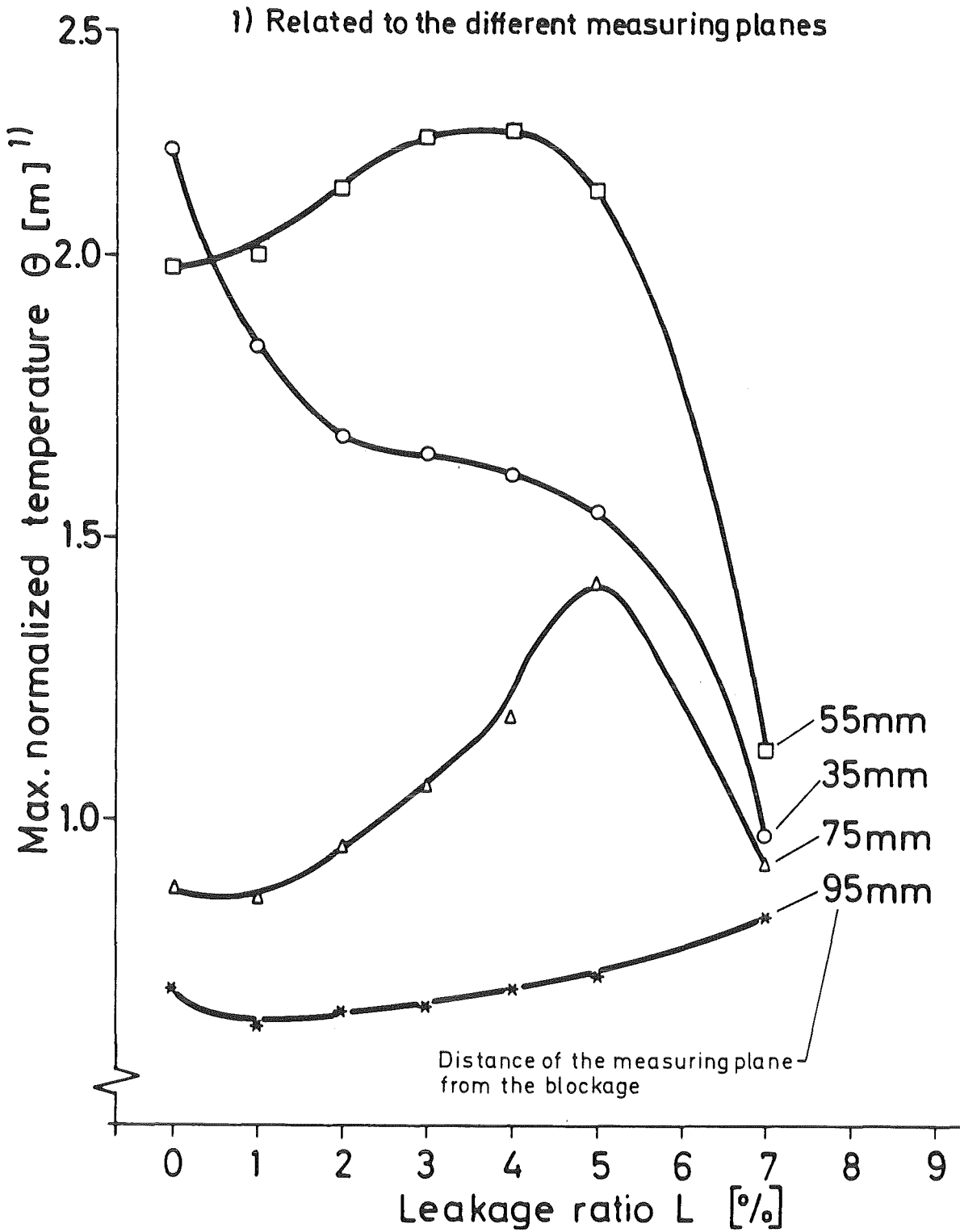
Variable Corner Blockage
Fig. 22: Influence of Blockage Size on Axial Peak Temperature Distribution



Line	Blockage Size	Run No.
————	10 %	10 Z 01
- - - -	20 %	20 Z 01
- . - -	33 %	33 Z 01
- . . -	49 %	49 Z 01
- - - -	55 %	55 Z 01
————	69 %	69 Z 01

$v_0 = 3 \text{ m/s}$ $q = 27 \text{ W/cm}^2$

Variable Central Blockage
Fig. 23: Influence of Blockage Size on Axial Peak Temperature Distribution



$v_0 = 5 \text{ m/s}$, $q = 27 \text{ W/cm}^2$

Fig.24 Influence of the Leakage Flow through the 21° Corner Blockage in Water

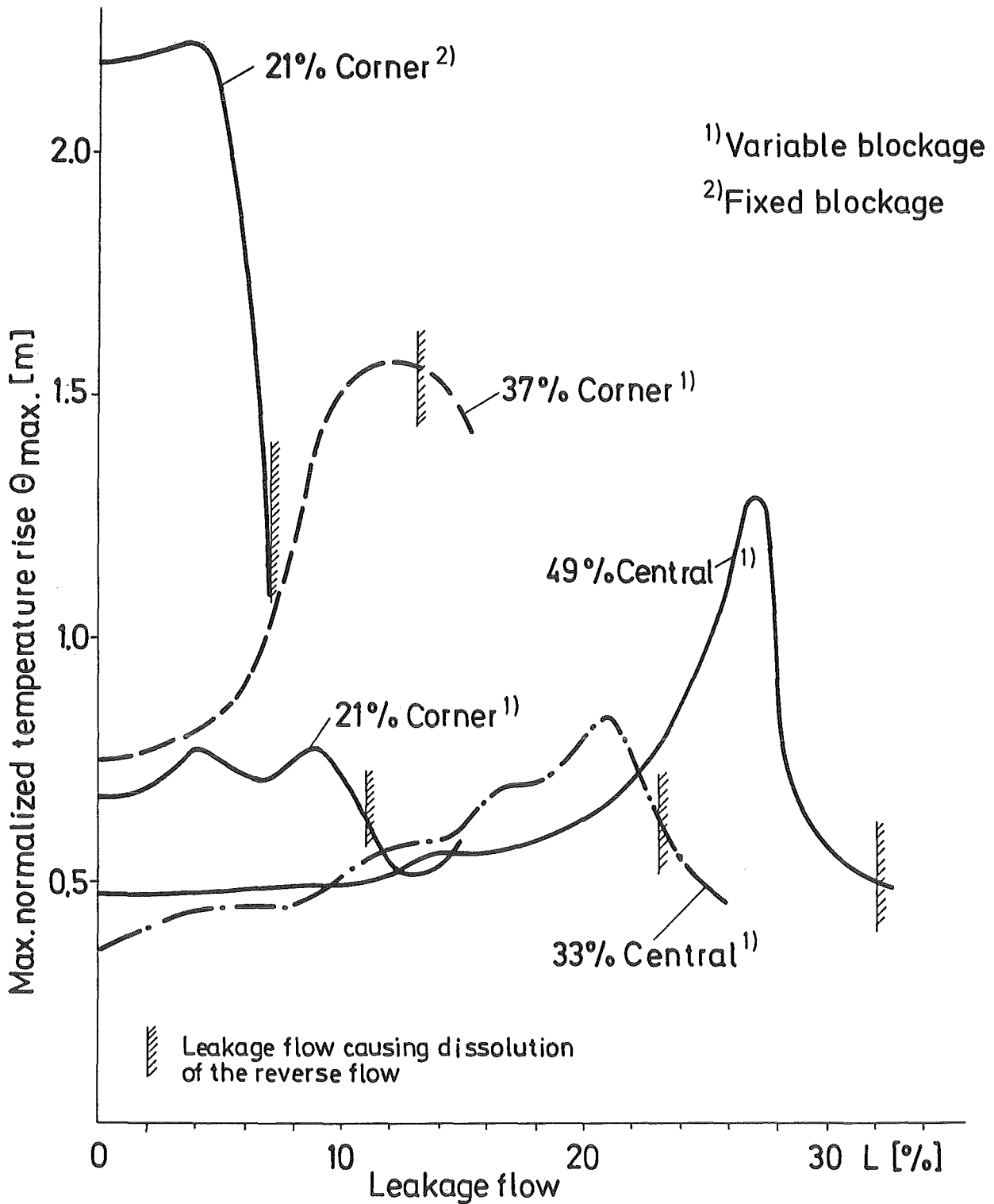
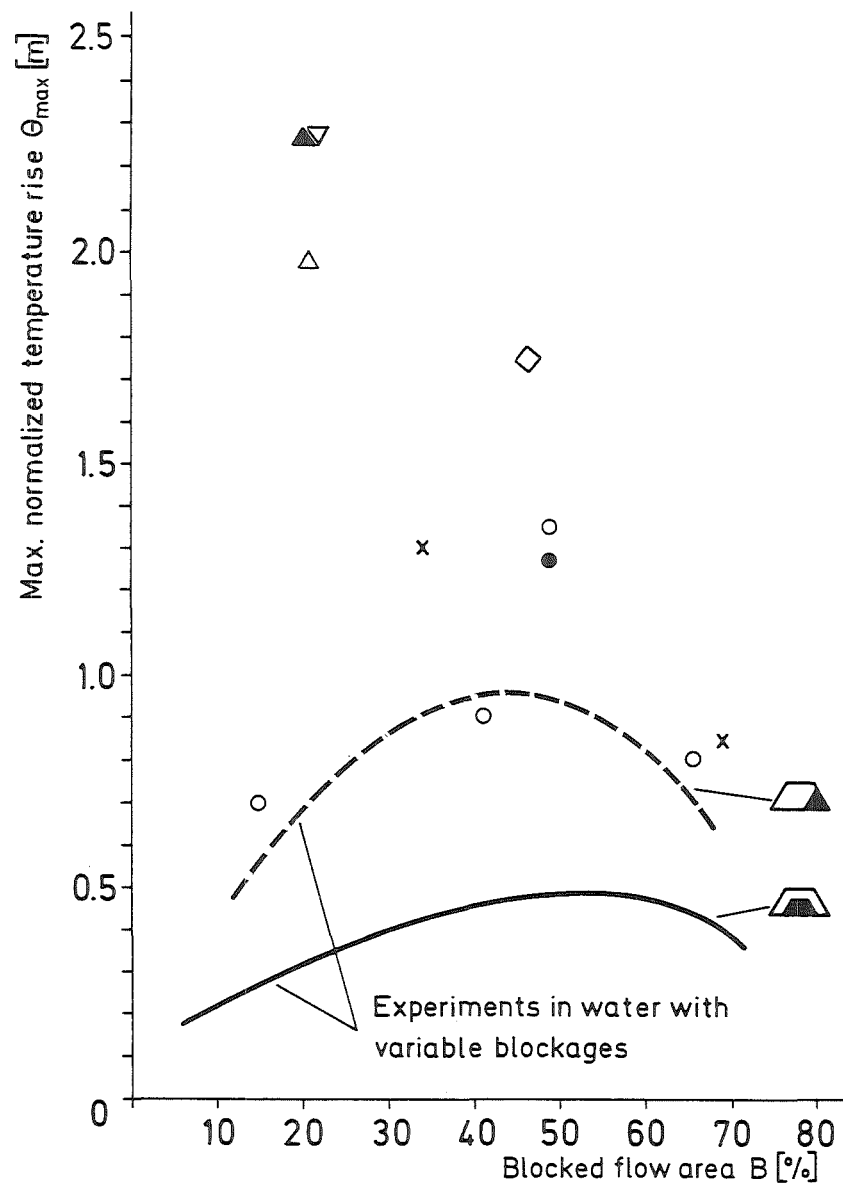
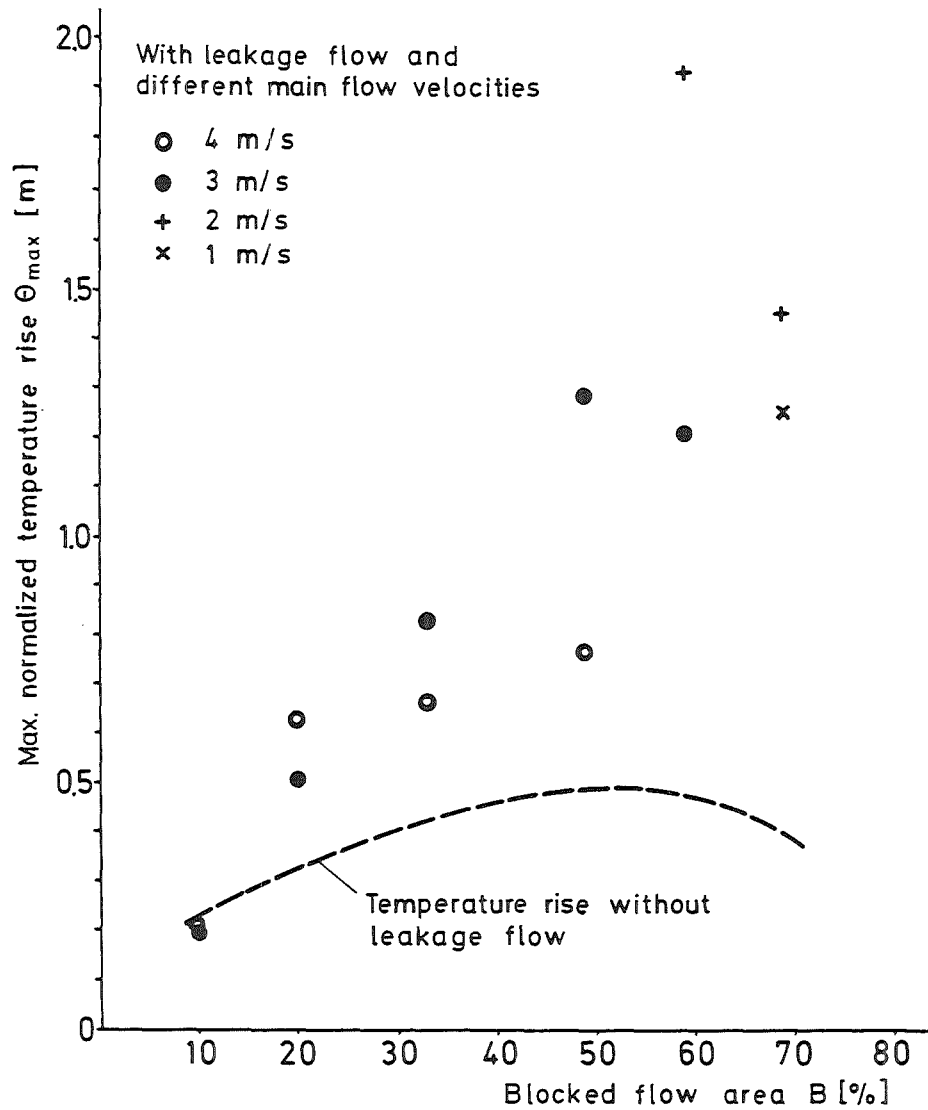


Fig.25 Influence of Leakage Flow on Max. Temperature Rise in the Wake



Symbol	Blockage		Coolant	Ref.
	Type	No		
—	Central	16 (variable)	Water	25,26
●		9	Sodium	12
○		3, 4, 8, 9	Water	9,10
x		(sector)	Sodium	55
- - -	Corner	16 (variable)	Water	25,26
▲		10	Sodium	16
△		10	Water	15
▽		15	Water	23
◇		5	Water	10

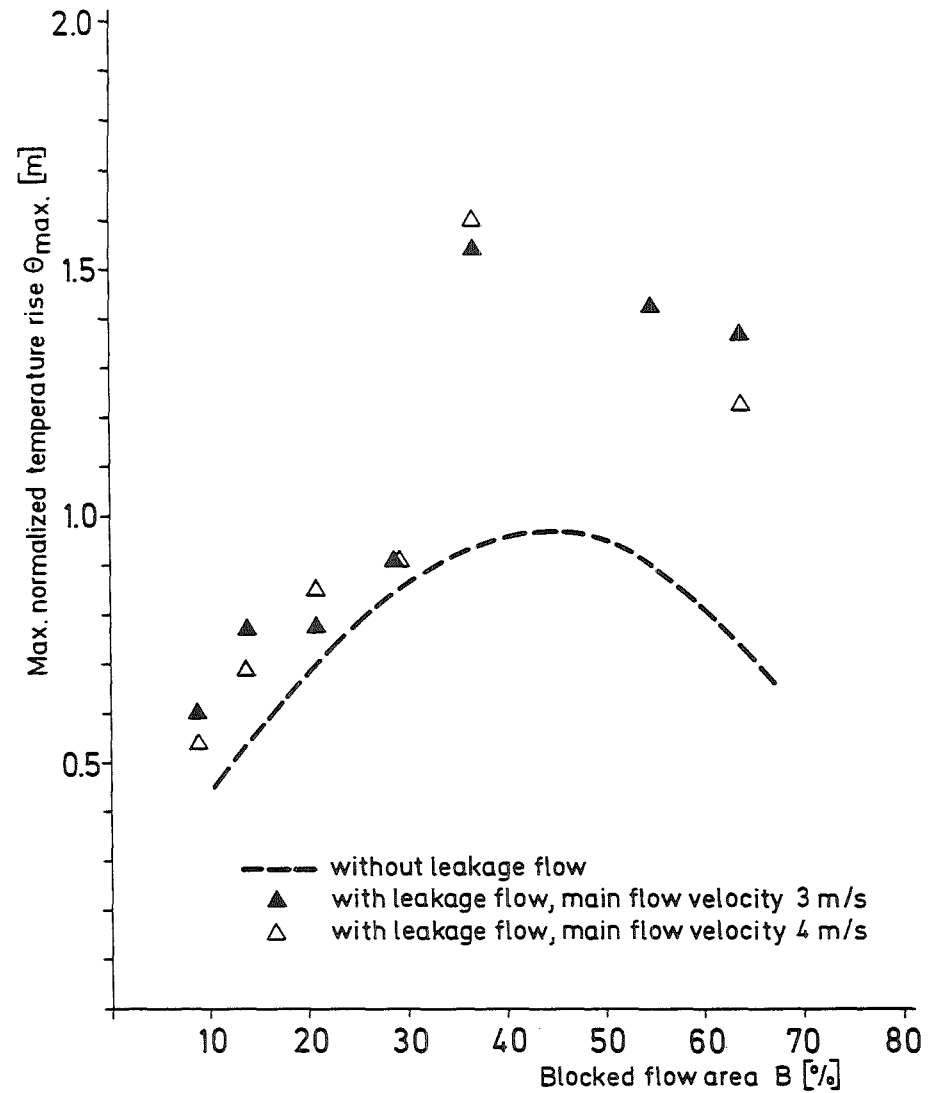
Fig.26 Max. Temperature Rise behind Different Blockages (Impermeable)



Central Blockage

IRE847869

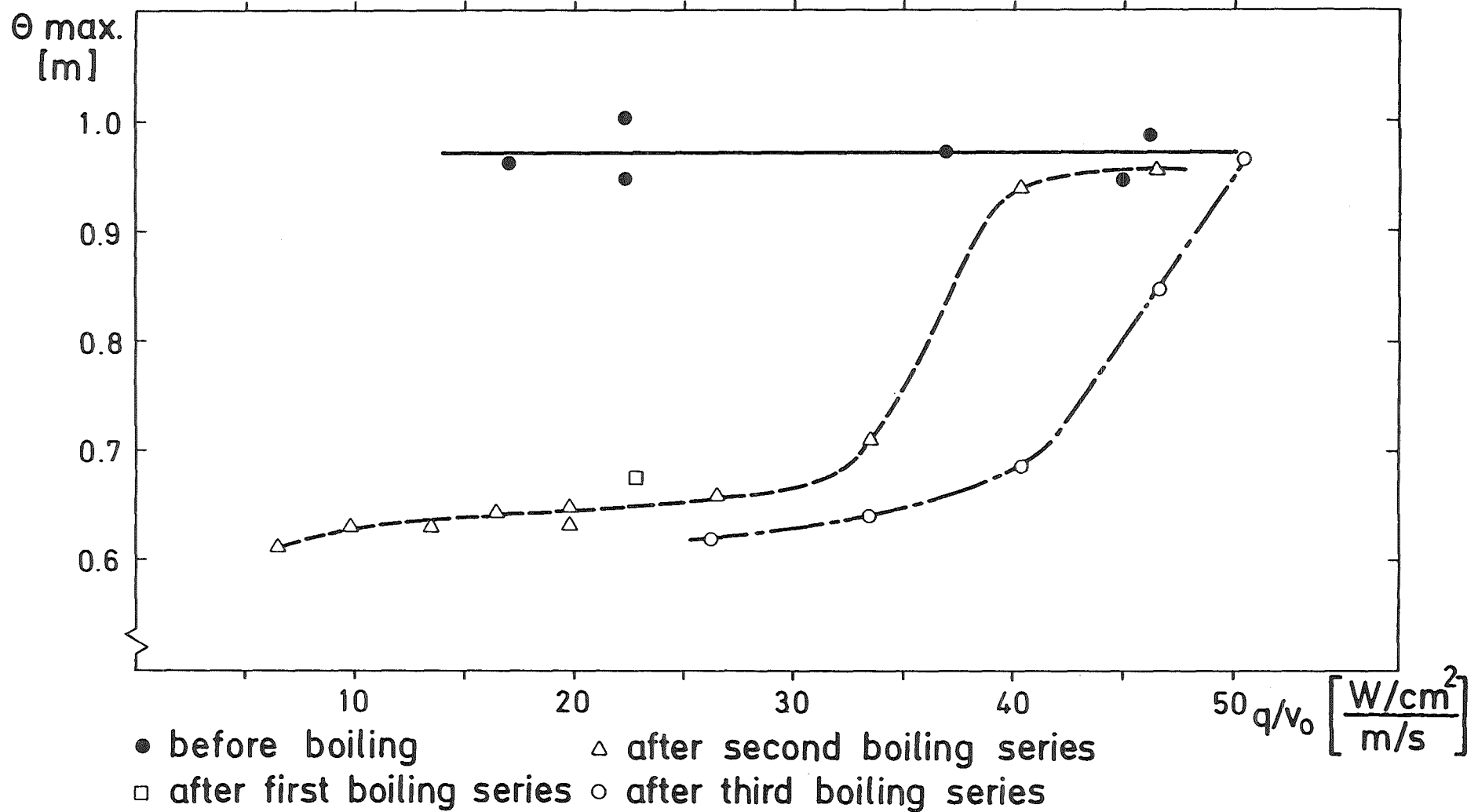
Fig. 27 Max. Temperature Rise with and without Leakage Flow



Corner Blockage

IRE847870

Fig. 28 Max. Temperature Rise with and without Leakage Flow



49% Central Blockage

KIK IRE847871

Fig.29 Influence of Boiling Experiments on the Maximum Temperature

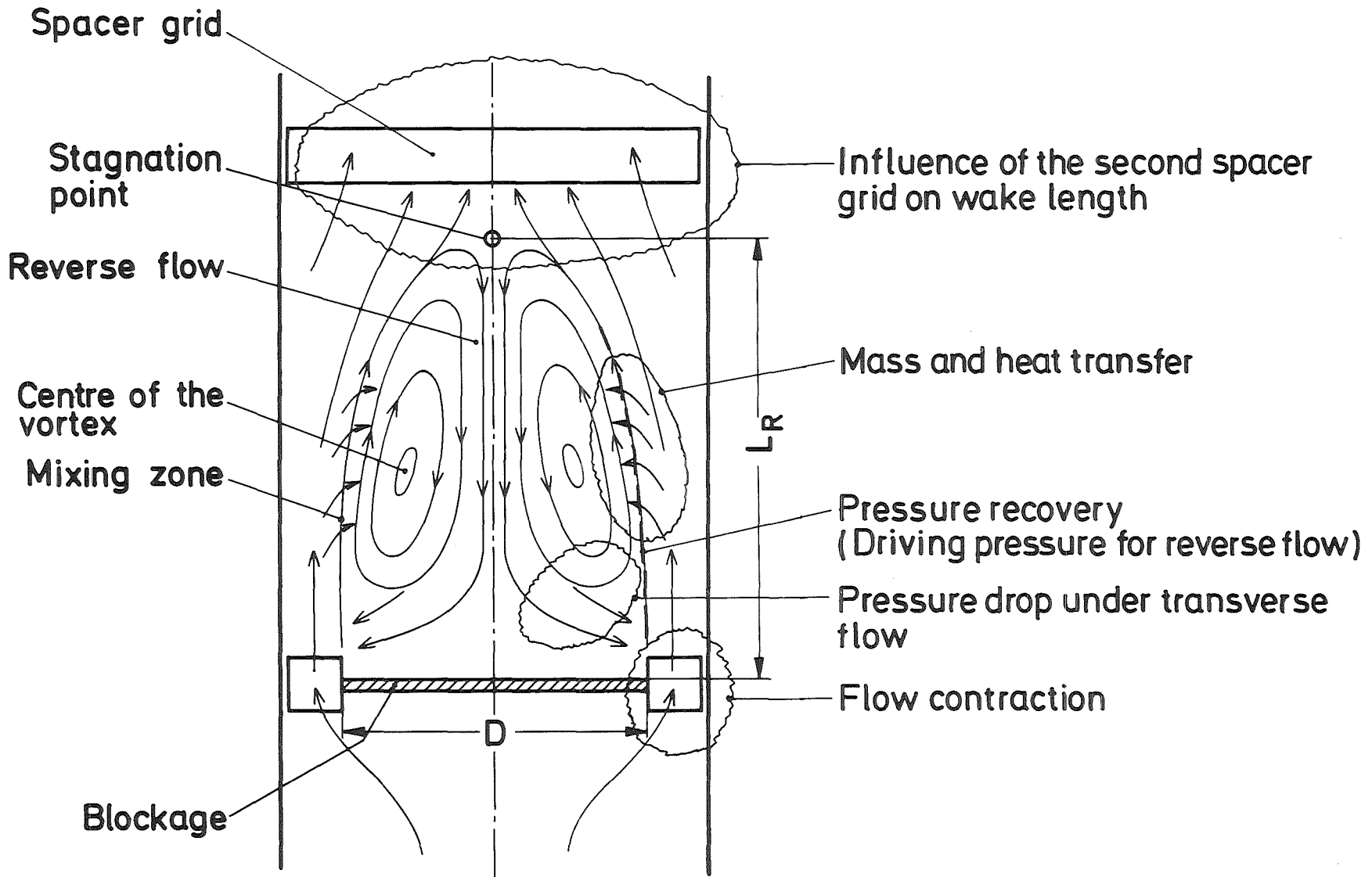
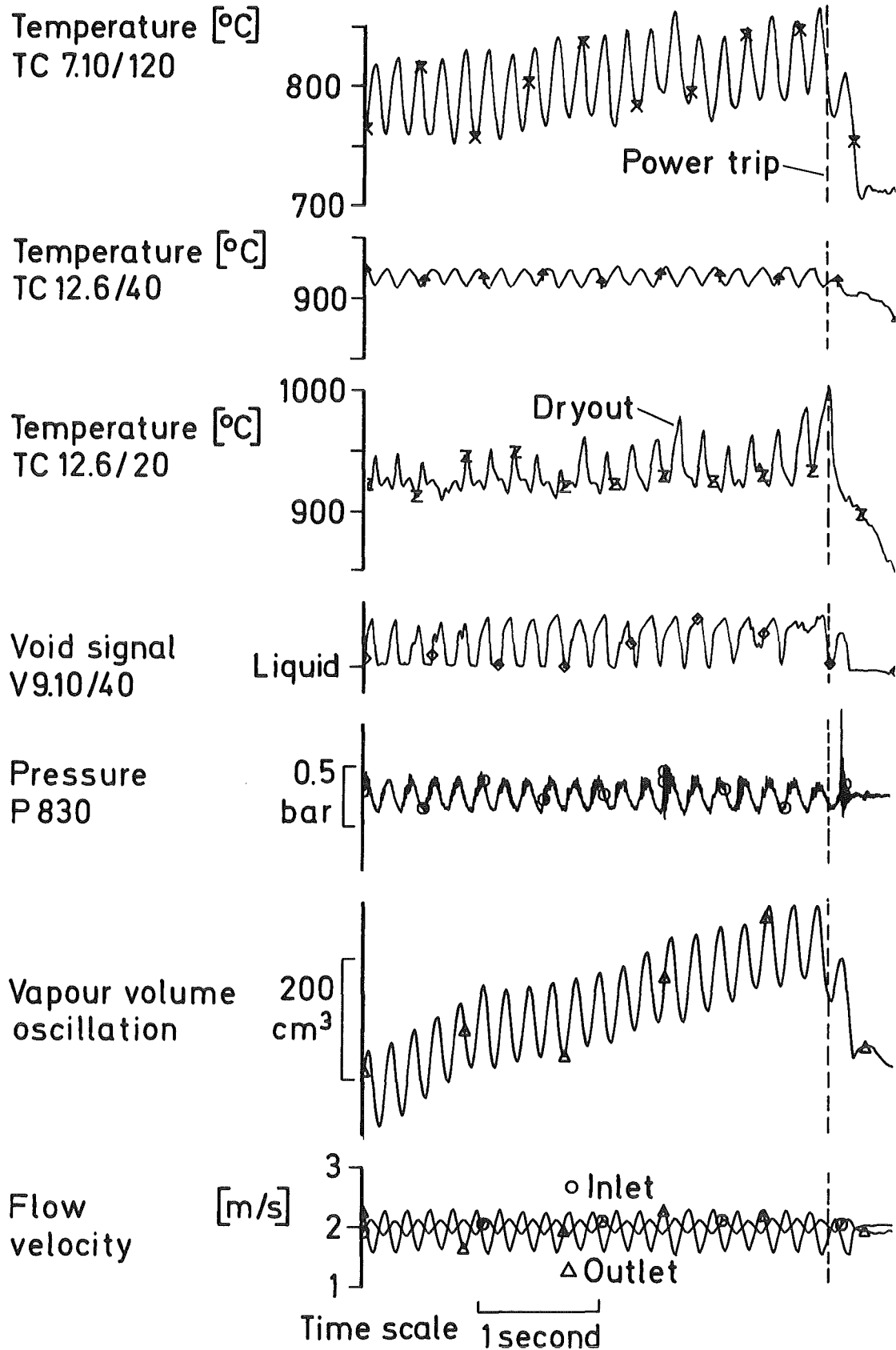


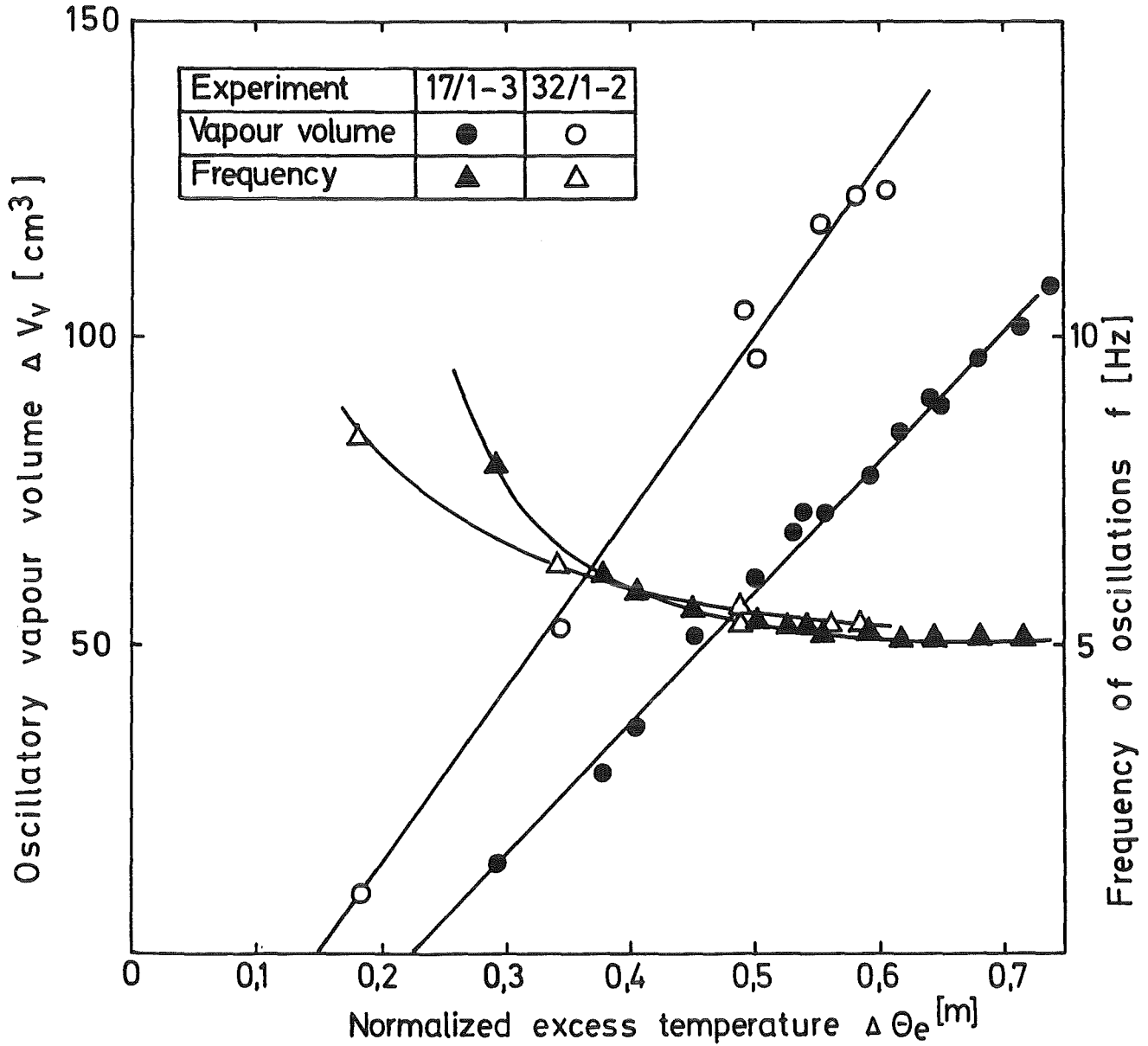
Fig.30 Identification of Important Thermo-Hydraulic Phenomena in the Wake of a Central Blockage



49% Central Blockage, Run 58E

KfK IRE847872

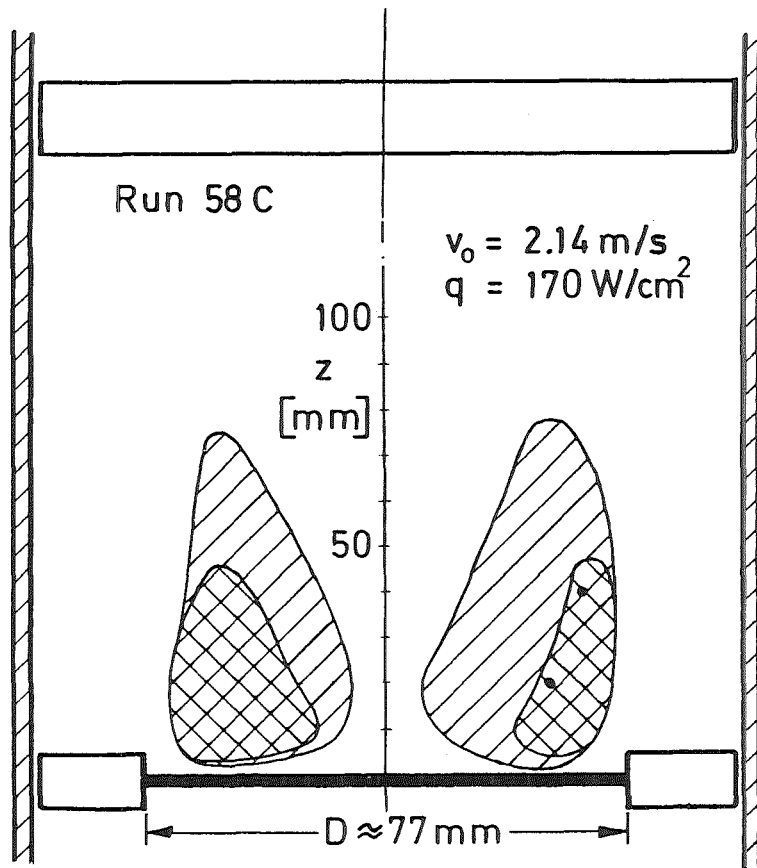
Fig.31 Typical Boiling Signals Recorded just before Permanent Dryout





49% Central Blockage

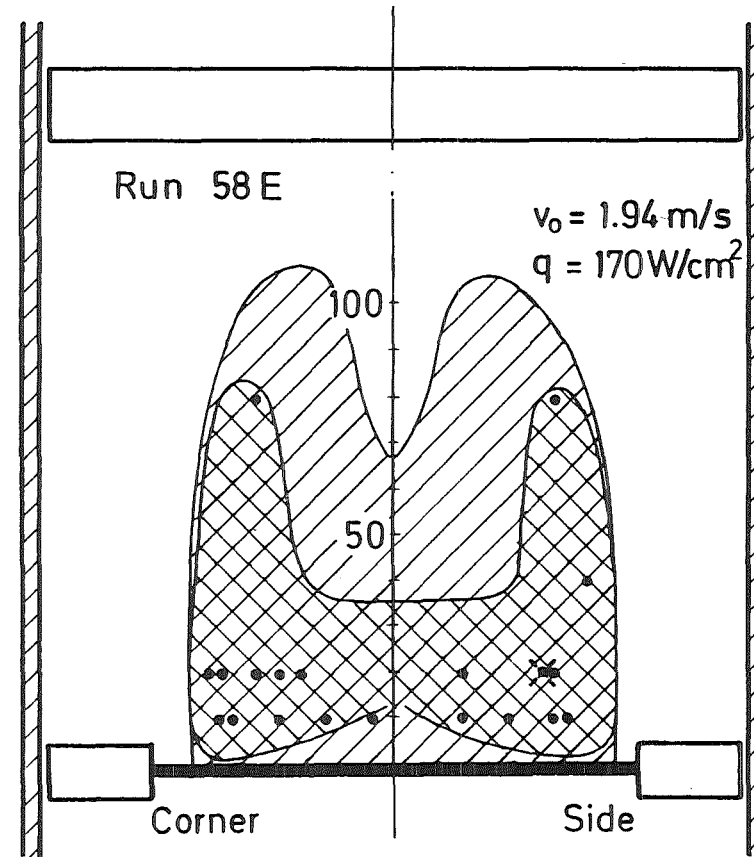
KfK IRE847873

Fig.32 Amplitude and Frequency of Vapour Volume Oscillations



$\Delta T_e \approx 310 \text{ K}$
 $\Delta \theta_e \approx 0.55 \text{ m}$
 $V_{B \text{ min}} \approx 70 \text{ cm}^3$
 $V_{B \text{ max}} \approx 170 \text{ cm}^3$

 Min. boiling region
 Max. boiling region



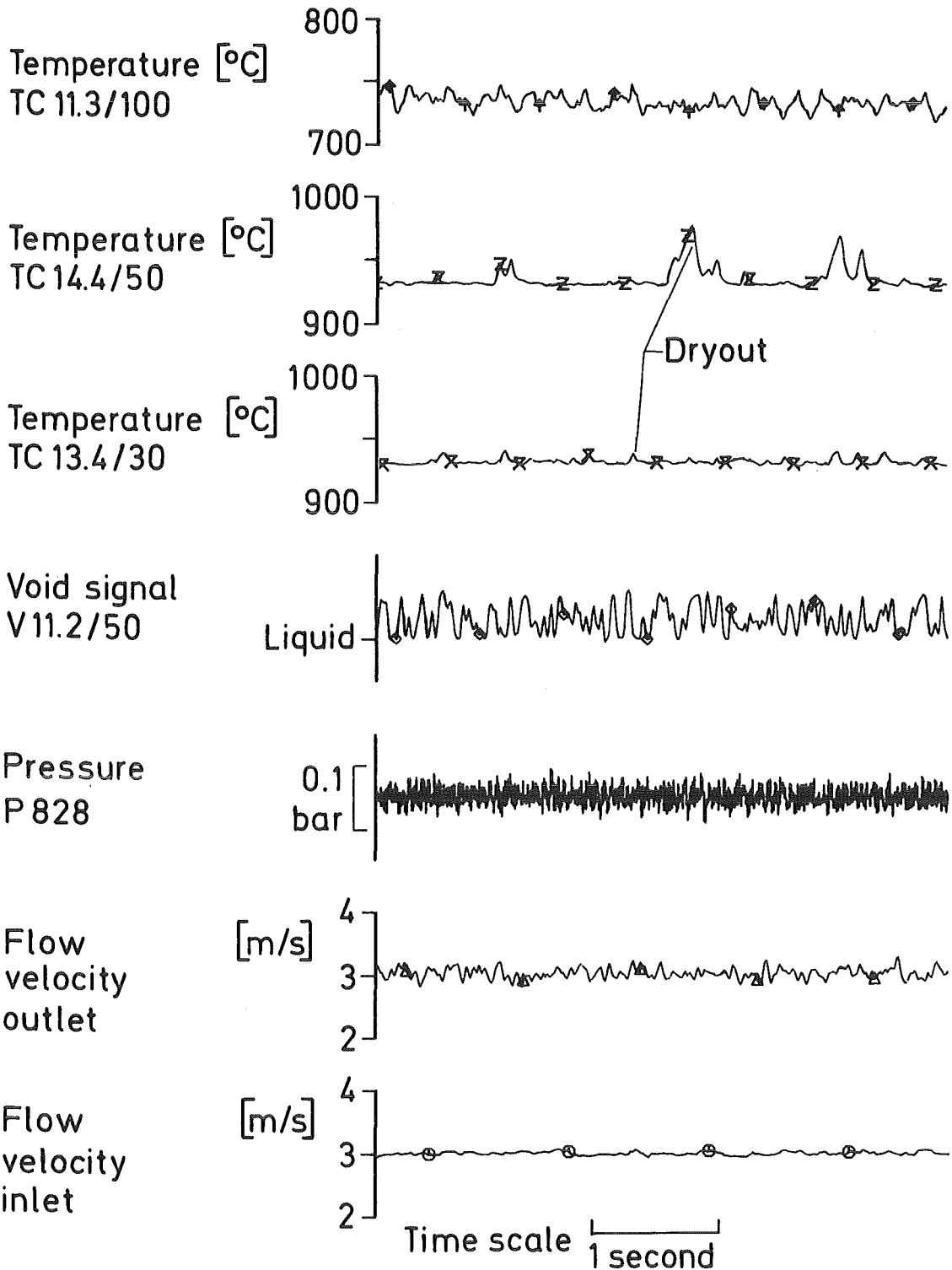
$\Delta T_e \approx 380 \text{ K}$
 $\Delta \theta_e \approx 0.61 \text{ m}$
 $V_{B \text{ min}} \approx 130 \text{ cm}^3$
 $V_{B \text{ max}} \approx 340 \text{ cm}^3$

• Brief dryout
 ✕ Permanent dryout

49% Central Blockage

 IRE847874

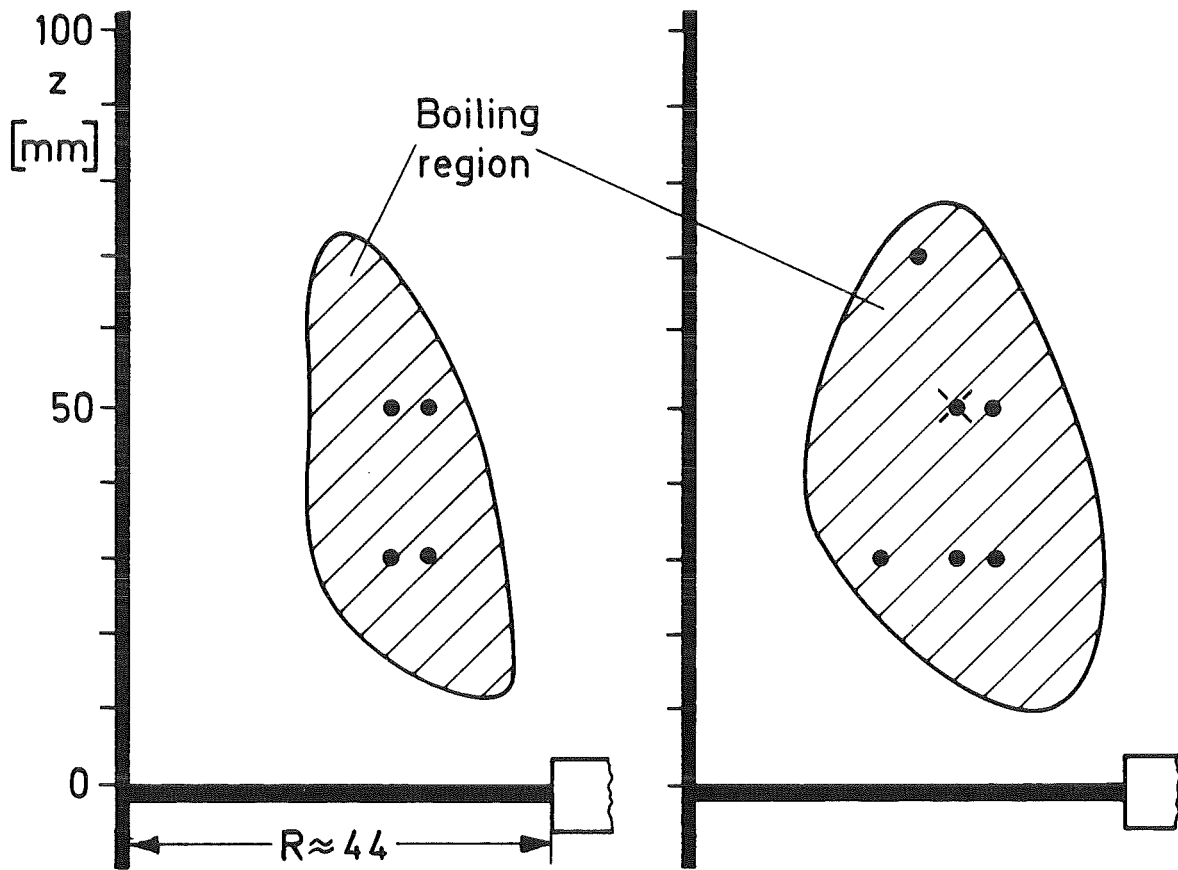
Fig.33 Estimated Minimum and Maximum Boiling Regions



21% Corner Blockage, Run 485

KfK IRE 847875

Fig.34 Typical Boiling Signals Recorded just before Permanent Dryout



Run 482

$\Delta\theta_e \approx 0.68\text{m}$

$\Delta T_e \approx 147\text{ K}$

$V_B \approx 48\text{ cm}^3$

Run 485

$\Delta\theta_e \approx 0.91\text{m}$

$\Delta T_e \approx 229\text{ K}$

$V_B \approx 67\text{ cm}^3$

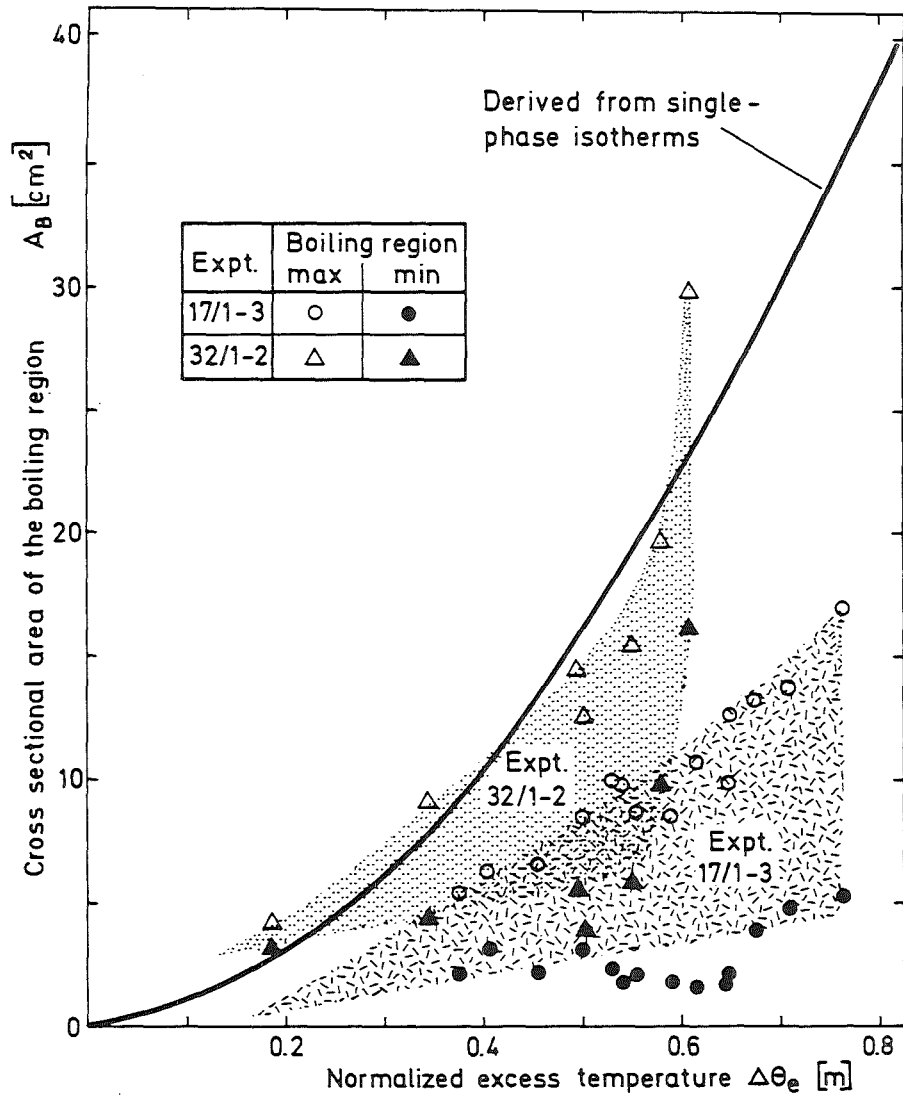
• Brief dryout

⊗ Max. temperature rise during brief dryout

21% Corner Blockage

KIK IRE 847876

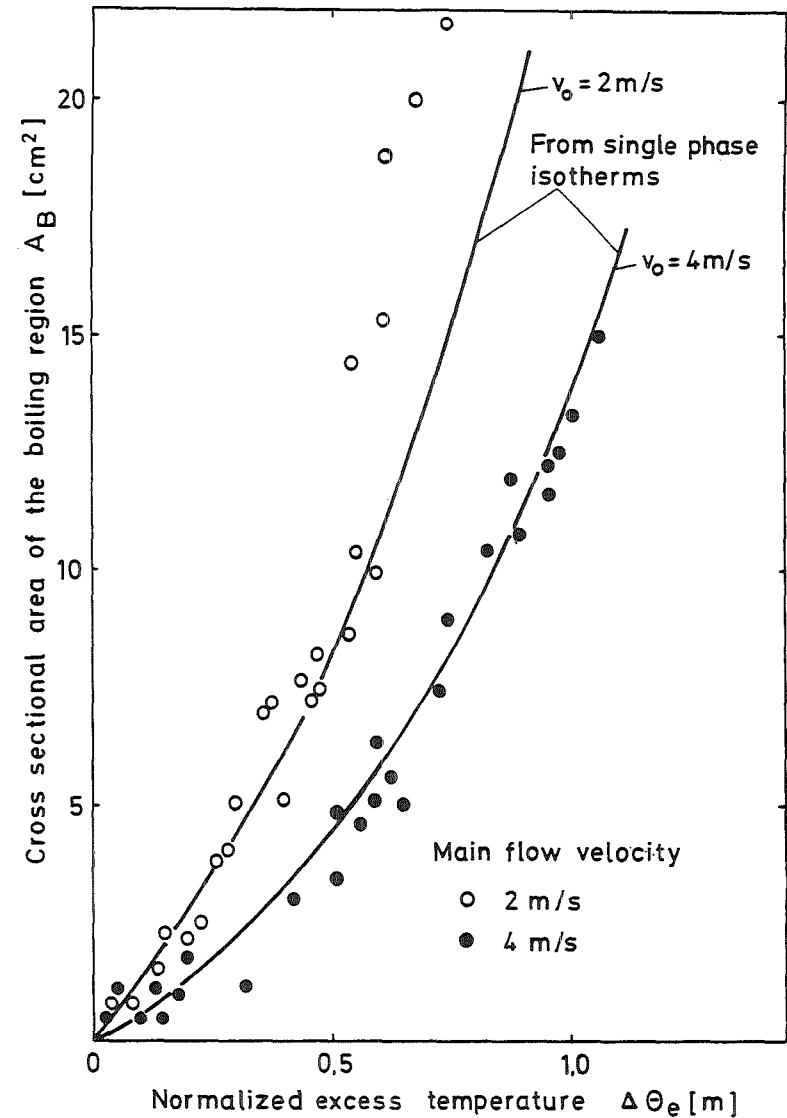
Fig.35 Approximated Boiling Regions



49% Central Blockage

IRE847877

Fig.36 Area of the Boiling Region Compared with Estimate from Single-Phase



21% Corner Blockage

IRE847878

Fig.37 Area of the Boiling Region Compared with Estimate from Single-Phase

Exp. No.	v_0 [m/s]	q [W/cm ²]	T_{in} [°C]
44/1	1	50 → 70	581
43/2	1.5	68 → 97	573
17/1-3	3.8 → 1.63	132	583
17/7	3.5 → 1.68	134	578
32/2	4 → 1.96	170	
215/2	2	61 → 97	505
216/3	2	47 → 79	588
214/2	3	92 → 135	427
215/1	3	82 → 128	498
216/2	3	62 → 107	581
224/3	3.8	76 → 155	627
214/1	4	121 → 165	422

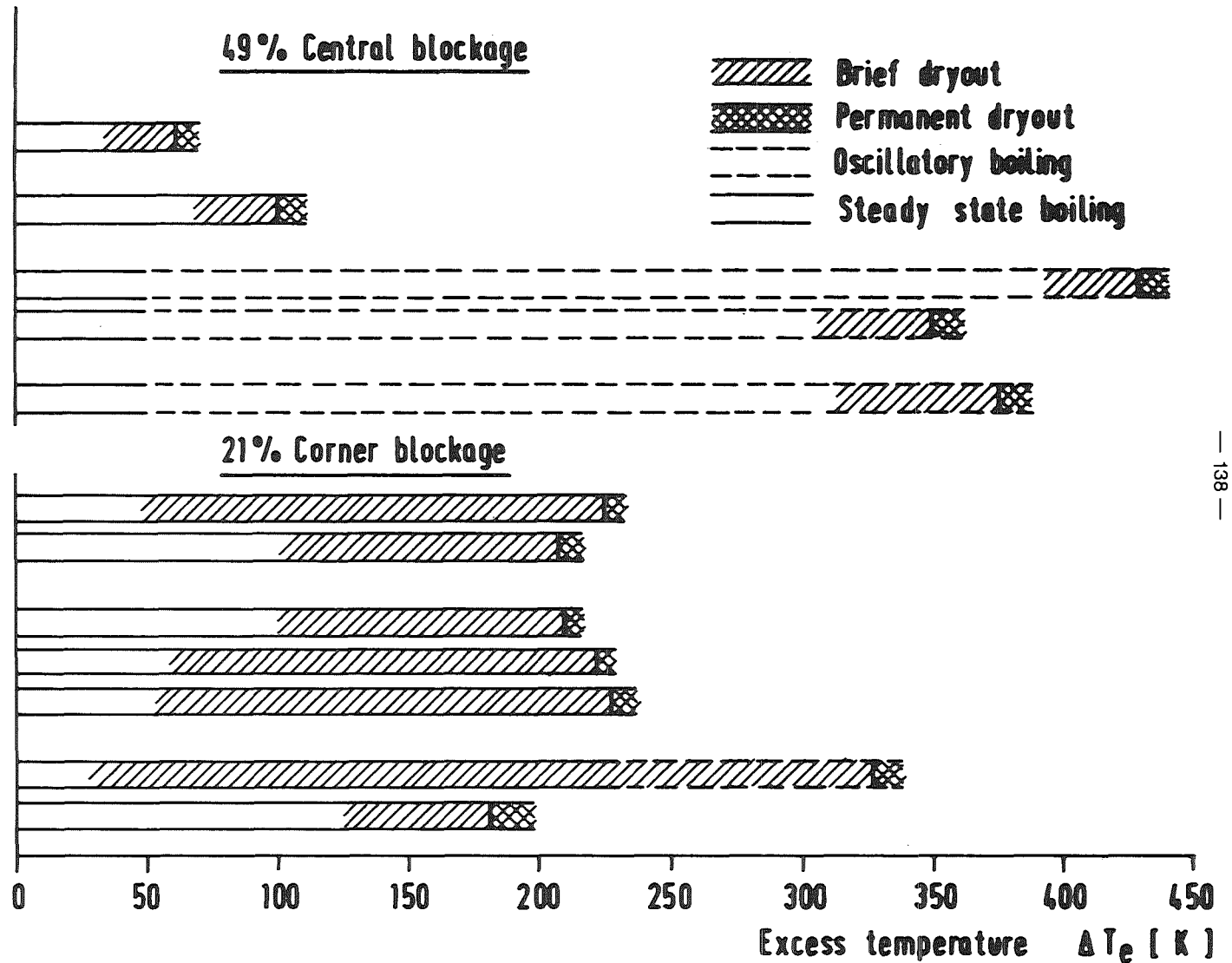


Fig. 38

Excess Temperatures at Dryout Conditions

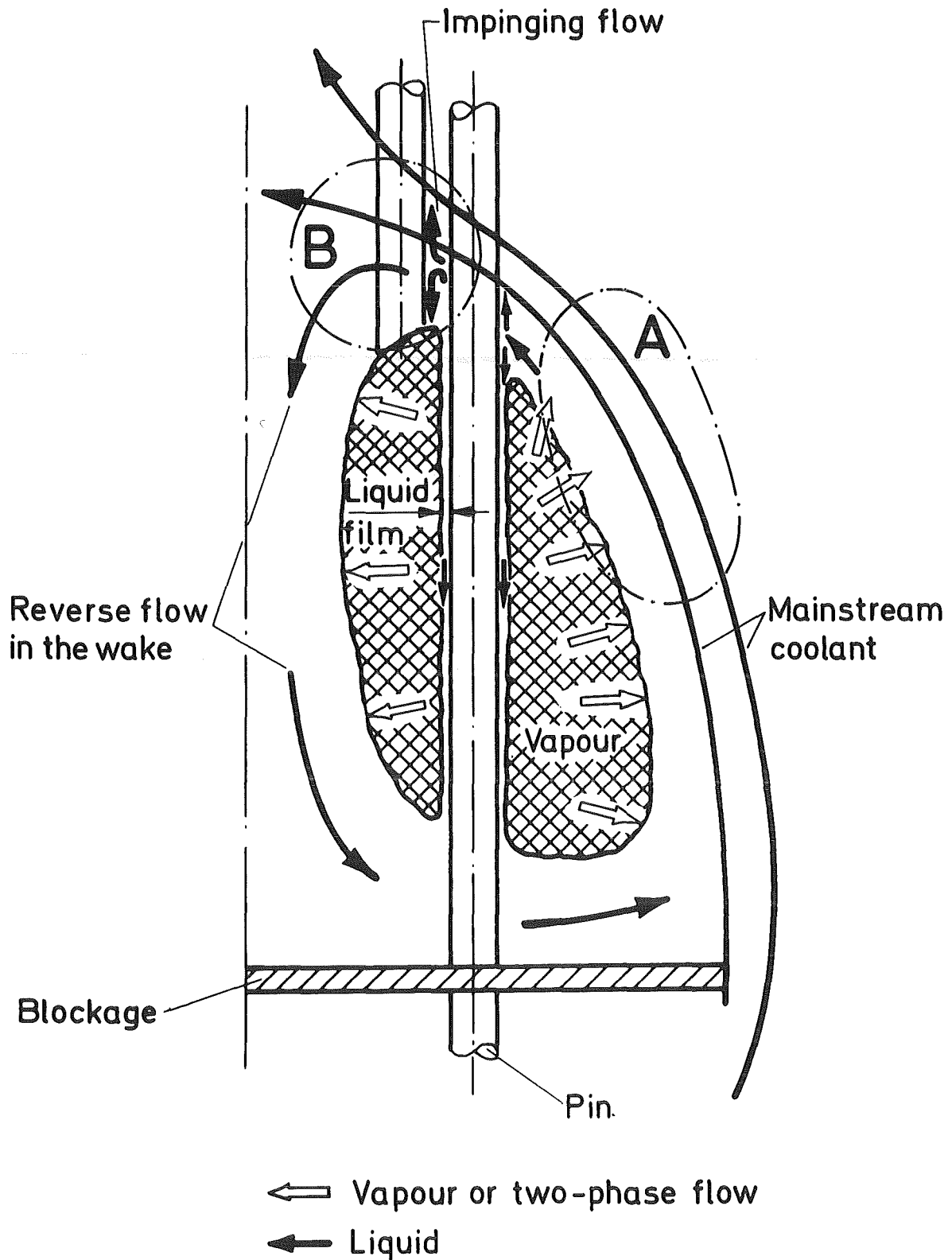


Fig. 39 Diagram Illustrating the Draining Liquid Film and the Vapour Flow

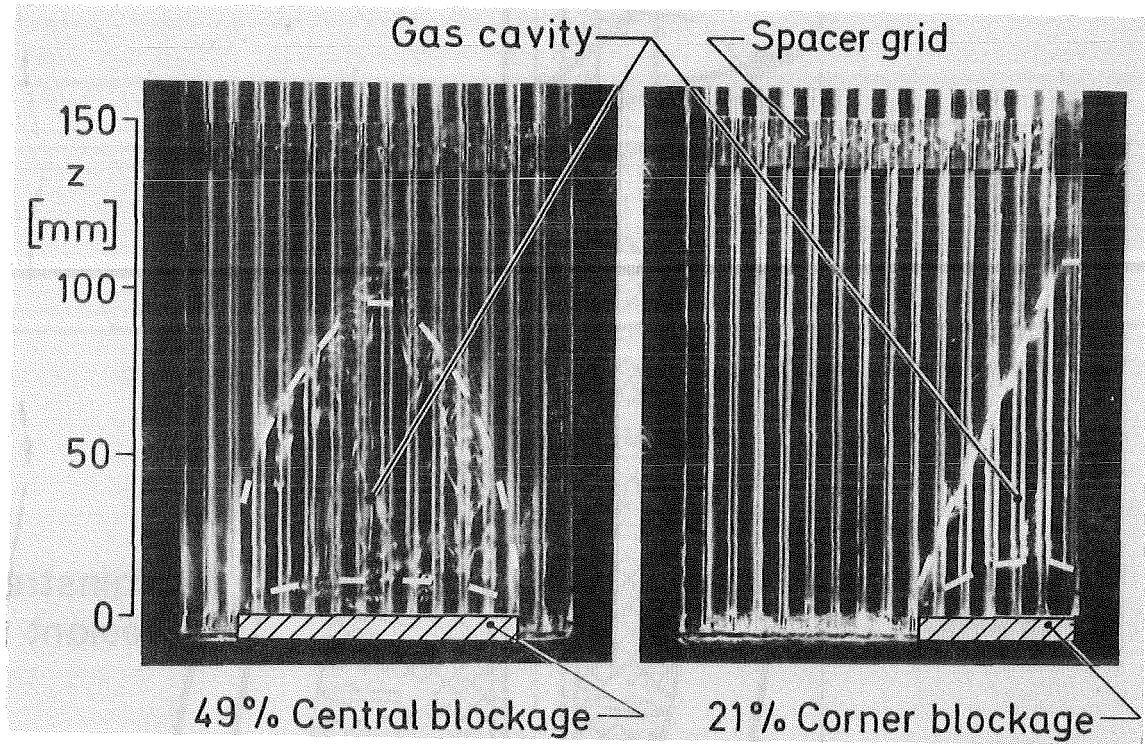
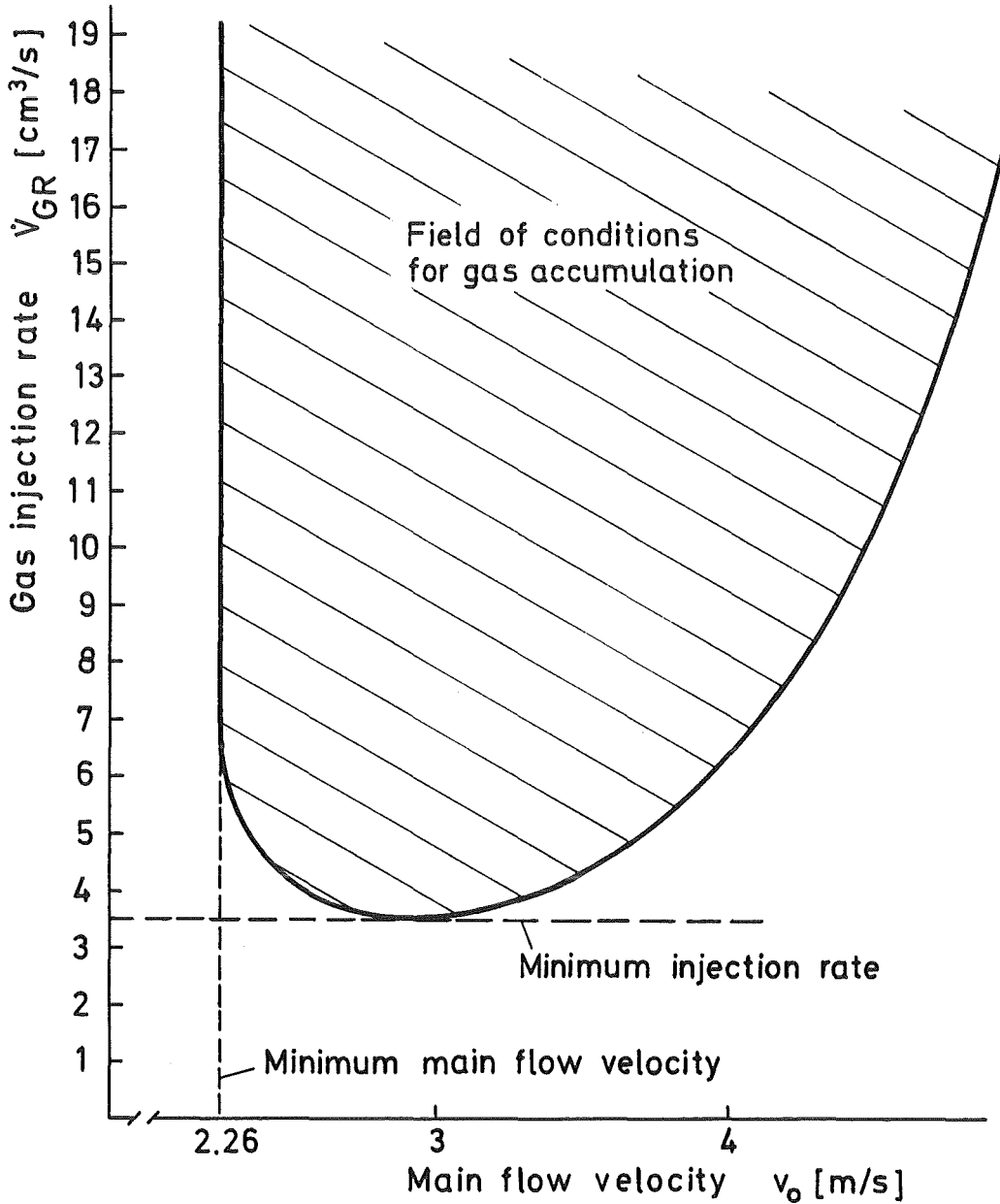


Fig.40 Gas Cavities in the Wake

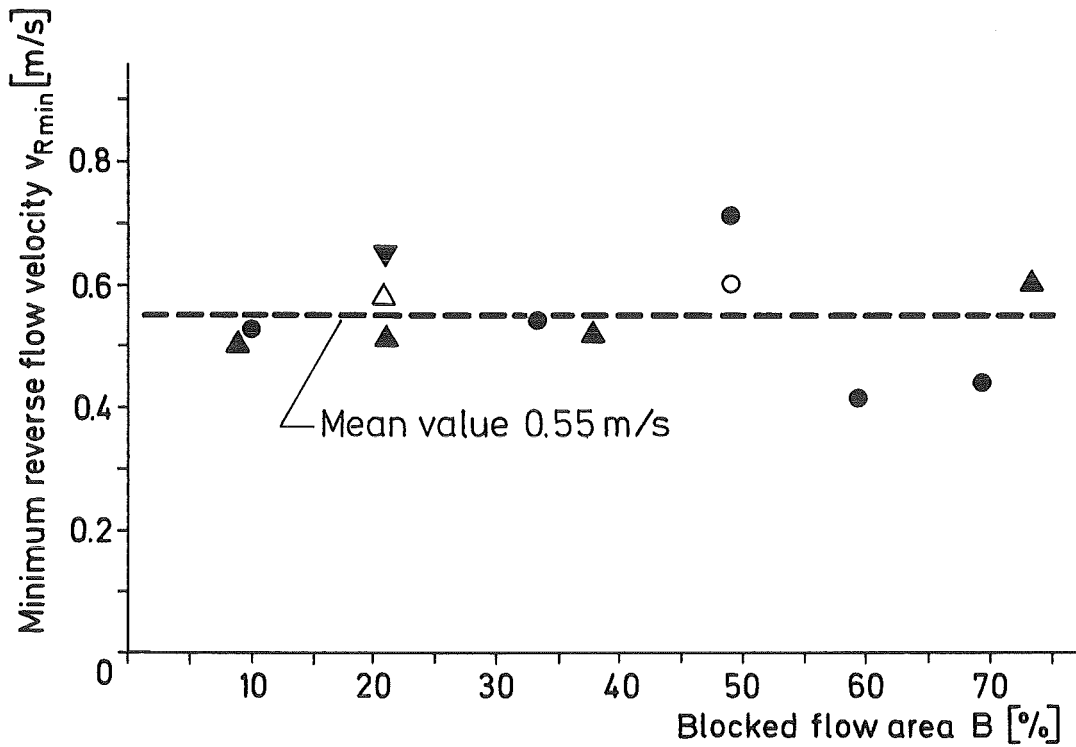


Gas injection into the wake

21% Corner Blockage

KfK IRE847882

Fig.41 Conditions of Gas Accumulation in Sodium



Symbol	Blockage		Coolant	Ref.
	Type	No		
●	Central	16(variable)	Water	24
○		9	Sodium	14
▲	Corner	16(variable)	Water	24
▼		14	Water	20
△		10	Sodium	18

Fig.42 Minimum Reverse Flow Velocity for Gas Accumulation from Different Experiments

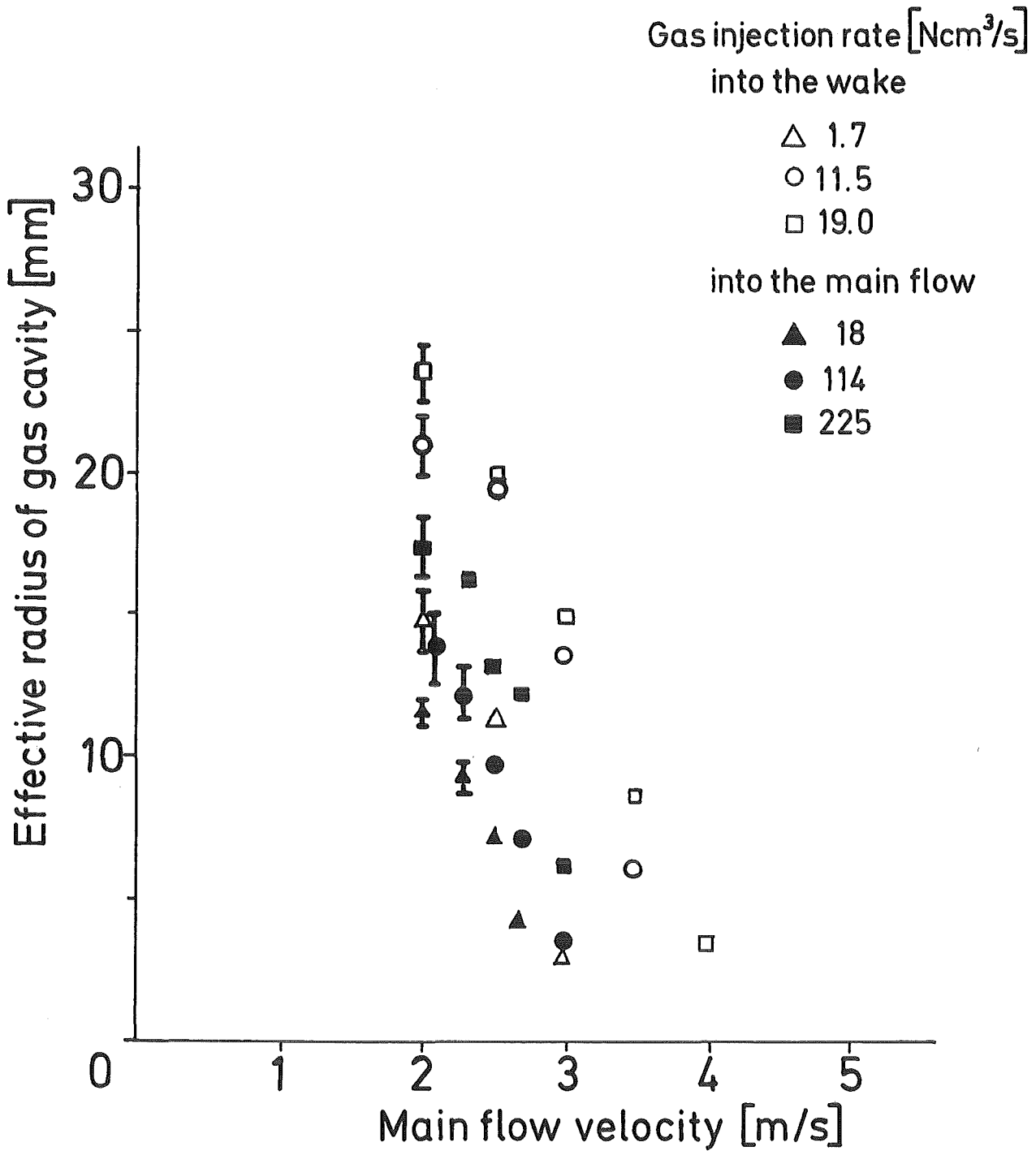
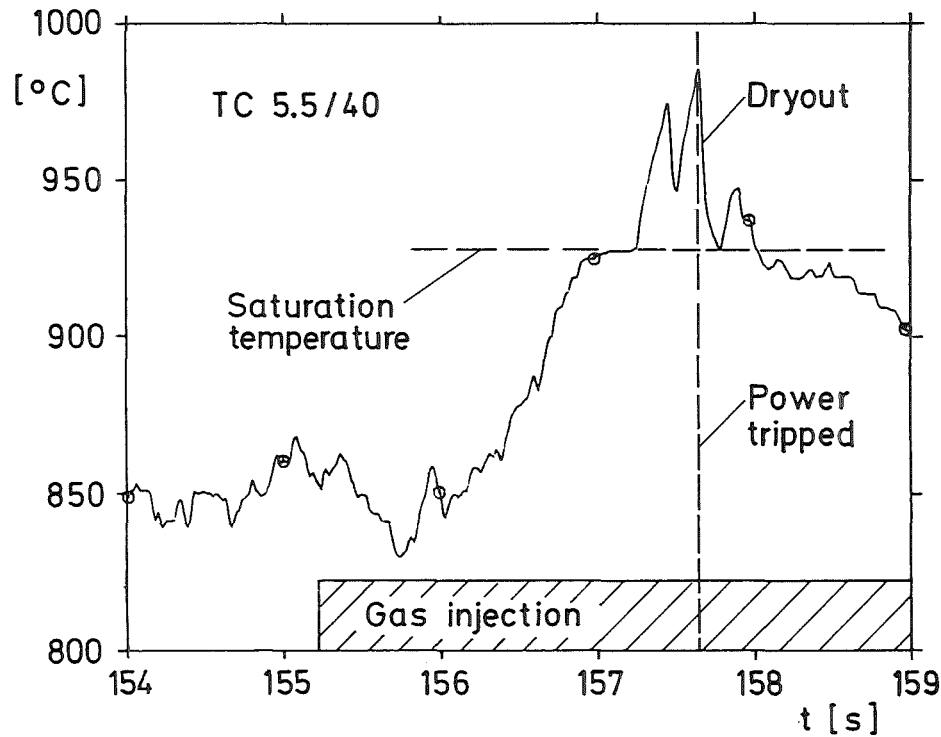


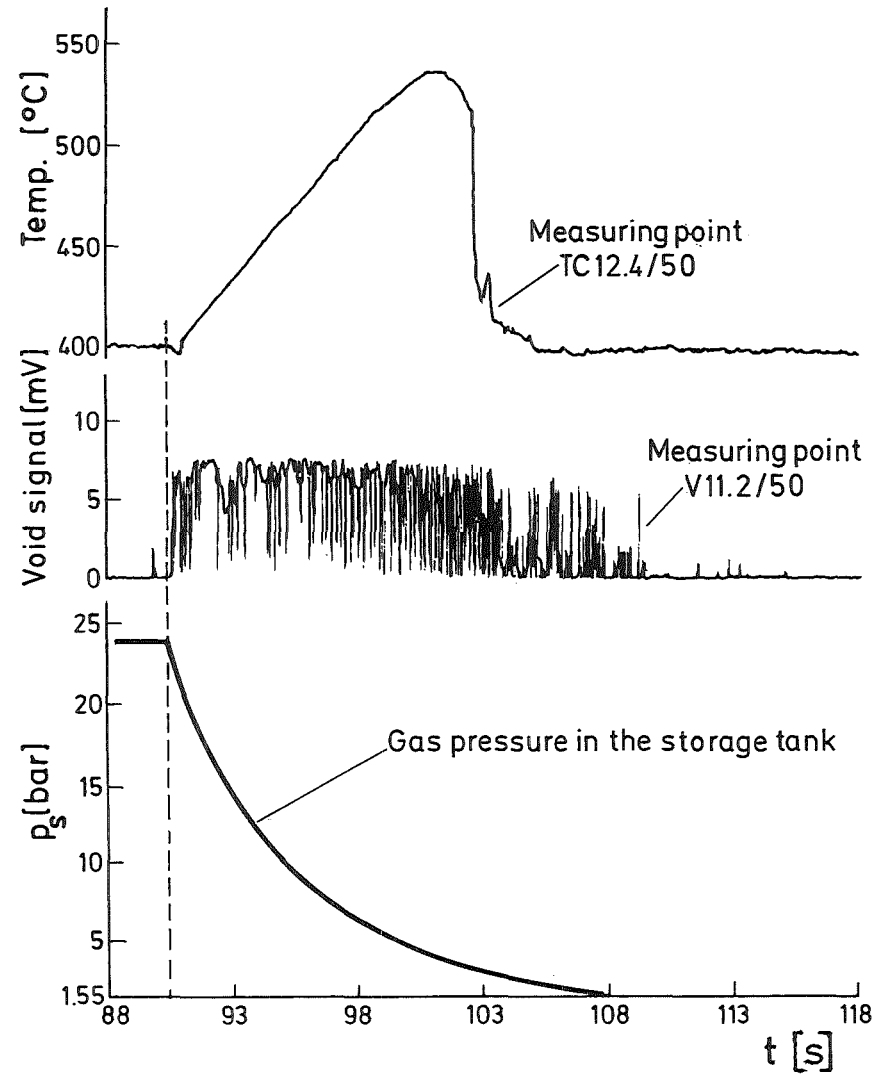
Fig.43 Dependence of Cavity Size on Main Flow Velocity and Gas Injection Rate



49% Central Blockage

IRE 847885

Fig.44 Course of Temperature During Gas Accumulation

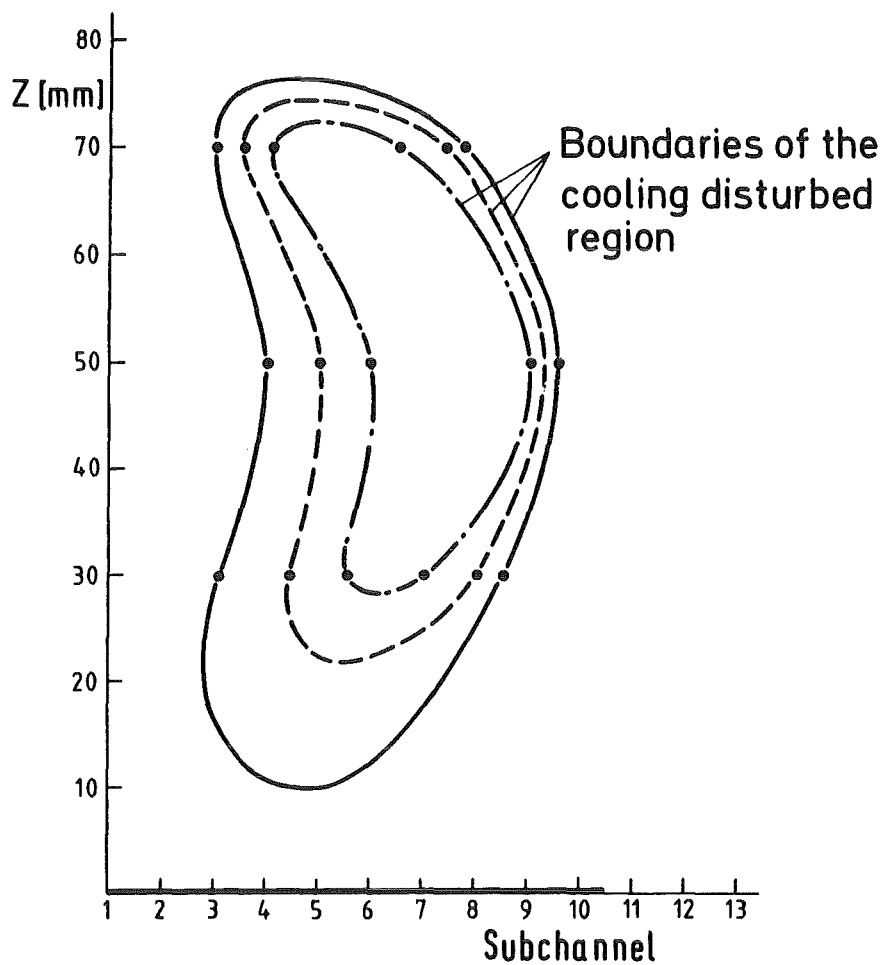


— 144 —

21% Corner Blockage

IRE 847886

Fig.45 Typical Signals of an Experiment with Pulswise Gas Injection



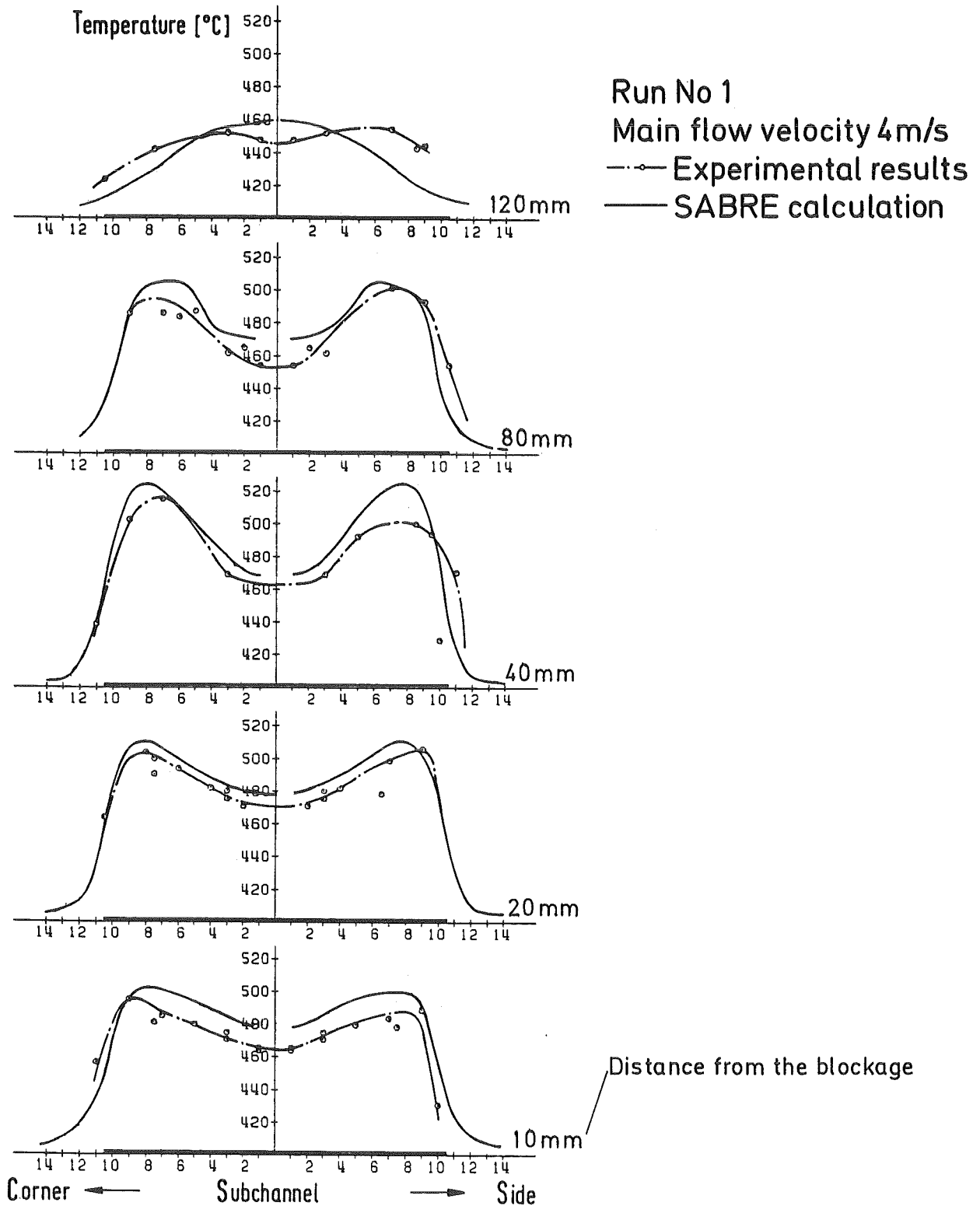
Gas injection rate [cm³/s]

- 19.3
- - - 16.1
- · - · 12.9

21% Corner Blockage

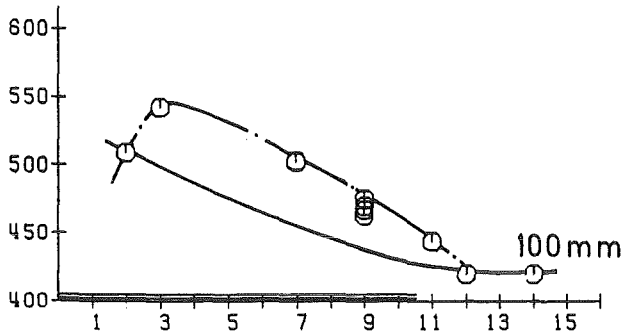
KfK IRE847887

Fig.46 Extension of the Cooling Disturbed Region in the Wake

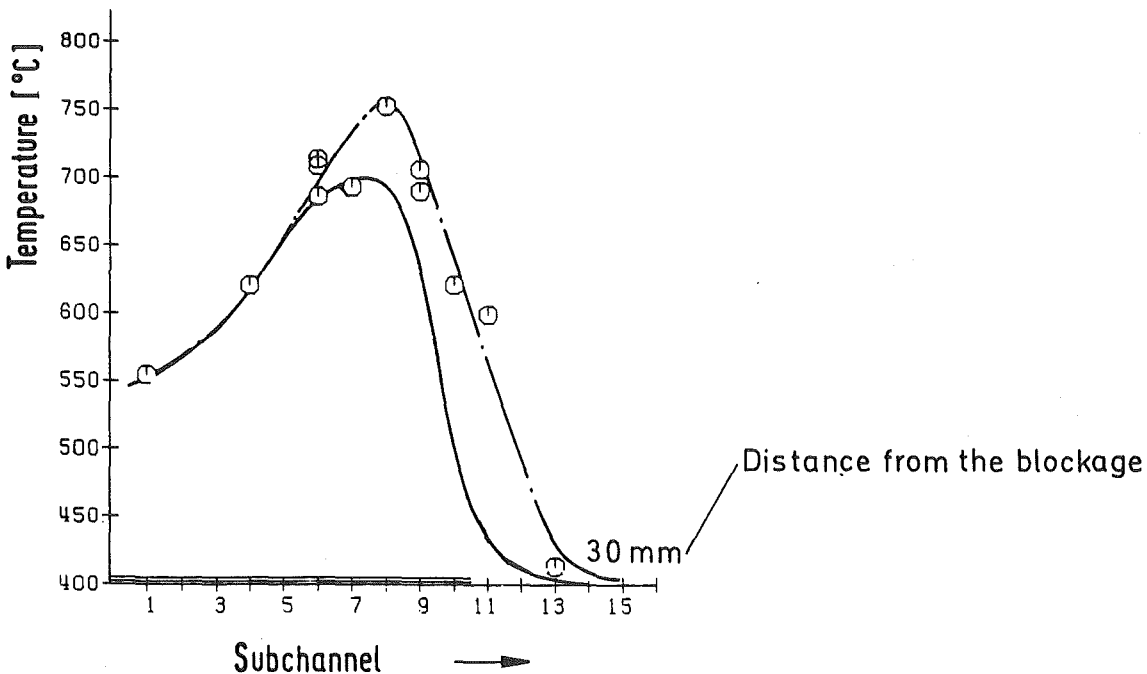
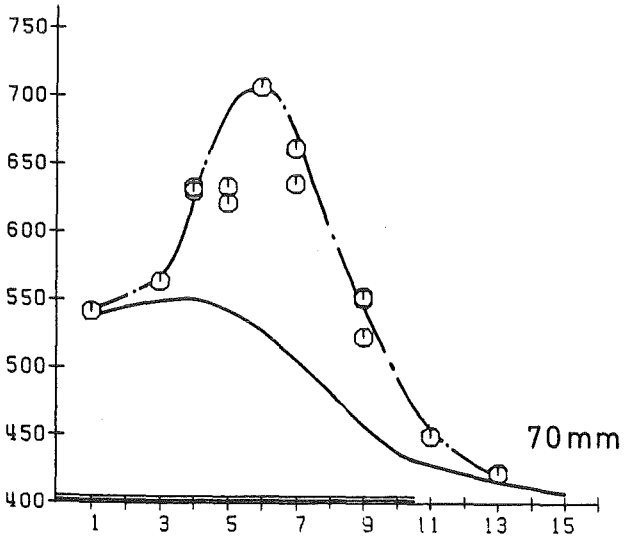


LMBWG Benchmark Calculations

Fig.47 49% Central Blockage, Sodium Radial Temperature Profile



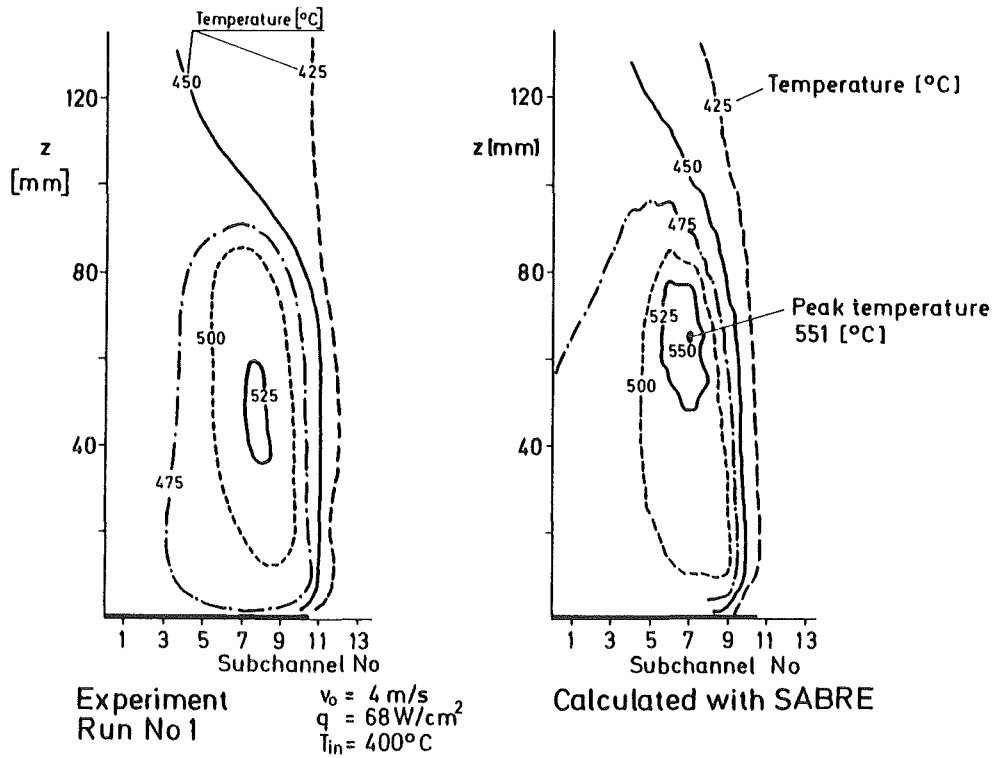
Run No 287
Main flow velocity 4 m/s
---○--- Experimental results
— SABRE calculation



LMBWG Benchmark Calculations

KIK IRE 847889

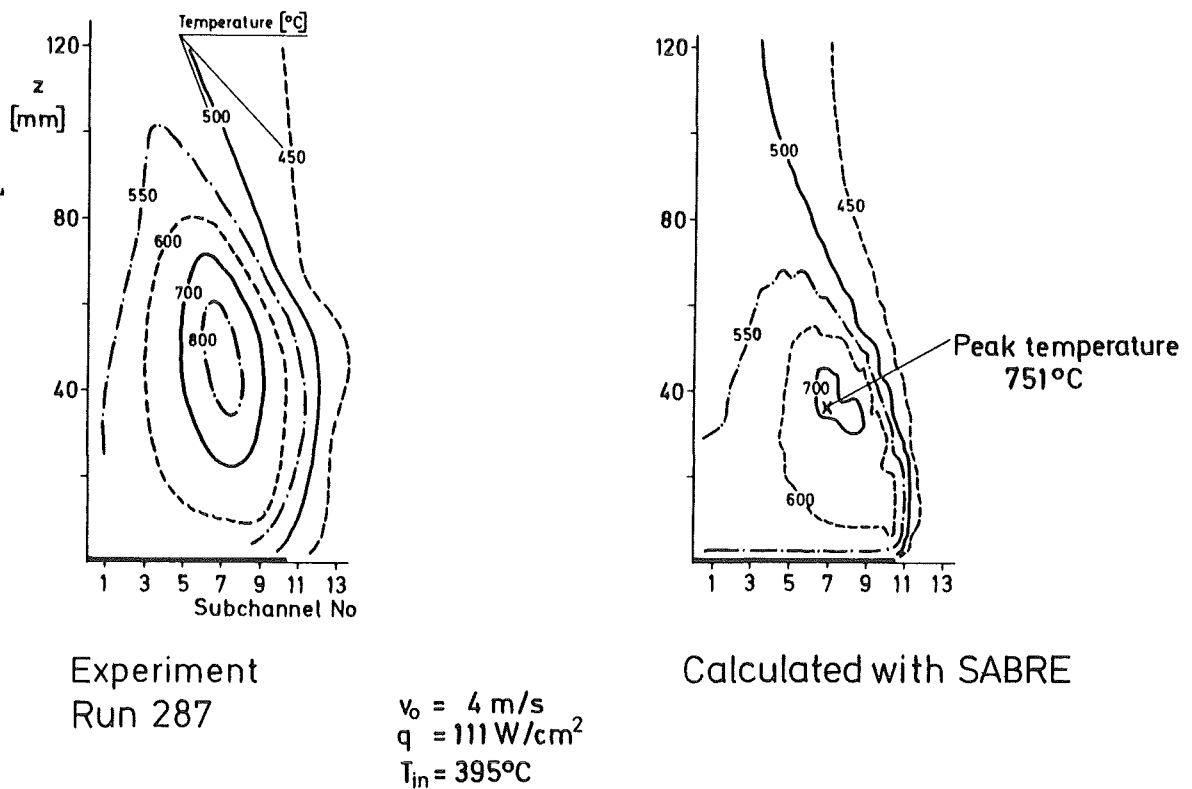
Fig.48 21% Corner Blockage, Sodium Radial Temperature Profile



LMBWG Benchmark Calculations

IRE 847890

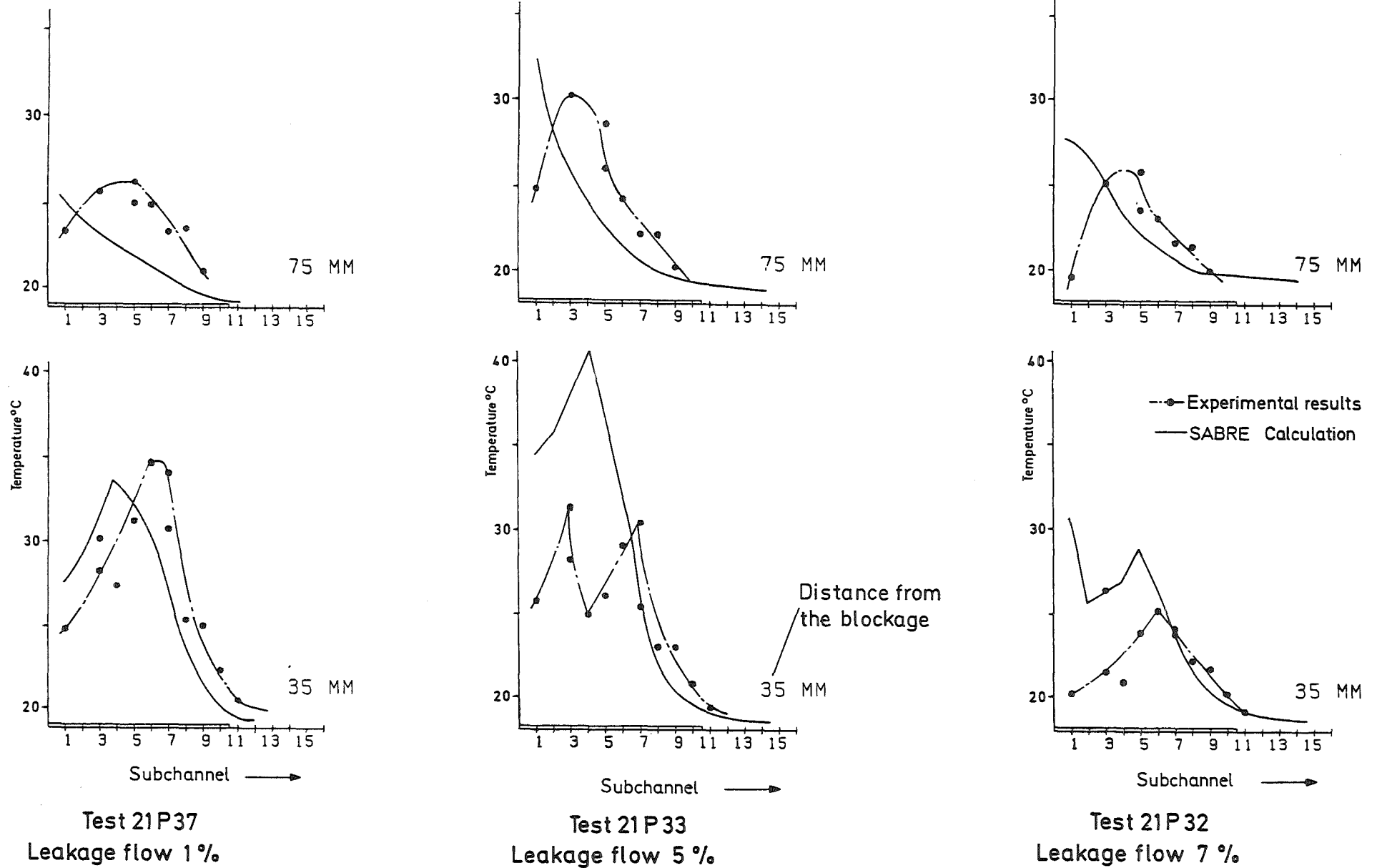
Fig.49 49% Central Blockage, Temperature Distribution



LMBWG Benchmark Calculations

IRE 847891

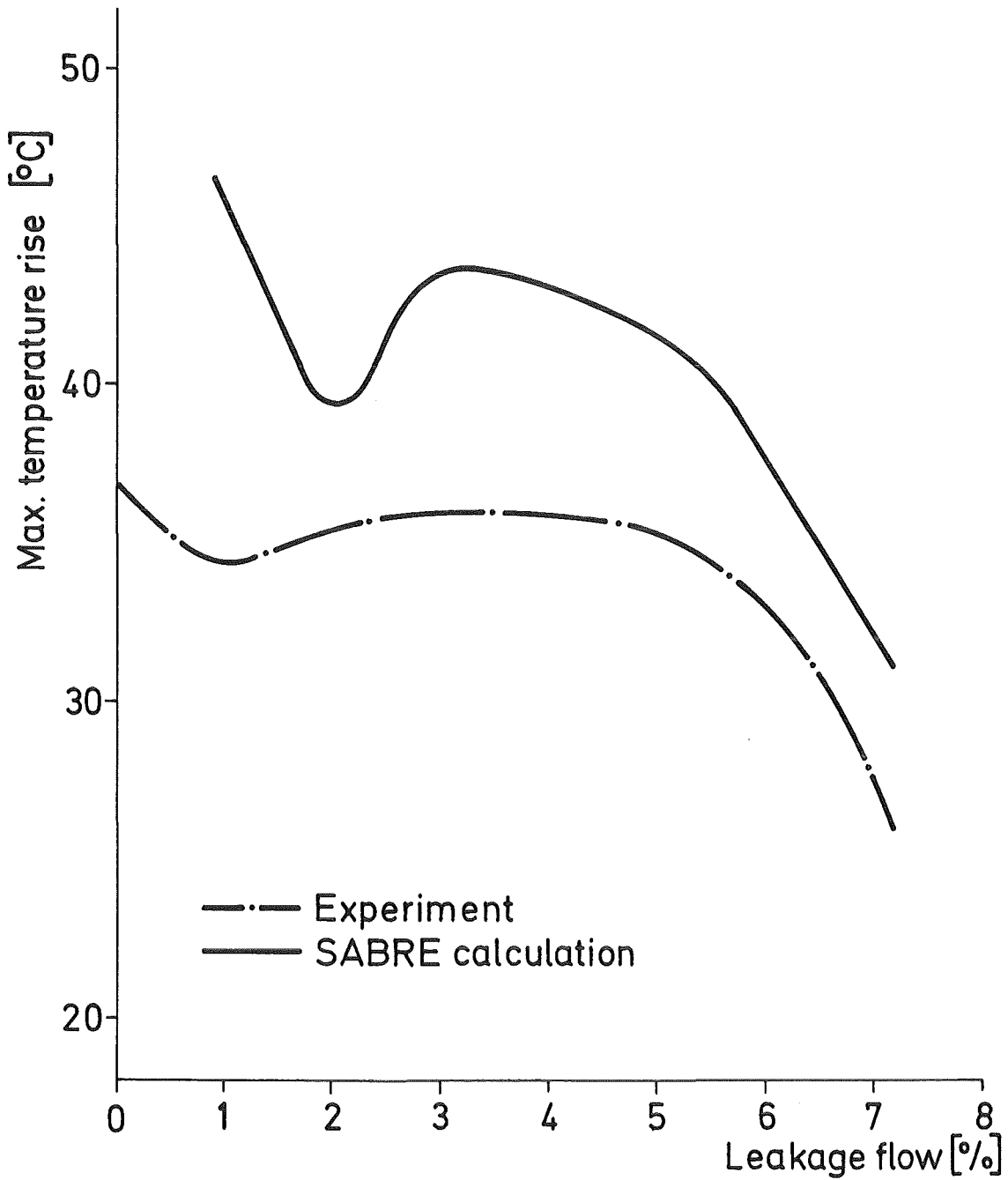
Fig.50 21% Corner Blockage, Temperature Distribution



LMBWG Benchmark Calculations

KIK IRE847892

Fig.51 21% Corner Blockage (Variable) with Leakage Flow Radial Temperature Profile



LMBWG Benchmark Calculations

Fig.52 21% Corner Blockage, Permeable Max. Temperature Rise vs. Leakage Flow

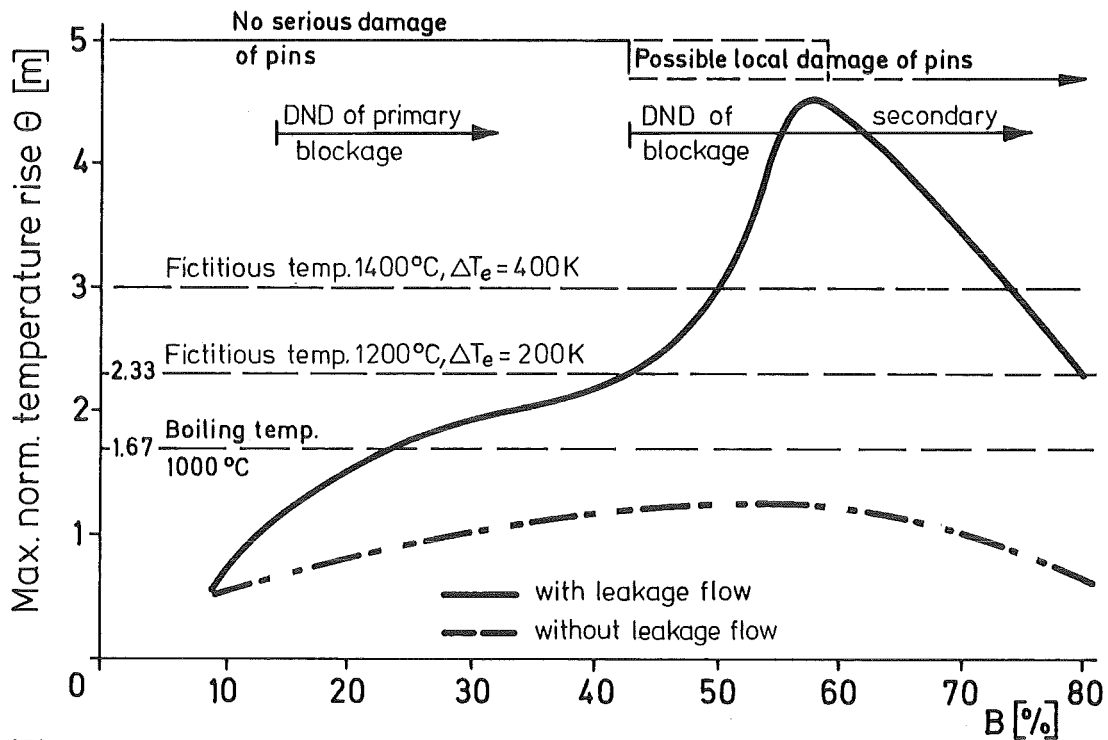


Fig.53a Max. Normalized Temperature Rise with and without Leakage Flow vs. Blockage Size

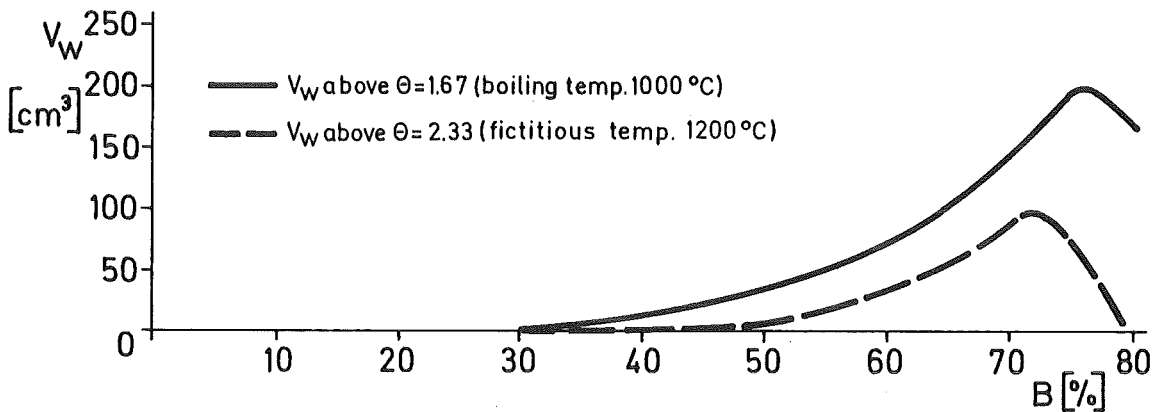


Fig.53b Volume of the Wake above Specified Normalized Temperatures under Leakage Flow Conditions

Central Blockage



Fig.53 Experimental Results Transferred to SNR 300 Conditions

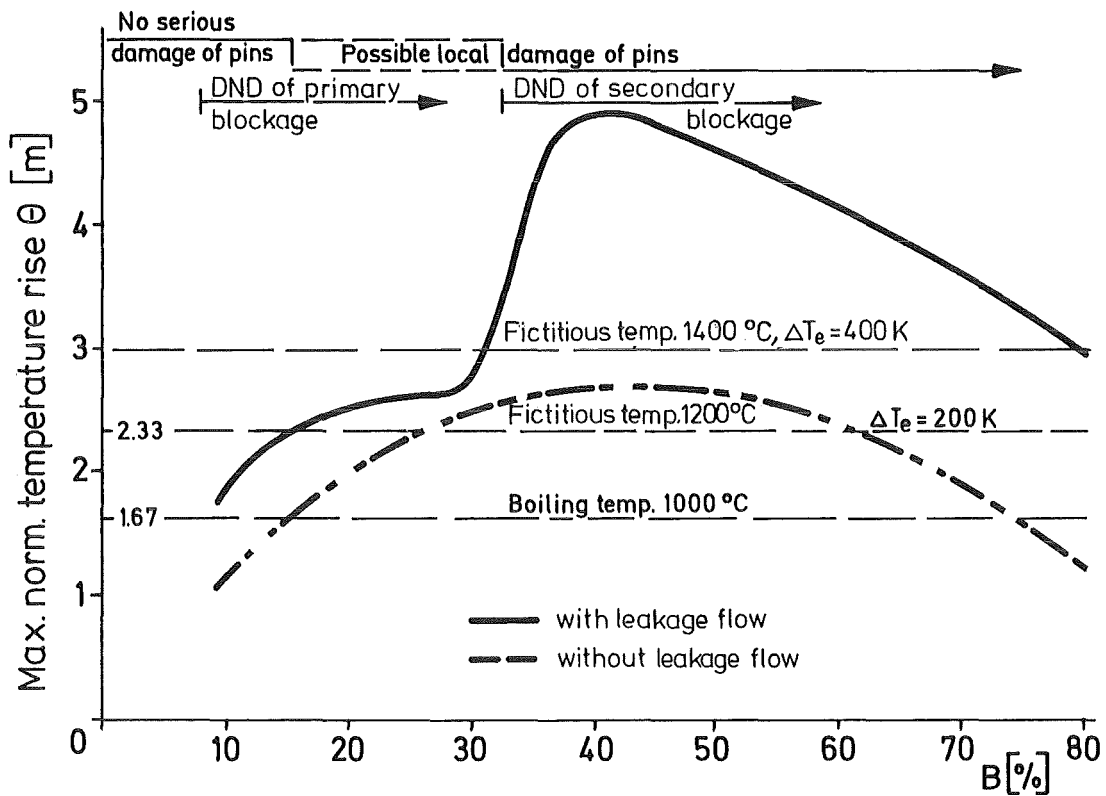


Fig.54a Max. Normalized Temperature Rise with and without Leakage Flow vs. Blockage Size

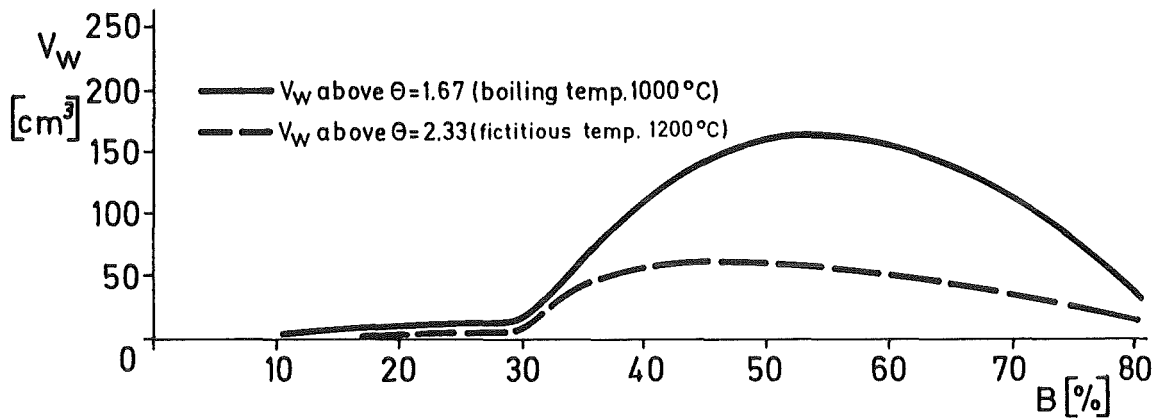
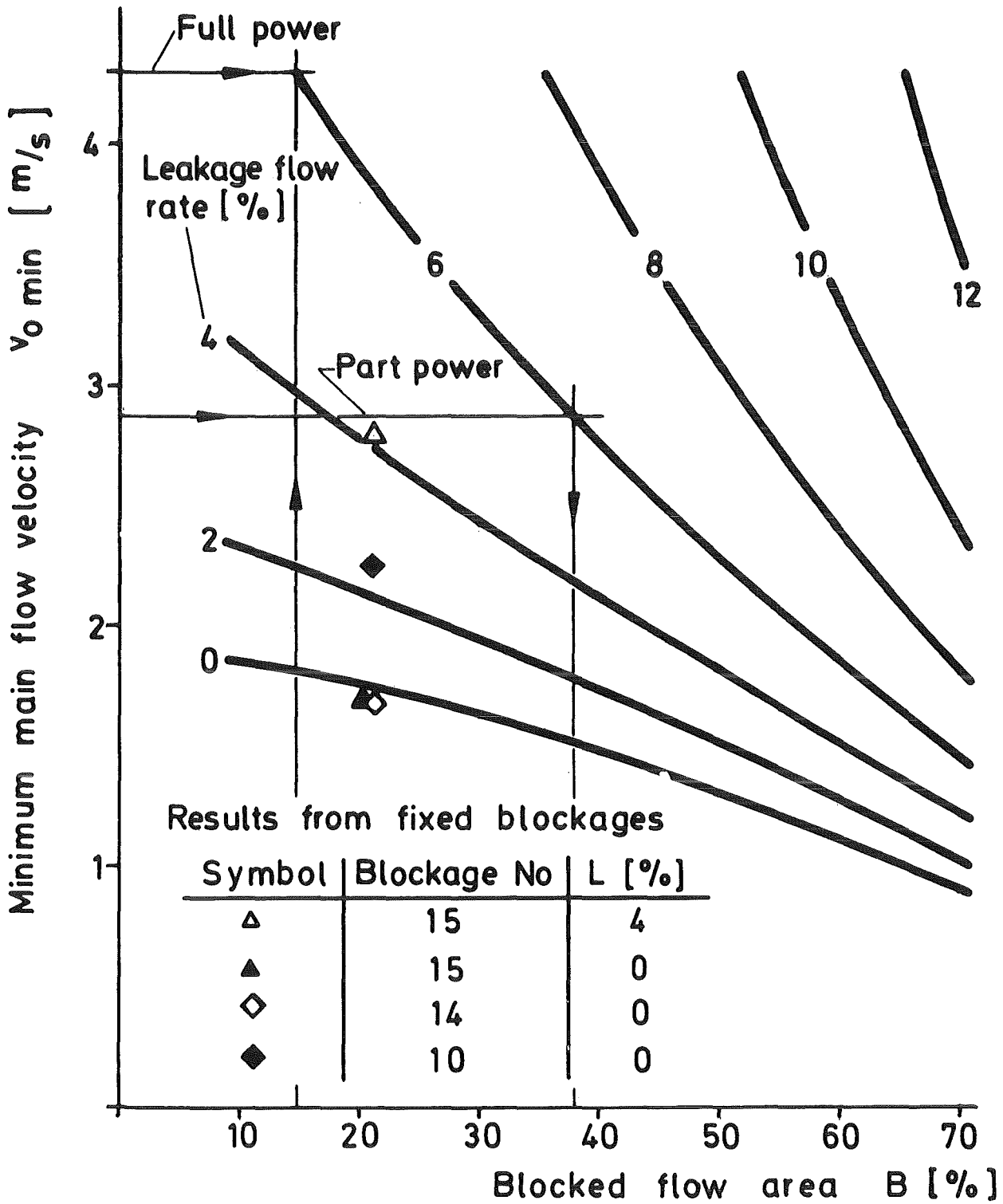


Fig.54b Volume of the Wake above Specified Normalized Temperatures under Leakage Flow Conditions

Based on main flow velocities of 3 and 4 m/s



No gas accumulation below the curves

Fig.55 Corner Blockage Minimum Main Flow Velocity for Gas Accumulation

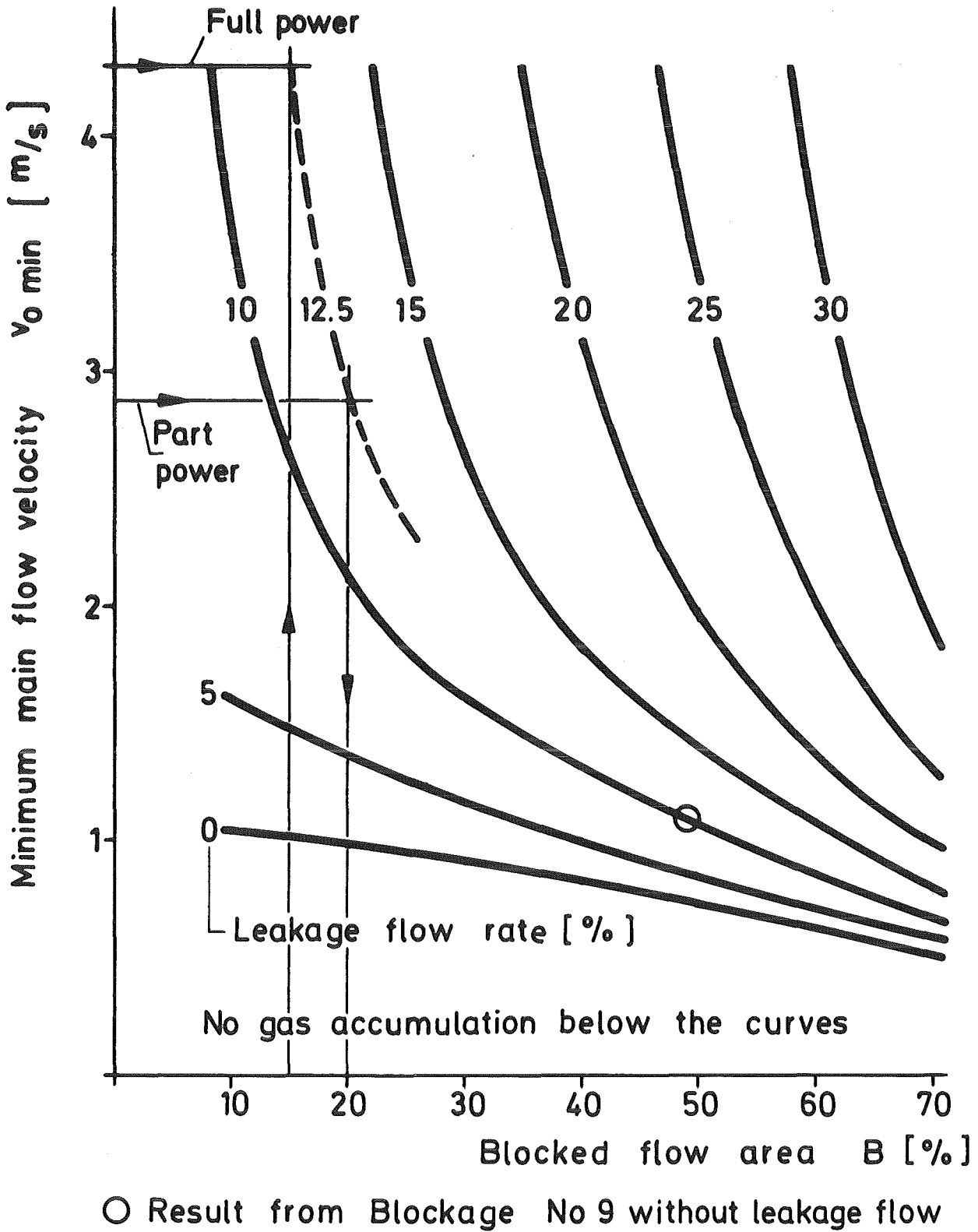
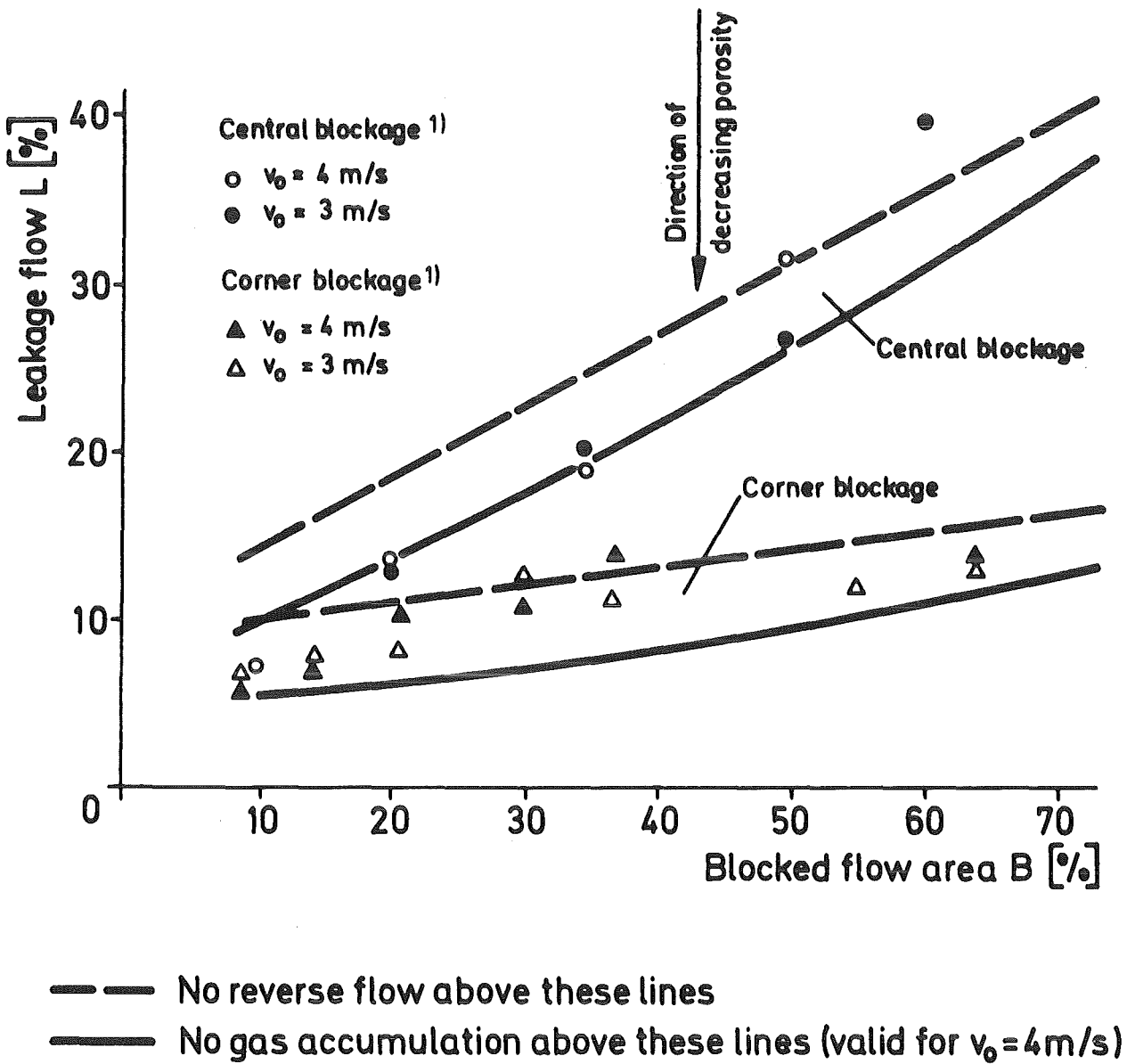
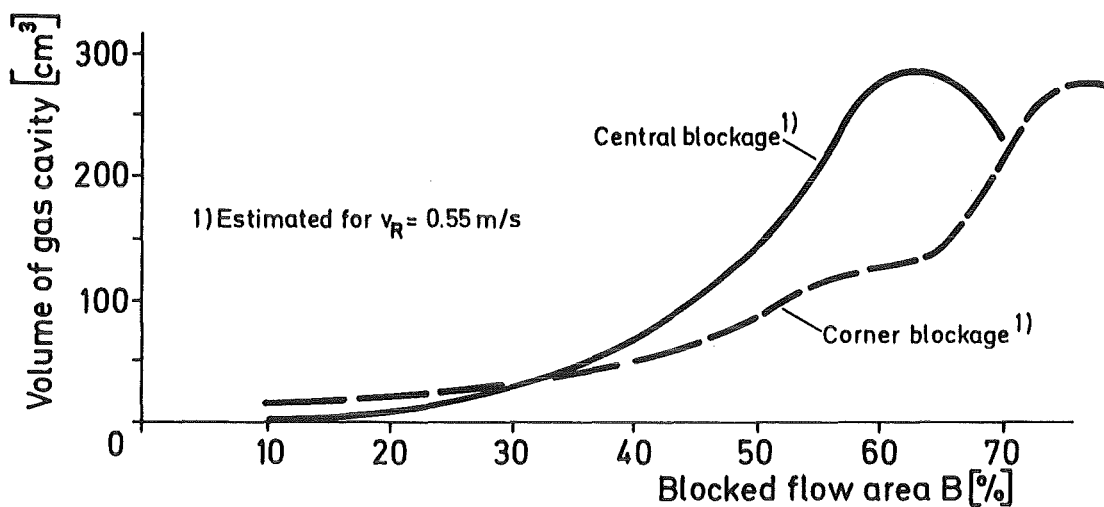


Fig.56 Central Blockage Minimum Main Flow Velocity for Gas Accumulation



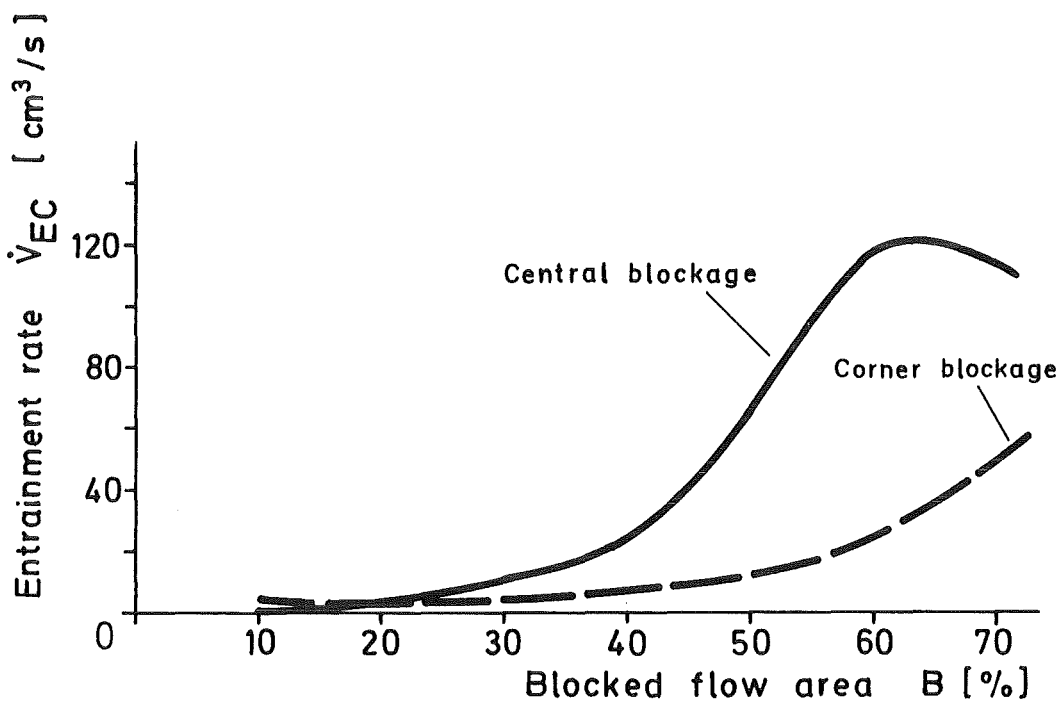
1) Experimental results causing max. temperature rise [25]

Fig.57 Leakage Flow Conditions Related to Reverse Flow and Gas Accumulation



IRE847899

Fig.58 Upper Limits of Gas Cavity Volumes



Valid for $v_0 = 4 \text{ m/s}$

IRE847900

Fig.59 Gas Entrainment Rate from the Cavity

Annex A

Definition of Normalized Temperatures

1. Normalization of Temperature Rise

The measured temperature rises in the wake were normalized to eliminate the different heater powers and coolant velocities and to facilitate comparison of results from different multi-pin blockage experiments. This form of normalization is based on the statement that in the wake the molecular momentum and energy transport (e.g. heat conduction) can be neglected. Details of these considerations are given in the report of D. Kirsch /9/. In the following paragraphs the theoretical axial temperature gradient in the undisturbed central subchannel is used. Thus, the normalized temperature is defined here as:

$$\theta = \frac{\Delta T}{dT/dz} \quad [m] \quad (A1)$$

A uniform axial temperature gradient is assumed which is given by:

$$\frac{dT}{dz} = \frac{4 \cdot q}{\rho \cdot c_p \cdot v_o \cdot d_h} \quad [K/m] \quad (A2)$$

In the experiments the inlet temperature of the blockage is not measured and therefore calculated assuming a uniform temperature gradient between the beginning of the heated section and the blockage position, a distance l_B ; thus, definition A1 may also be expressed as

$$\theta = \frac{T - T_{in}}{dT/dz} - l_B \quad [m] \quad (A3)$$

2. Definition of Excess Temperature

As a measure of characterizing the boiling intensity in different experiments the excess and normalized temperatures, respectively, must be introduced.

The excess temperature is defined as the difference between the fictitious peak temperature \hat{T} , in the absence of boiling, and the saturation temperature.

$$\Delta T_e = \hat{T} - T_{\text{sat}} \quad [\text{K}] \quad (\text{A4})$$

T is not known from the experiment under actual conditions. It is therefore calculated from the normalized peak temperature $\hat{\theta}$ deduced from the onset of boiling or from the single-phase conditions.

$$\hat{T} = (\hat{\theta} + 1_B) \frac{dT}{dz} + T_{\text{in}} \quad [\text{K}] \quad (\text{A5})$$

3. Definition of Normalized Excess Temperature

The normalized excess temperature is given by

$$\Delta \theta_e = \hat{\theta} - \theta_{\text{sat}} \quad [\text{m}] \quad (\text{A6})$$

from (A4) using the definition (A1),

$$\Delta \theta_e = \frac{\Delta T_e}{dT/dz} \quad [\text{m}]$$

Annex B

Definition of Leakage Flow

The leakage flow through th blockage is defined as the ratio of the flow through the blocked area to the flow through the same area that would prevail in the absence of the blockage.

$$L = \frac{\dot{m}_L}{\dot{m}_B \cdot B} \quad (B1)$$

Annex C

Boundary Conditions for a Gas Cavity Formation

As described in Chapt. 8, all experiments in water and in sodium as well have shown that below a certain main flow velocity, irrespective of the gas injection rate, no gas collects behind a blockage. Instead of the main flow velocities measured in different experiments it is more appropriate to compare the related reverse flow velocities. Therefore, in Table C1 the minimum reverse flow velocities measured or calculated for the lower limiting conditions of gas cavity formation are listed.

Blockage			Coolant	v_{Rmin}
No	Type	Size %		m/s
9	Central, impermeable	49	sodium	0.6
10	Corner, impermeable	21	sodium	0.58
14	Corner, impermeable	21	water	0.65
15	Corner, permeable	21	water	0.48
16	Central, variable	10	water	0.53
		21		0.6
		39		0.53
		49		0.6
		75		0.59
16	Corner, variable	9	water	0.5
		21		0.58
		30		0.54
		50		0.72
		61		0.62
		71		0.45

Table C1 Minimum Reverse Flow Velocities for Gas Cavity Formation found with different Blockage Configurations

These velocities - the average value is 0.55 m/s - are close together and about the same as the buoyancy velocity of bubbles of a diameter of about 3 mm /20/. It is assumed that for gas accumulation the reverse flow velocity must be higher than the buoyancy velocity of the gas bubbles.

To evaluate the field of conditions for a possible gas cavity formation the relation between the minimum main flow velocity and the blockage size will be deduced below with the leakage flow through the blockage as the main parameter.

For the wake region an average main flow velocity \bar{v} is defined (see Fig. 9):

$$\bar{v} = \frac{v_o + v_B}{2}$$

v_B is expressed by a relation between v_o and B, the blocked flow area in %/

$$\bar{v} = \frac{v_o (200-B)}{2 (100-B)} \quad (C1)$$

It was found in the experiments with zero leakage (see Fig. 11) that the relation v_R/\bar{v} can be assumed to be nearly independent of the blockage size for a specified blockage type, either corner or central. Therefore, it is convenient to introduce this relation in (C1)

$$\frac{v_R}{\bar{v}} = \frac{v_R}{v_o} \cdot \frac{2(100-B)}{200-B} \quad (C2)$$

Because the minimum reverse flow velocity v_{Rmin} is known too, the minimum main flow velocity v_{omin} can be determined from (C3)

$$v_{o \min} = v_{R \min} \cdot \frac{1}{v_R/\bar{v}} \cdot \frac{2(100-B)}{200-B} \quad (C3)$$

Equation (C3) is valid only for the case of leak-tight blockages using the values for the relation v_R/\bar{v} .

The values for the relation v_R/\bar{v} in the table below are taken from the experiments (see Fig. 11).

Type and Size of the Blockage		Coolant	v_R/\bar{v}
Central	variable	water	0.5
	49 % fixed	sodium	0.4
Corner	variable	water	0.28
	21 % fixed	sodium	0.18
		water	0.25

Table C2 Normalized Reverse Flow Velocities of Different Blockages

The influence of the leakage flow through a porous blockage is included in the following. It was observed in the experiments that at constant main flow velocity v_0 the reverse flow velocity v_R is roughly proportionally decreasing with increasing leakage flow L (see also Fig. 12). For a certain leakage flow L_K the reverse flow v_R becomes zero. The dependence is expressed by Eq. C4

$$\frac{v_{RL}}{\bar{v}} = \frac{v_R}{\bar{v}} \left(1 - \frac{L}{L_K} \right) \tag{C4}$$

Equation (C4) is introduced in (C3) for v_{RL}/v

$$v_{o \min} = v_{R \min} \cdot \frac{1}{v_R/\bar{v}} \cdot \frac{\frac{100-B}{200-B}}{\left(1 - \frac{L}{L_K}\right)} \quad (C5)$$

The values for $L_K = f(B)$ of the experiments with the variable blockage (see Fig. 13) can be reproduced by two functions:

Central blockage

$$L_{KCe} = 9.6 + 0.448 \cdot B \quad (C6)$$

Corner blockage

$$L_{KCr} = 8.8 + 0.104 \cdot B \quad (C7)$$

Equations (C6) and (C7) together with the values for v_{\min} and v_R/\bar{v} from the experiments in water with the variable blockage are introduced in Eq. (C5).

Central blockage

$$v_{o \min} = 2.2 \frac{\frac{100-B}{200-B}}{1 - \frac{L}{9.6+0.448 \cdot B}} \quad (C8)$$

Corner blockage

$$v_{o \min} = 3.93 \frac{\frac{100-B}{200-B}}{1 - \frac{L}{8.8+0.104 \cdot B}} \quad (C9)$$

With these two equations the field of conditions was calculated for gas cavity formation with impermeable and permeable blockages, was described in Chapt. 10.1.3 (Figs. 55 and 56) was calculated.

Annex D

Graphs of characteristic boiling signals

To describe the two different boiling regimes - oscillatory boiling and steady state boiling - in chapter 6 typical signals of two tests are shown, but only during the last run of the experiments just before switch off of the power. To give more information to the course of these two experiments in the following the characteristic signals of every run are plotted with the excess temperature as a measure of boiling intensity.

Fig. D1 Oscillatory boiling, experiment 32/1-2, Run No. 57A-58E

Fig. D2 Steady state boiling, experiment 216/2, Run No.478-485.

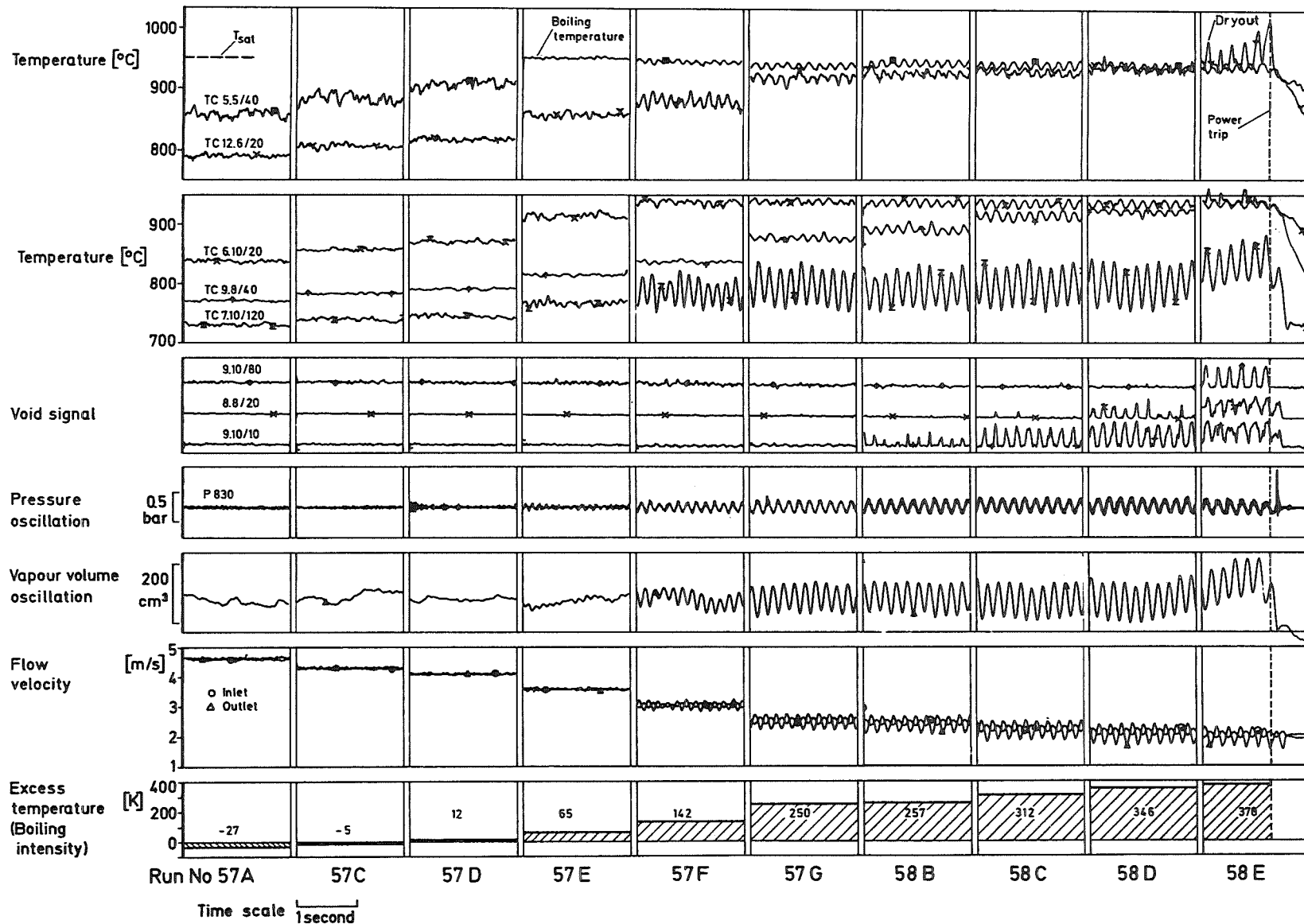


Fig. D1 Characteristic Oscillatory Boiling Signals (Experiment 32/1,2)

IRE849891

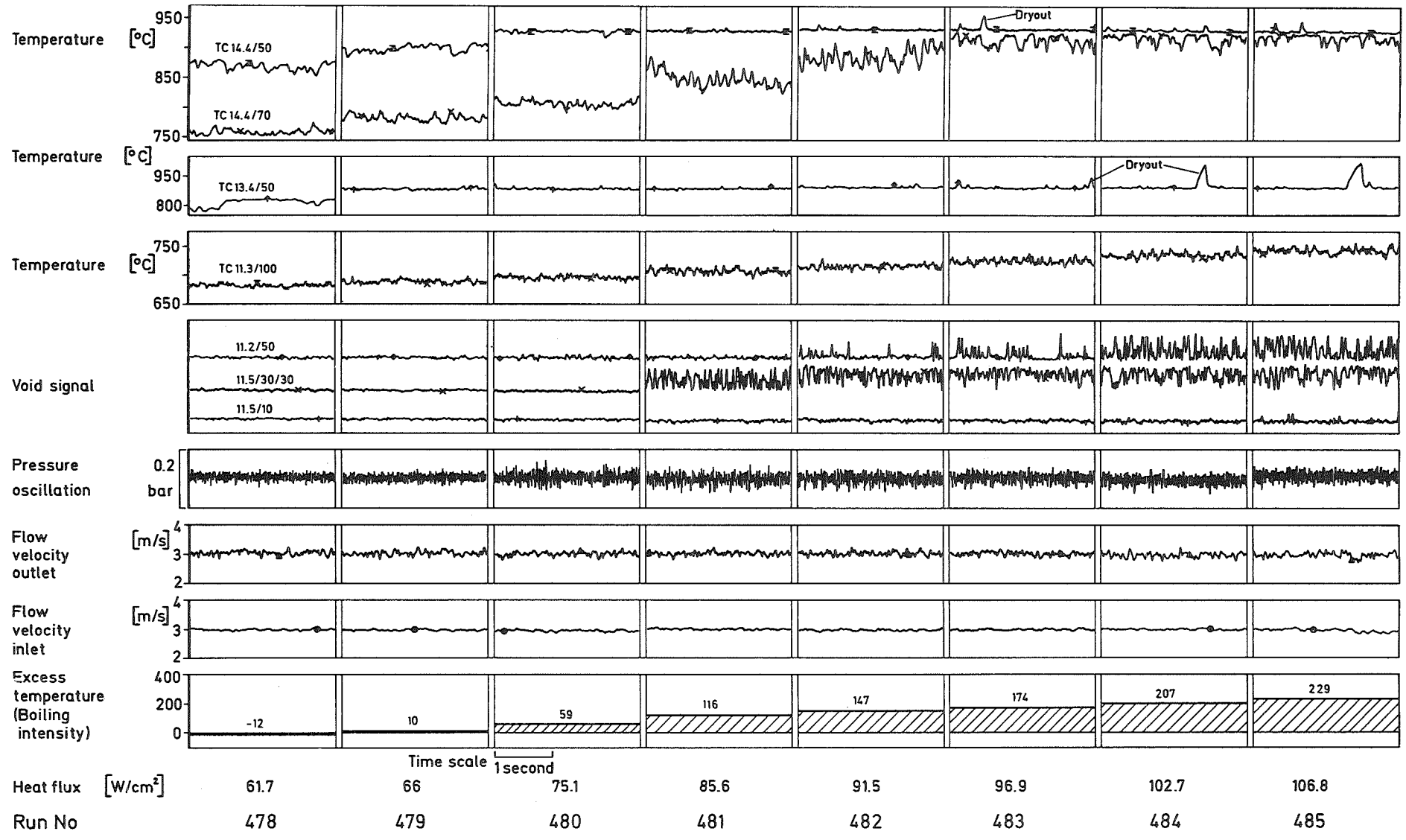


Fig. D2 Characteristic Steady-State Boiling Signals (Experiment 216/2) IRE849892